Supporting Information

Synthesis and Comparative Study of (NHC_F)$PdCl_2Py$ and (NHC_F)Ni(Cp)Cl Complexes: Investigation of the Electronic Properties of NHC Ligands and Complex Characteristics

Roman O. Pankov[a], Ignatii R. Tarabrin[a,b], Alexandra G. Son[c], Mikhail E. Minyaev[a], Darya O. Prima[a], Valentine P. Ananikov[a*]

[a] *Zelinsky Institute of Organic Chemistry, Russian Academy of Sciences, Leninsky prospekt 47, Moscow, 119991, Russia;*

[b] *Department of Chemistry, Lomonosov Moscow State University, Leninskie Gory 1-3, Moscow 119991, Russia;*

[c] *Kurnakov Institute of General and Inorganic Chemistry, Russian Academy of Sciences, Leninskii pr. 31, Moscow 119991, Russia;*

**e-mail: val@ioc.ac.ru; http://AnanikovLab.ru*

1. General information

Chemicals were obtained from P&M Invest, Sigma-Aldrich and Acros Organics. The samples for the ESI-TOF-HRMS experiments were prepared in 1.8 mL glass vials with screw-top caps fitted with Teflon-lined septa (Agilent Technologies). NMR spectra were recorded by using Bruker Avance-NEO 300 or Bruker Fourier 300HD spectrometers operating at 300.1 MHz for ^{1}H, 75 MHz for ^{13}C, 57 MHz for ^{77}Se and 282.4 MHz for ^{19}F. ^{1}H and ^{13}C NMR chemical shifts are reported relative to the solvent signals as internal standards: 2.5 ppm/39.5 ppm for DMSO-d_6 and 7.26 ppm/77.16 for $CDCl_3$. ^{19}F NMR chemical shifts are reported relative to C_6F_6 ($\delta^{19}F$ = –162.9 with respect to $CFCl_3$). ^{77}Se chemical shifts are given in parts per million relative to internal Ph_2Se_2 ($\delta^{77}Se$ = 463.27).

The electronic absorption spectra of the solutions were measured using a Cary 5000 UV-Vis-NIR spectrometer with a wavelength resolution of 0.05 nm in the range of 200–650 nm. Photoluminescence spectra were obtained using a Perkin Elmer LS-55 luminescence spectrometer with a spectral resolution of 0.5 nm and spectral slit width of 10 nm, in the range 350–700 nm. All measurements were performed at room temperature using a standard quartz cuvette with a 1 cm optical path length and a single-position cuvette holder for liquid samples. All measurements were performed at room temperature.

Oxidation and reduction behavior of complexes **4** were analyzed by cyclic voltammetry using a digital potentiostat IPC-Pro-MF (Econix). The solution preparation and all measurements were made in an argon-filled glovebox with water and oxygen contents below 0.1 ppm. Before that, acetonitrile (HPLC grade, Acros) with an initial water content of <100 ppm, were stored over 4 Å molecular sieves preliminarily dried under oil-pump vacuum at 200–250 °C for 4 h. Bu_4NBF_4 (Sigma-Aldrich) was dried under oil-pump vacuum at 80 °C for 4 h. The water content in 0.1 M Bu_4PF_6/MeCN did not exceed 20 ppm as determined by Karl Fischer titration using a Mettler-Toledo Titrator C10SD. The compounds **4** dissolved in the supporting electrolyte with a concentration of 2.5×10^{-3} M were electrochemically tested in a standard three-electrode glass cell at a potential sweep rate of 100 mV/s. The working electrode was a glassy carbon disc electrode with a diameter of 1.7 mm. Before use, it was polished with abrasive paper and then GOI paste until the surface attained a mirror shine. The counter electrode was a Pt wire preannealed in a gas burner flame to remove oxides and other possible contaminations. The potentials of the studied processes were measured versus the Ag wire coated with AgCl (prepared by galvanostatic anodization in 5% HCl solution) separated from the bulk electrolyte solution by an electrolytic bridge filled with the supporting electrolyte. The reference electrode was calibrated versus the ferrocene–ferrocenium redox couple. Also, ferrocene was used as a standard to establish a one-electron current level under experimental conditions.

Instrumentation. High-resolution mass spectra were recorded on Bruker micrOTOF (time-of-flight mass analyzer), on a Bruker maXis Q-TOF instrument (Bruker Daltonik GmbH, Germany) equipped with an electrospray ionization (ESI) source. The experiments were performed in positive (+) MS ion mode (HV capillary: 4500 V; HV end plate offset: -500 V) with a scan range of *m/z* 50–1500. External calibration of the mass spectrometer was performed using a low-concentration tuning mix solution (Agilent Technologies) for microTOF and maXis. Samples were injected using a 500 μL Hamilton RN 1750 syringe (Switzerland). Direct syringe injection was applied to the analyzed solutions in CH_3CN (flow rate: 3 μL/min) for analytical characterization. Nitrogen was applied as the nebulizer gas (1 bar) and dry gas (4.0 L/min, 200 °C). The spectra

were processed using Bruker Data Analysis 4.0 software. The error is determined by the most intense peak.

2. Catalytic activity studies

Table S1. Catalytic testing of Pd and Ni/NHC$_F$ complexes

№	Reaction	Conditions, cat = 1mol%	Pd, % yield	Ni, % yield
1	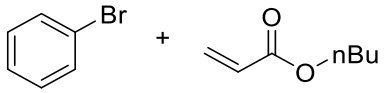	cat, DMF K_2CO_3, 100°C	10	0
2	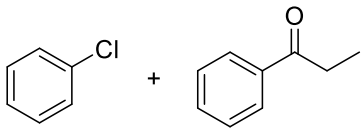	cat, toluene *t*BuONa, 110°C	0	0
3	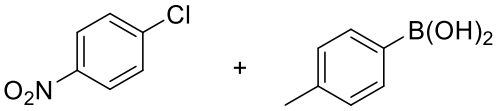	cat, dioxane *t*BuOK, rt	15	0
4	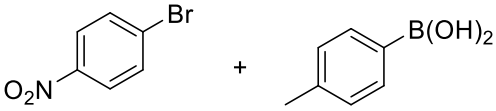	cat, DMF K_2CO_3, rt	0	0
5		cat, DME *t*BuOK, rt	0	0
6		cat, DME *t*BuOK, 70°C	t = 70 °C - 10% t = 50 °C - 15%	26
7	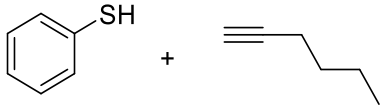	cat, toluene Et_3N, terpinene, 110°C	0	0

General Synthetic Procedure for Arylthiols Addition to Alkynes.[1] Complex **4** (1 mol %, 0.02 mmol), ArSH (2.0 mmol), and triethylamine (1 mol %, 2.0 mg, 0.02 mmol) were placed in a scintillation vial fitted with a Teflon-sealed screw cap and purged with nitrogen. The color of the solution changed from crimson to dark brown upon addition of Et_3N. The alkyne was added in three portions after 15 min, 1 h, and 2 h (1.0, 0.5, and 0.5 mmol, respectively) while the reaction mixture was stirring and heated at 80 °C. Total reaction time was 5 h. After completion, the yield was measured by ^{1}H NMR.

3. Characterization of the obtained compounds

3.1 NMR spectra of the obtained compounds

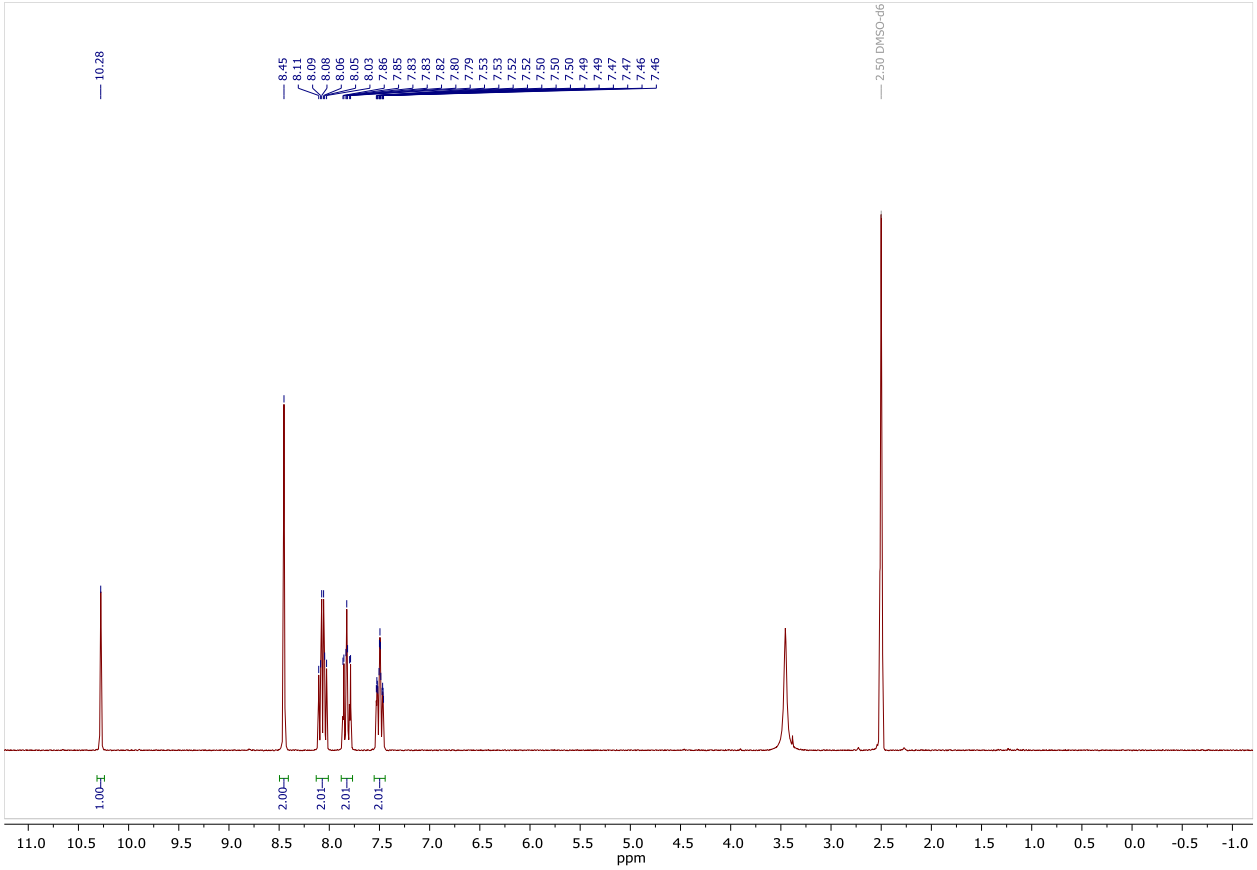

Figure S1. ^{1}H NMR spectrum of **2c**. Solvent: DMSO-d_6, 300 MHz.

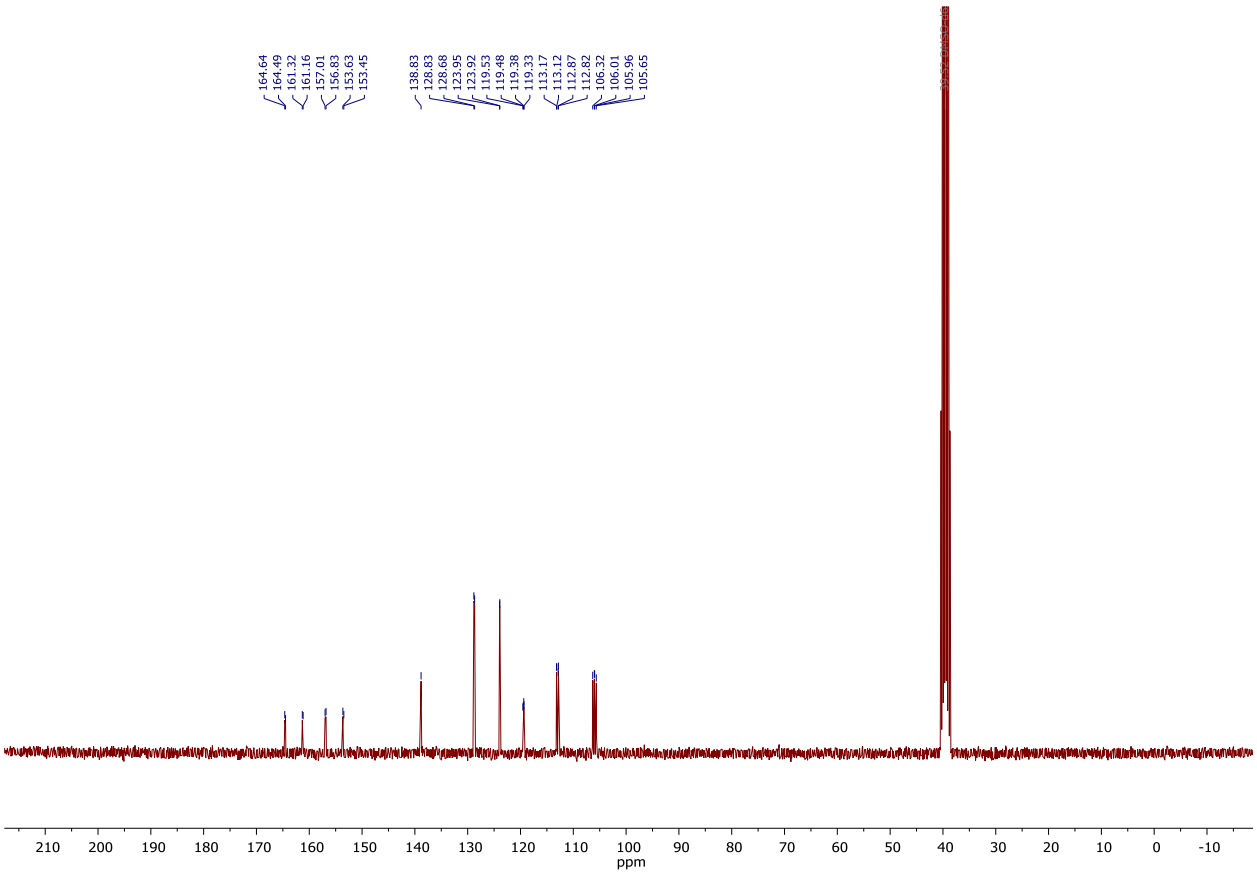

Figure S2. $^{13}C\{^{1}H\}$ NMR spectrum of **2c**. Solvent: DMSO-d_6, 75 MHz.

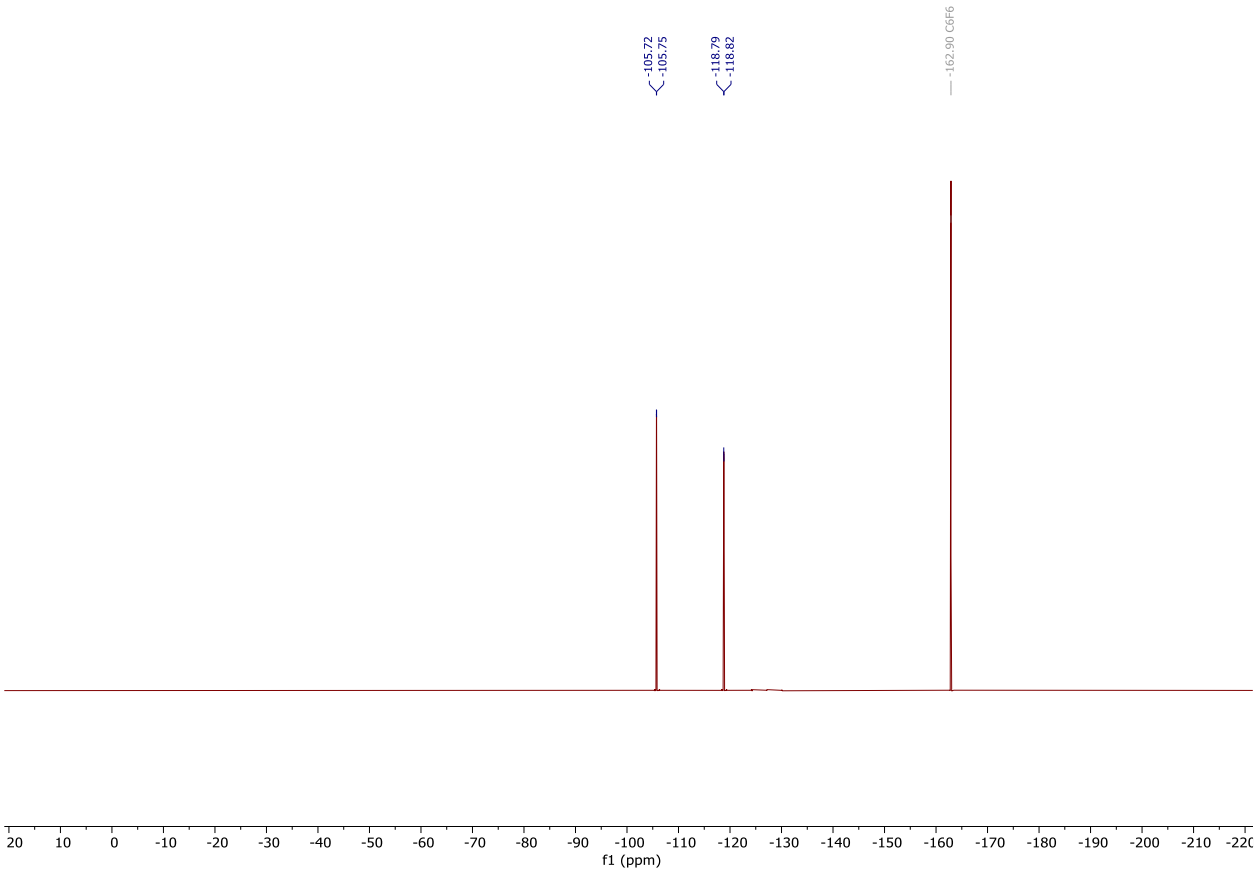

Figure S3. $^{19}F\{^{1}H\}$ NMR spectrum of **2c**. Solvent: DMSO-d_6, 282.4 MHz. Standard: C_6F_6 with respect to $CFCl_3$.

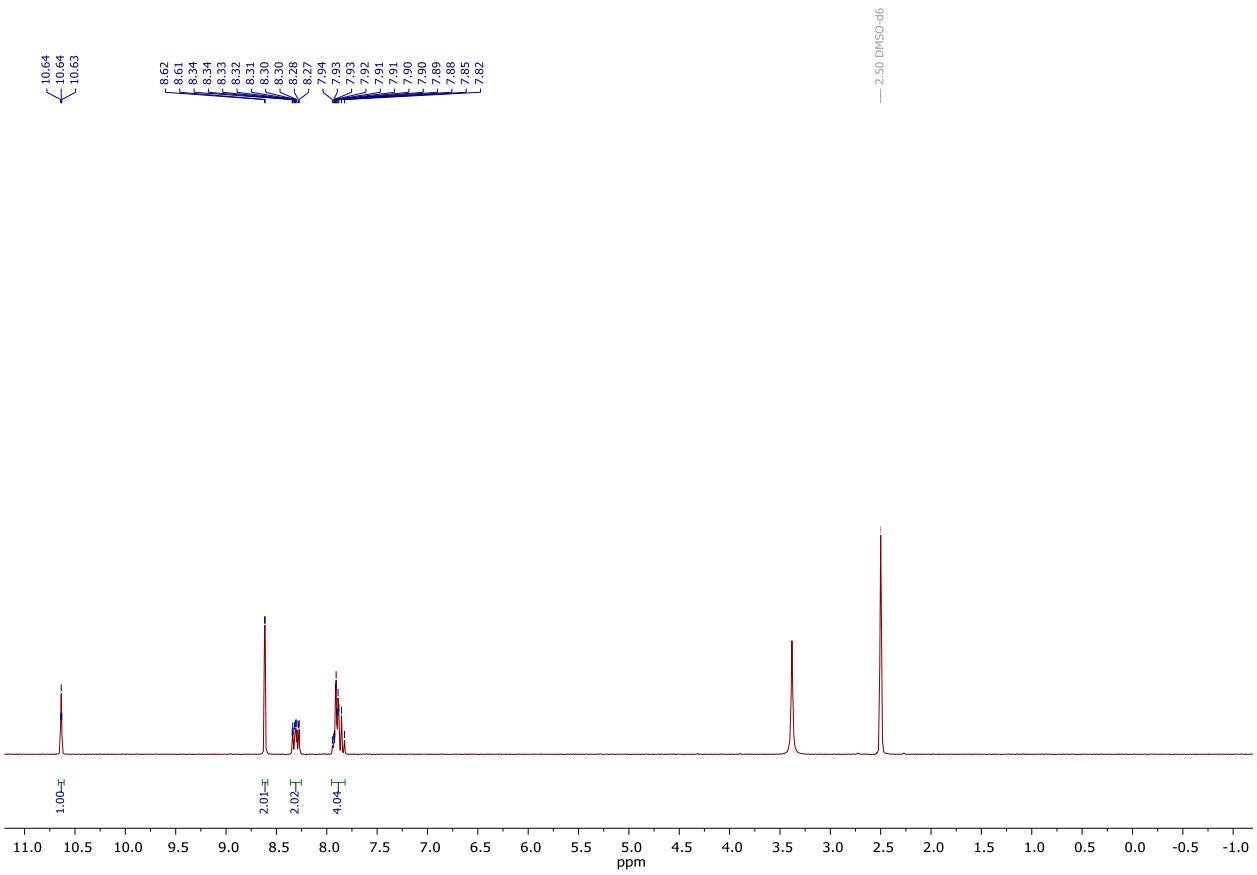

Figure S4. ^{1}H NMR spectrum of **2d**. Solvent: DMSO-d_6, 300 MHz.

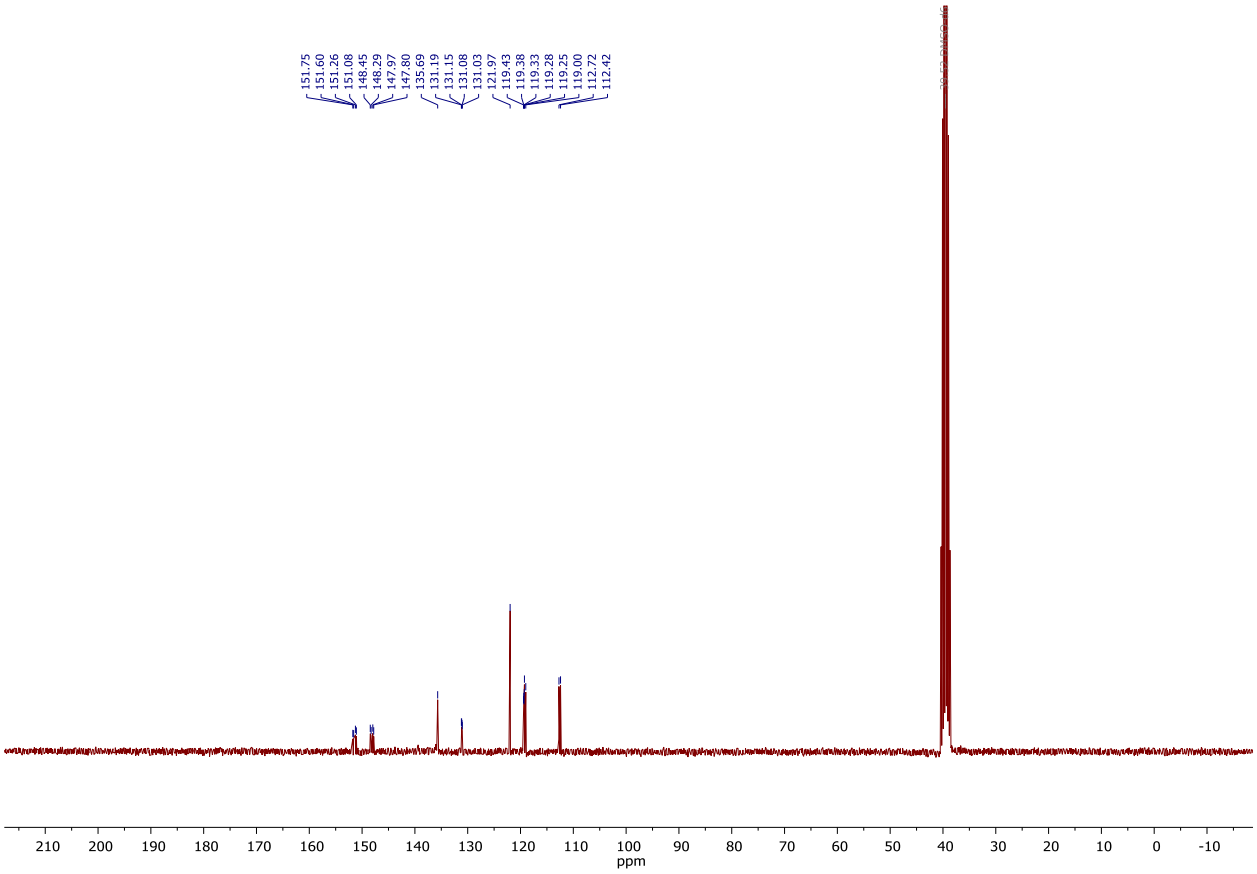

Figure S5. ^{13}C{^{1}H} NMR spectrum of **2d**. Solvent: DMSO-d_6, 75 MHz.

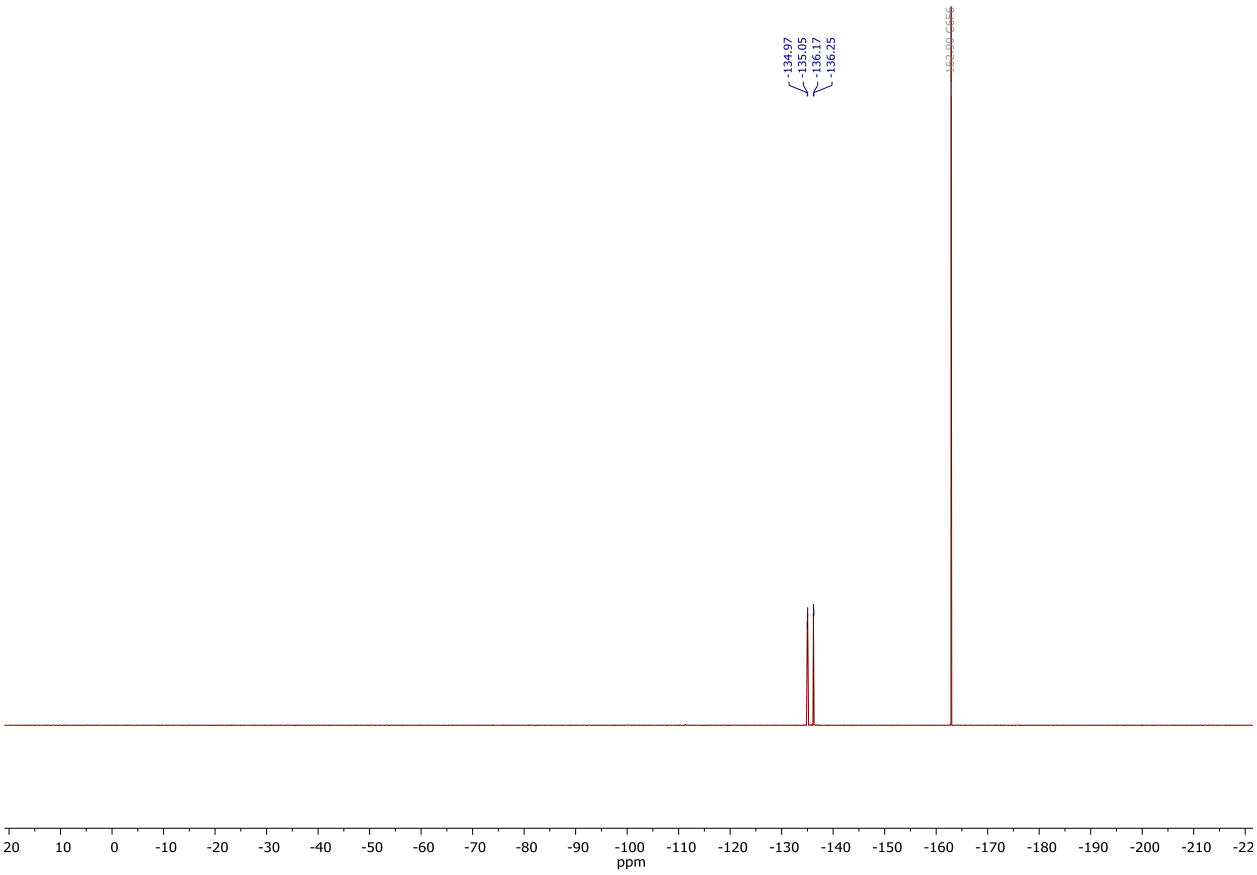

Figure S6. $^{19}F\{^{1}H\}$ NMR spectrum of **2d**. Solvent: DMSO-d_6, 282.4 MHz. Standard: C_6F_6 with respect to $CFCl_3$.

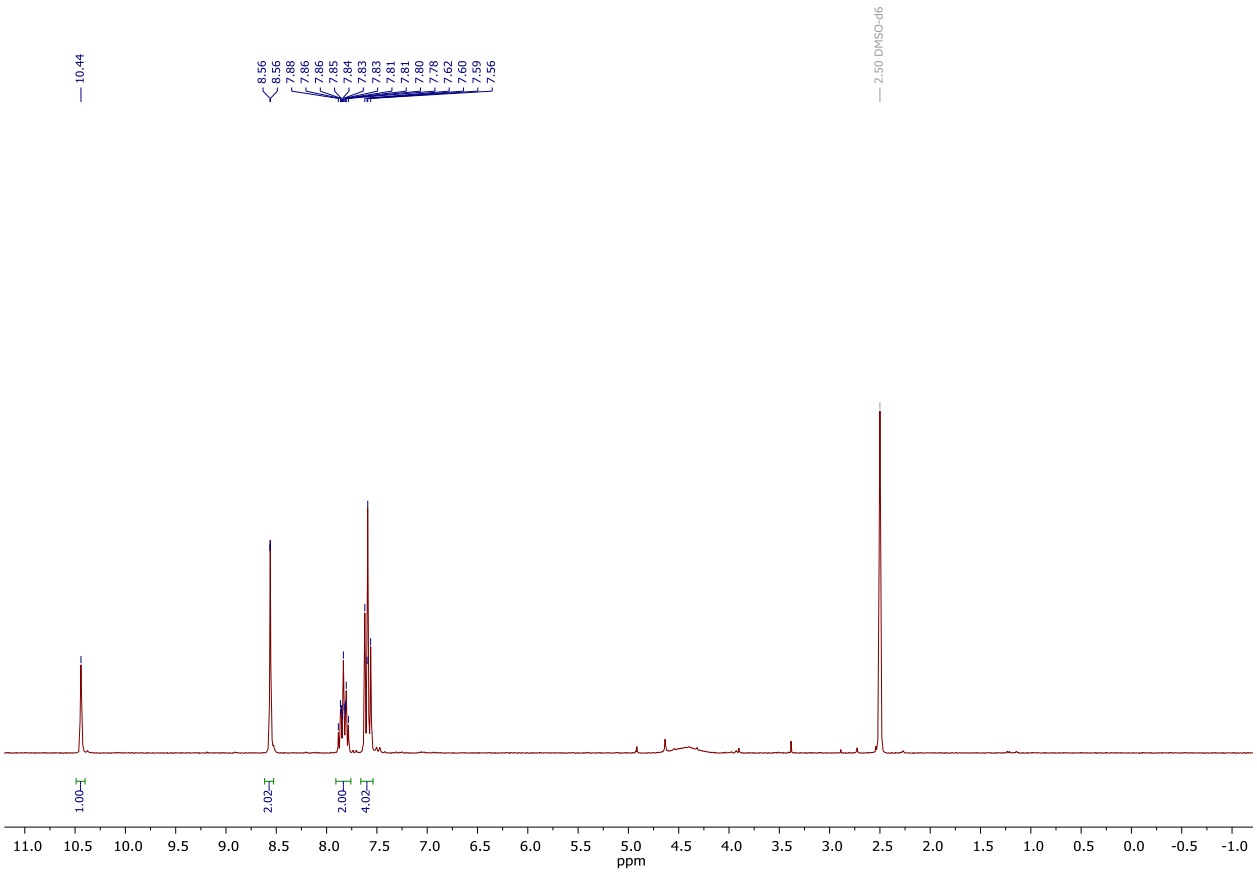

Figure S7. ^{1}H NMR spectrum of **2e**. Solvent: DMSO-d_6, 300 MHz.

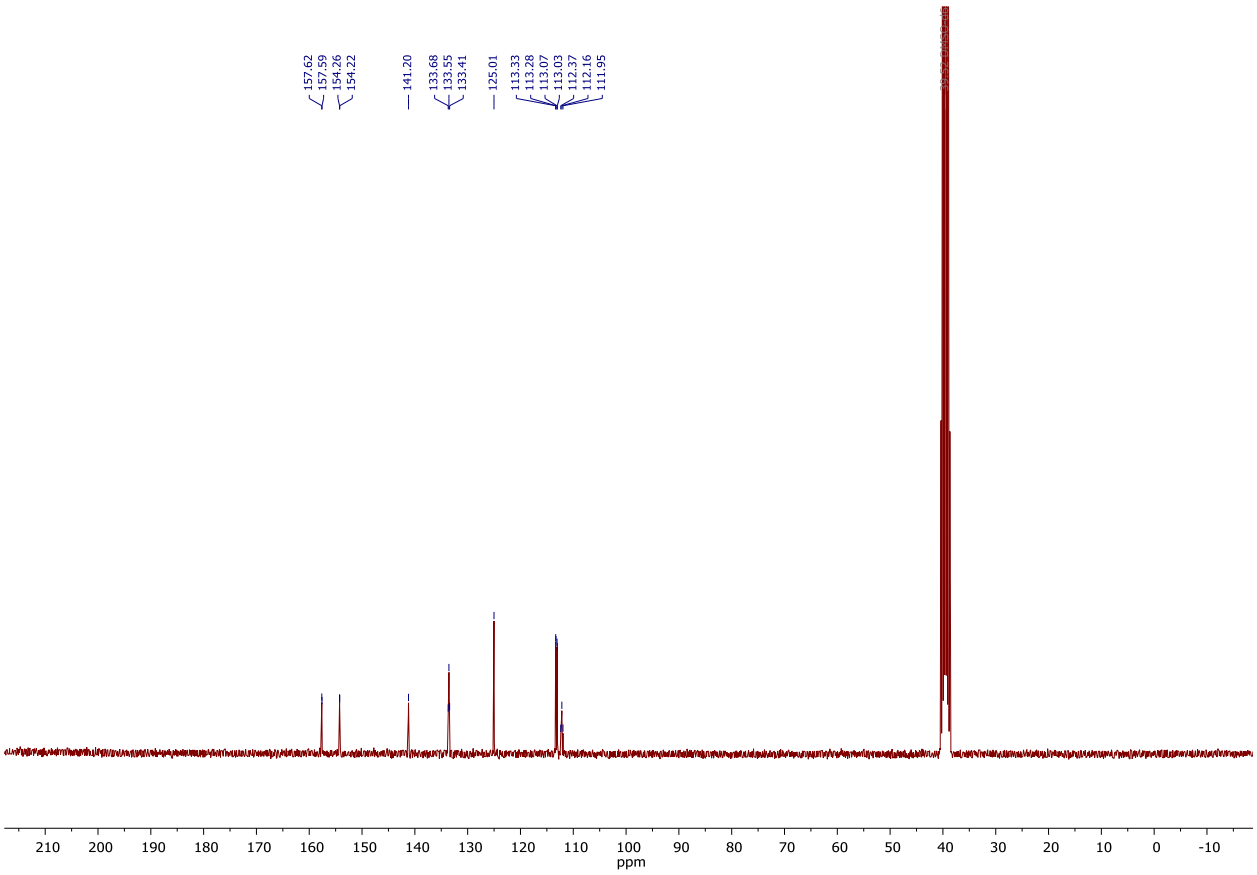

Figure S8. $^{13}C\{^{1}H\}$ NMR spectrum of **2e**. Solvent: DMSO-d_6, 75 MHz.

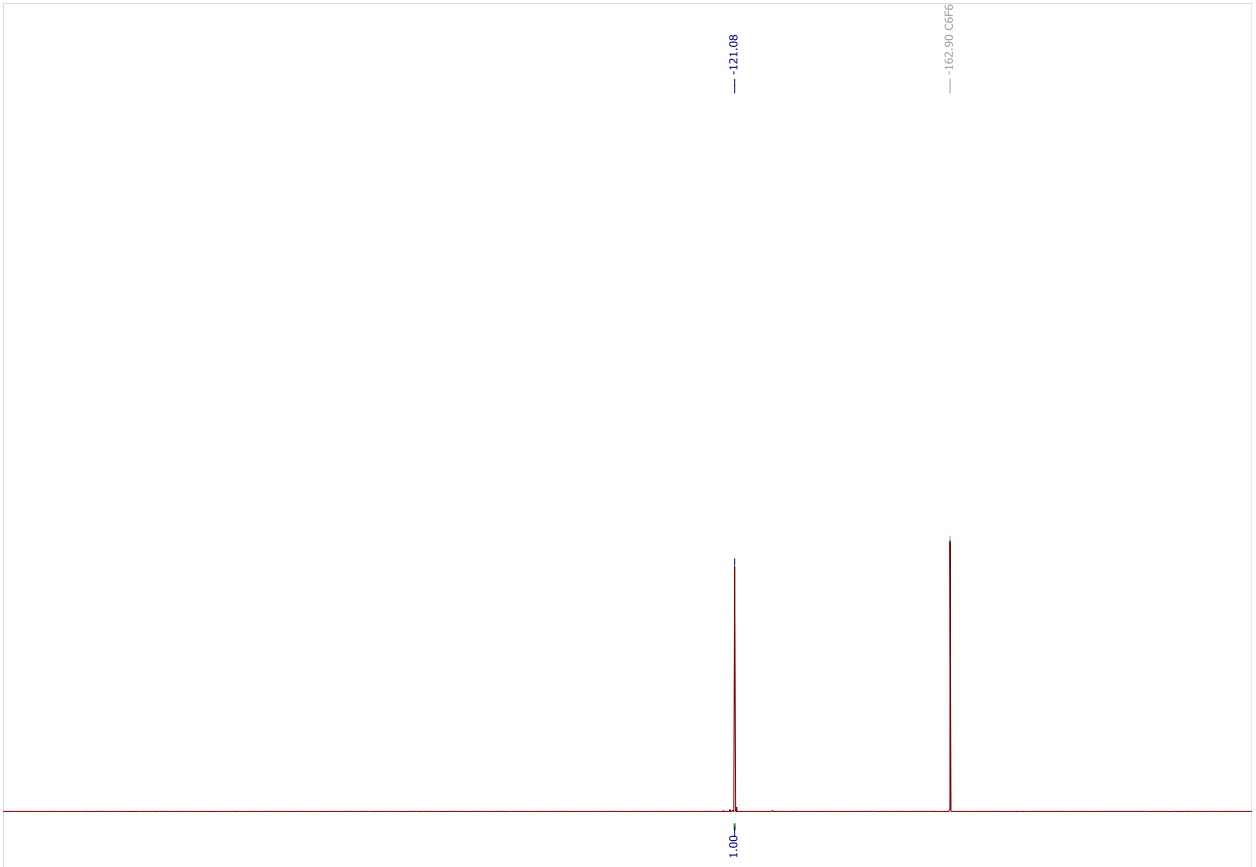

Figure S9. $^{19}F\{^{1}H\}$ NMR spectrum of **2e**. Solvent: DMSO-d_6, 282.4 MHz. Standard: C_6F_6 with respect to $CFCl_3$.

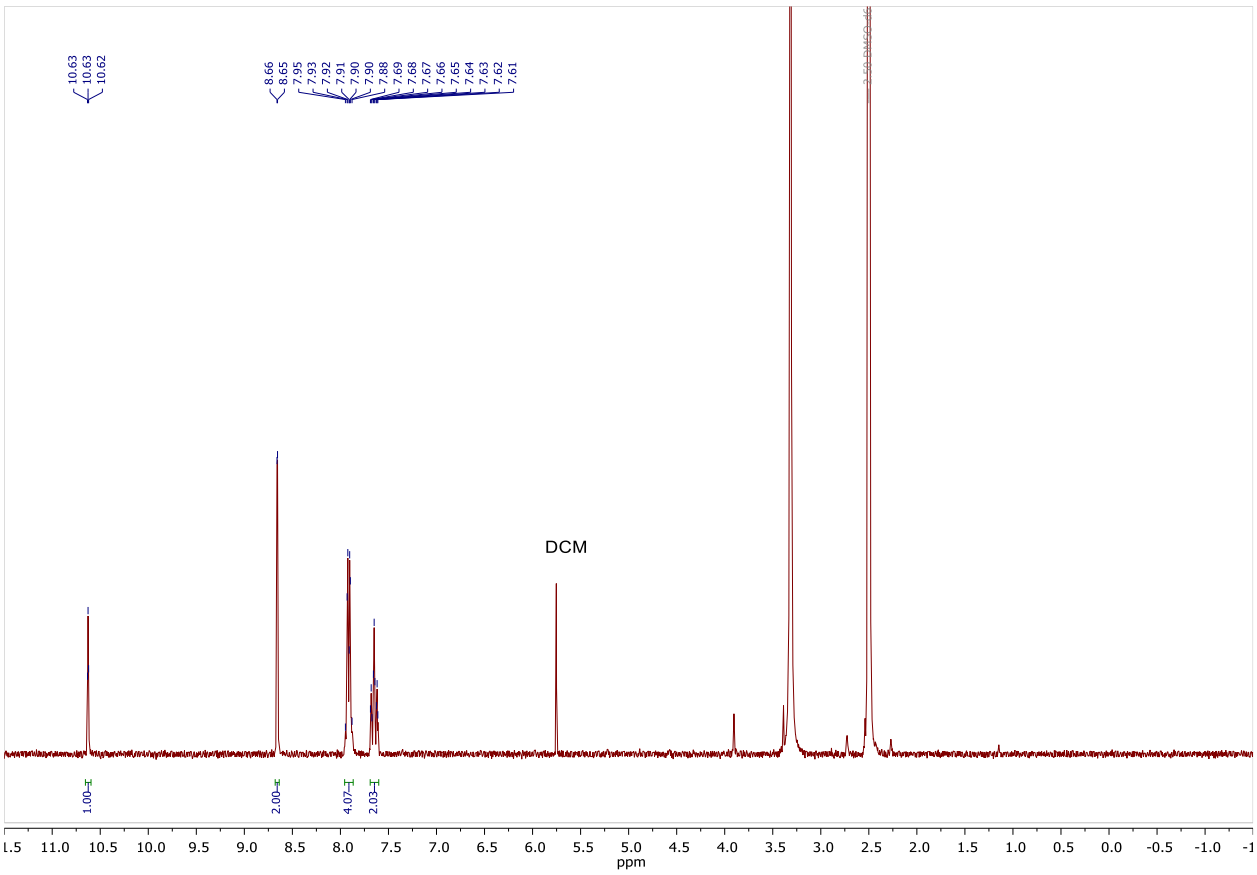

Figure S10. ^{1}H NMR spectrum of **2f**. Solvent: DMSO-d_6, 300 MHz.

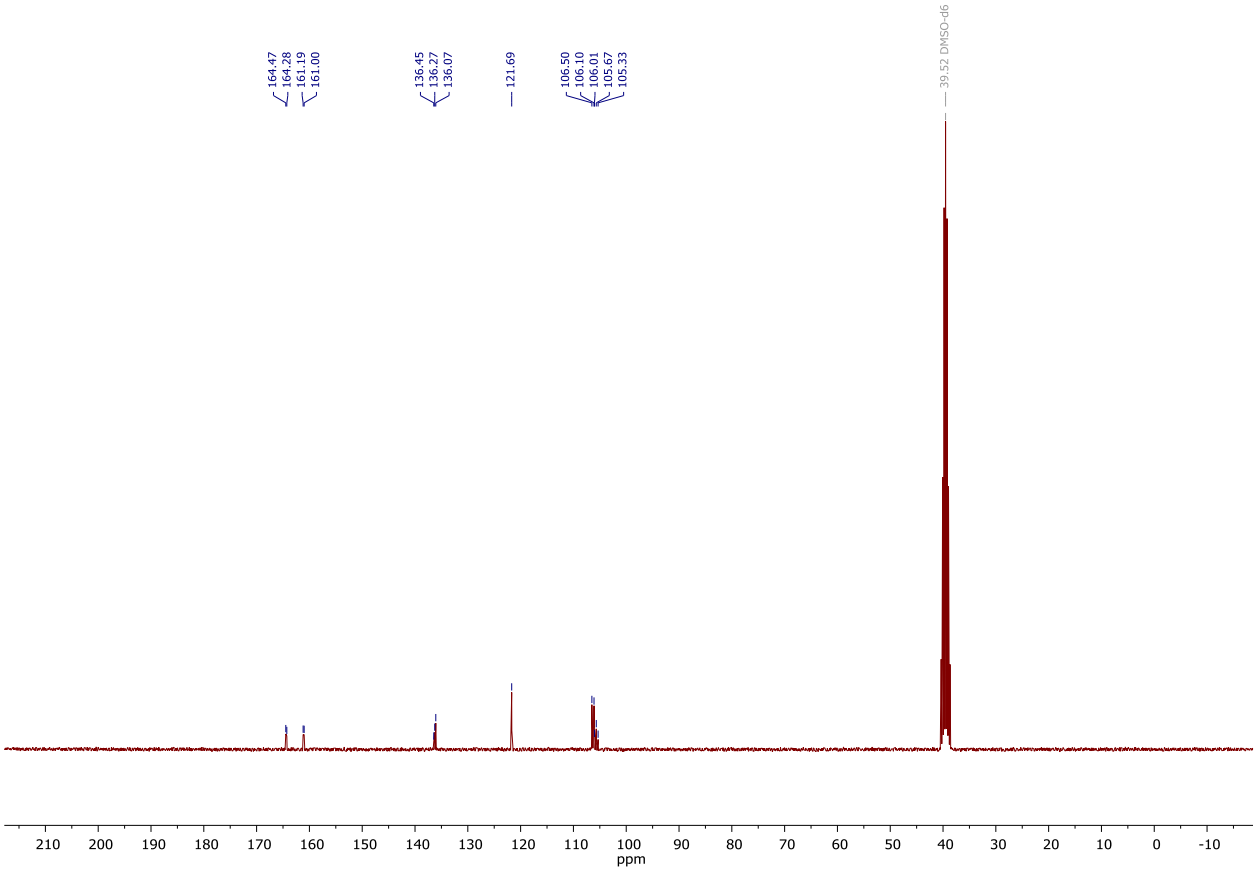

Figure S11. ^{13}C{^{1}H} NMR spectrum of **2f**. Solvent: DMSO-d_6, 75 MHz.

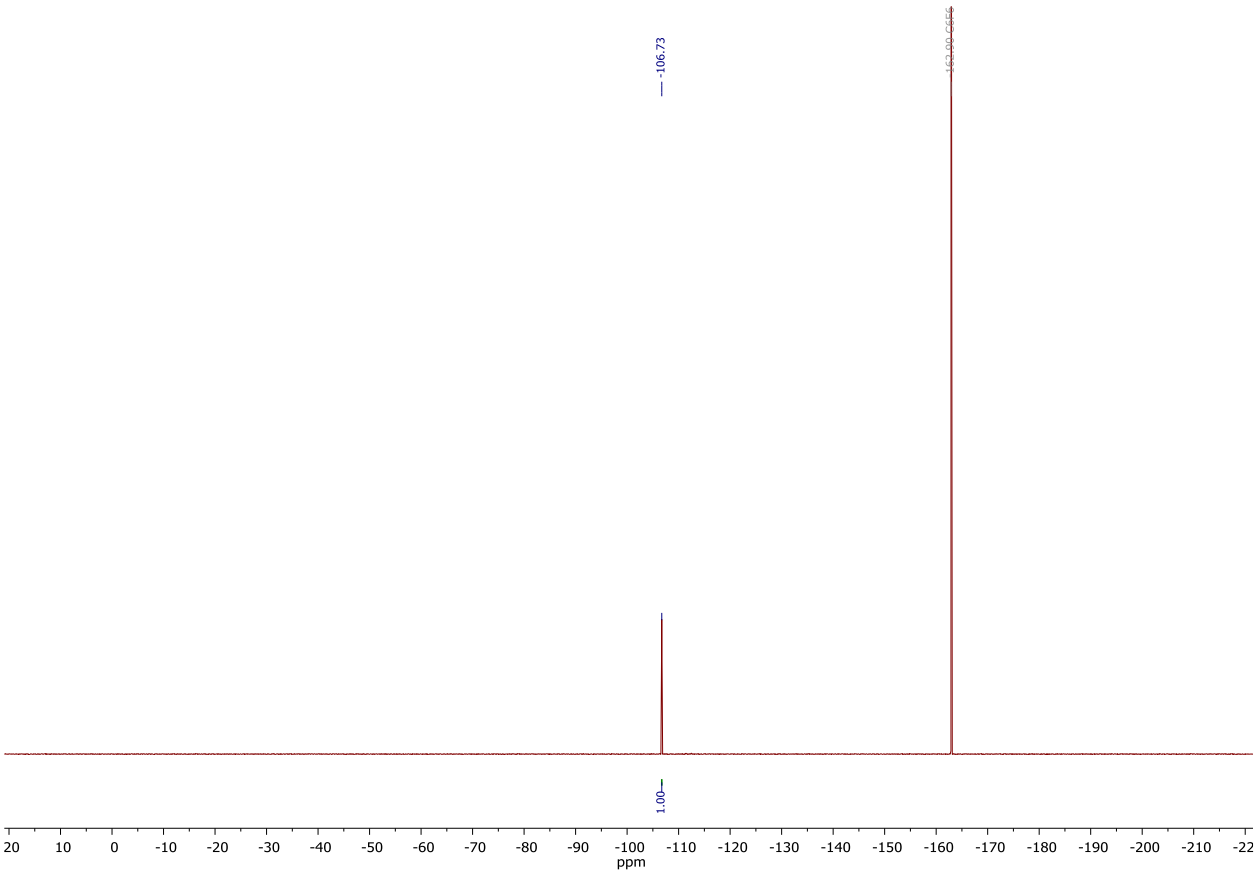

Figure S12. $^{19}F\{^{1}H\}$ NMR spectrum of **2f**. Solvent: DMSO-d_6, 282.4 MHz. Standard: C_6F_6 with respect to $CFCl_3$.

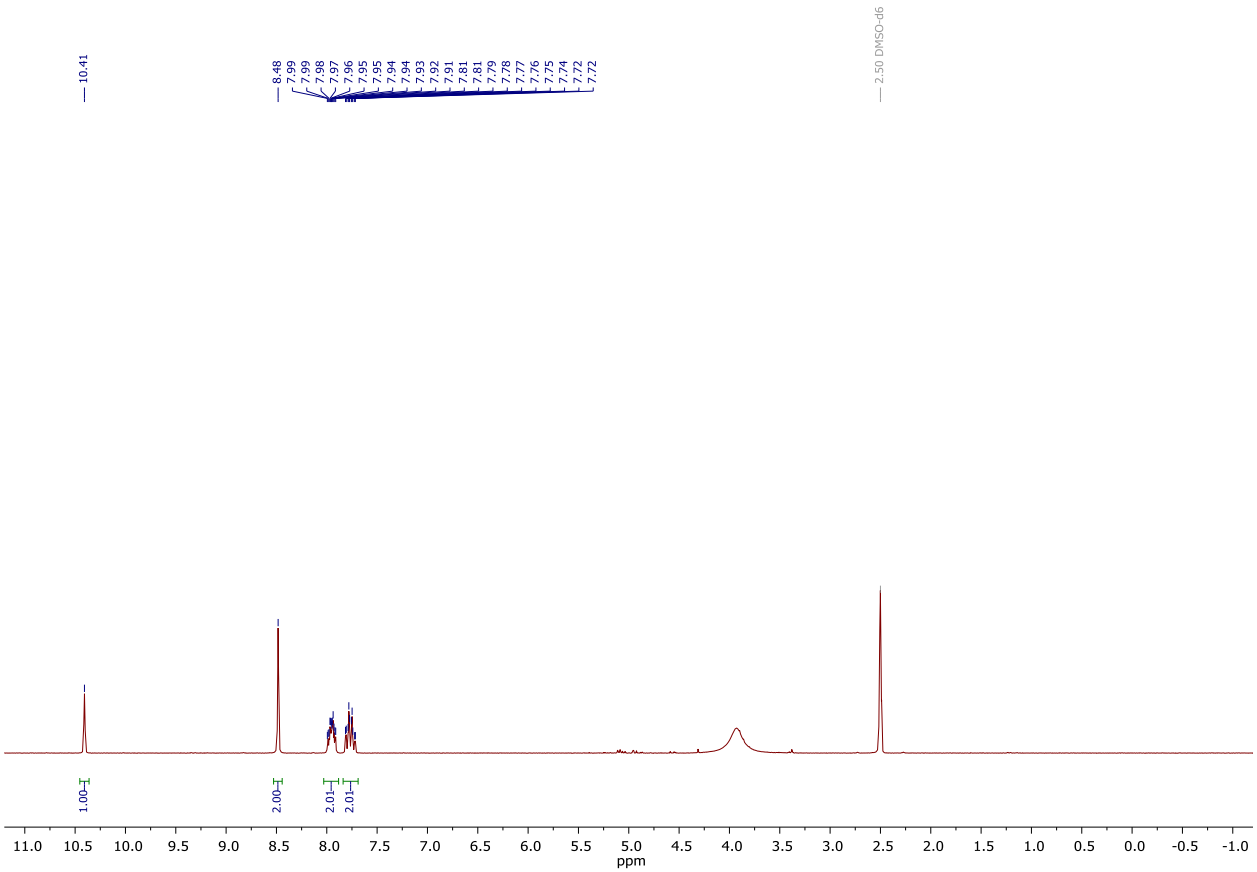

Figure S13. ^{1}H NMR spectrum of **2g**. Solvent: DMSO-d_6, 300 MHz.

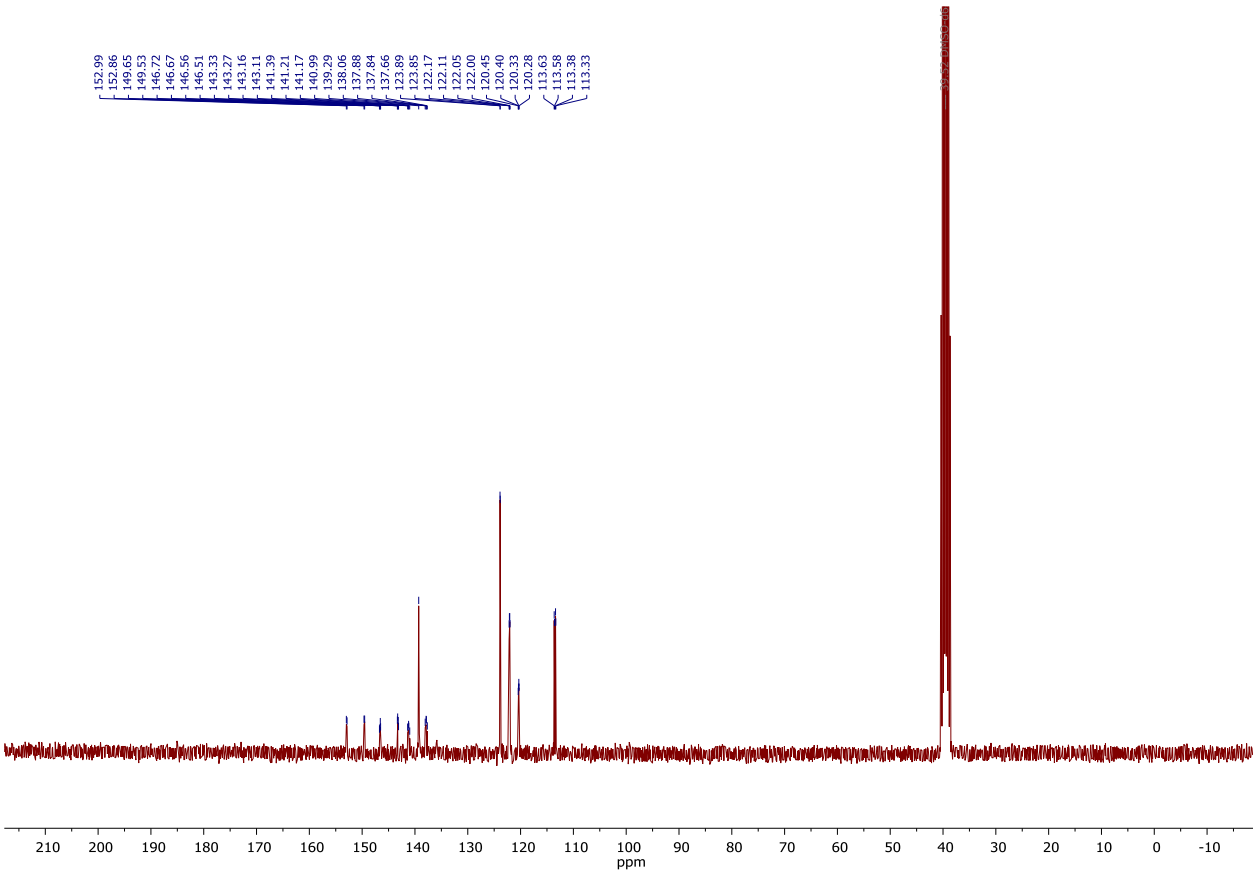

Figure S14. $^{13}C\{^{1}H\}$ NMR spectrum of **2g**. Solvent: DMSO-d_6, 75 MHz.

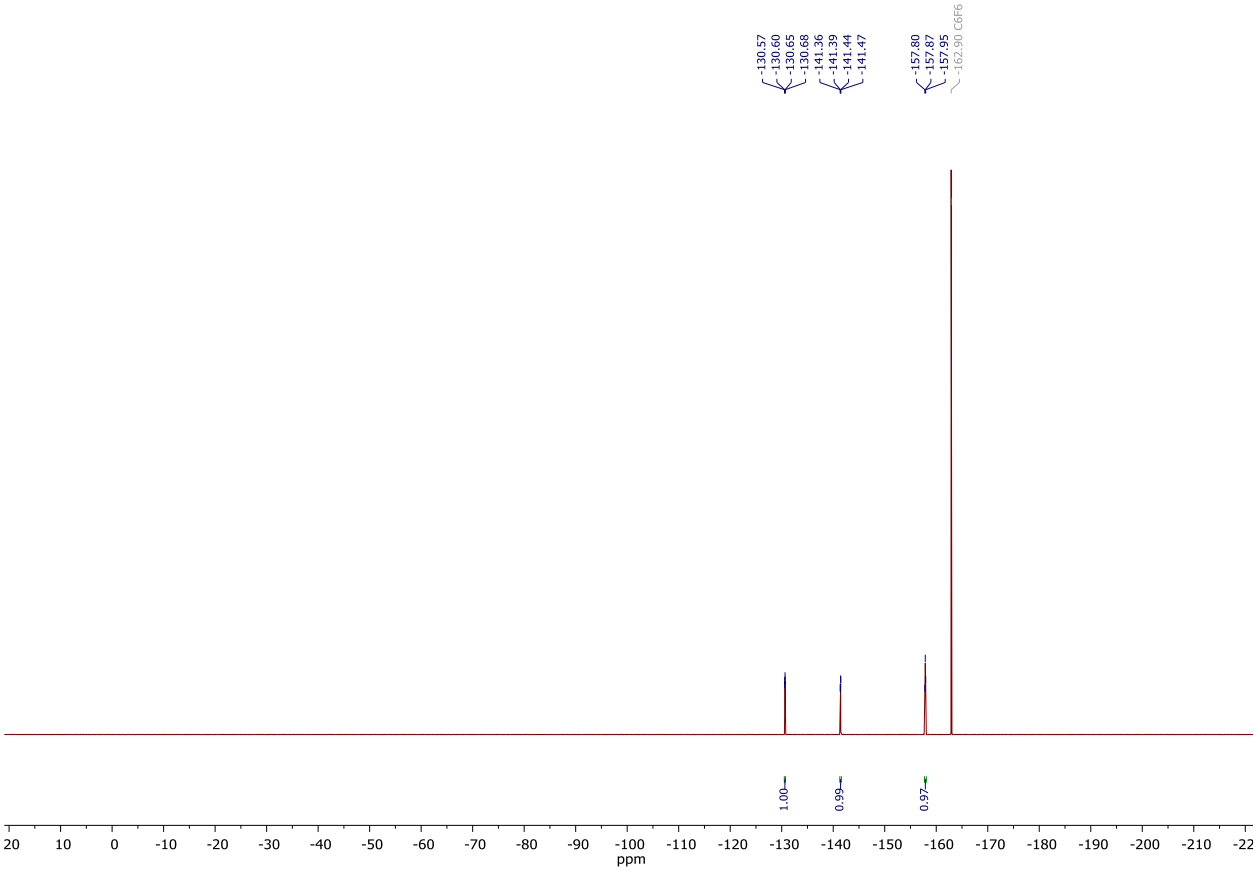

Figure S15. $^{19}F\{^{1}H\}$ NMR spectrum of **2g**. Solvent: DMSO-d_6, 282.4 MHz. Standard: C_6F_6 with respect to $CFCl_3$.

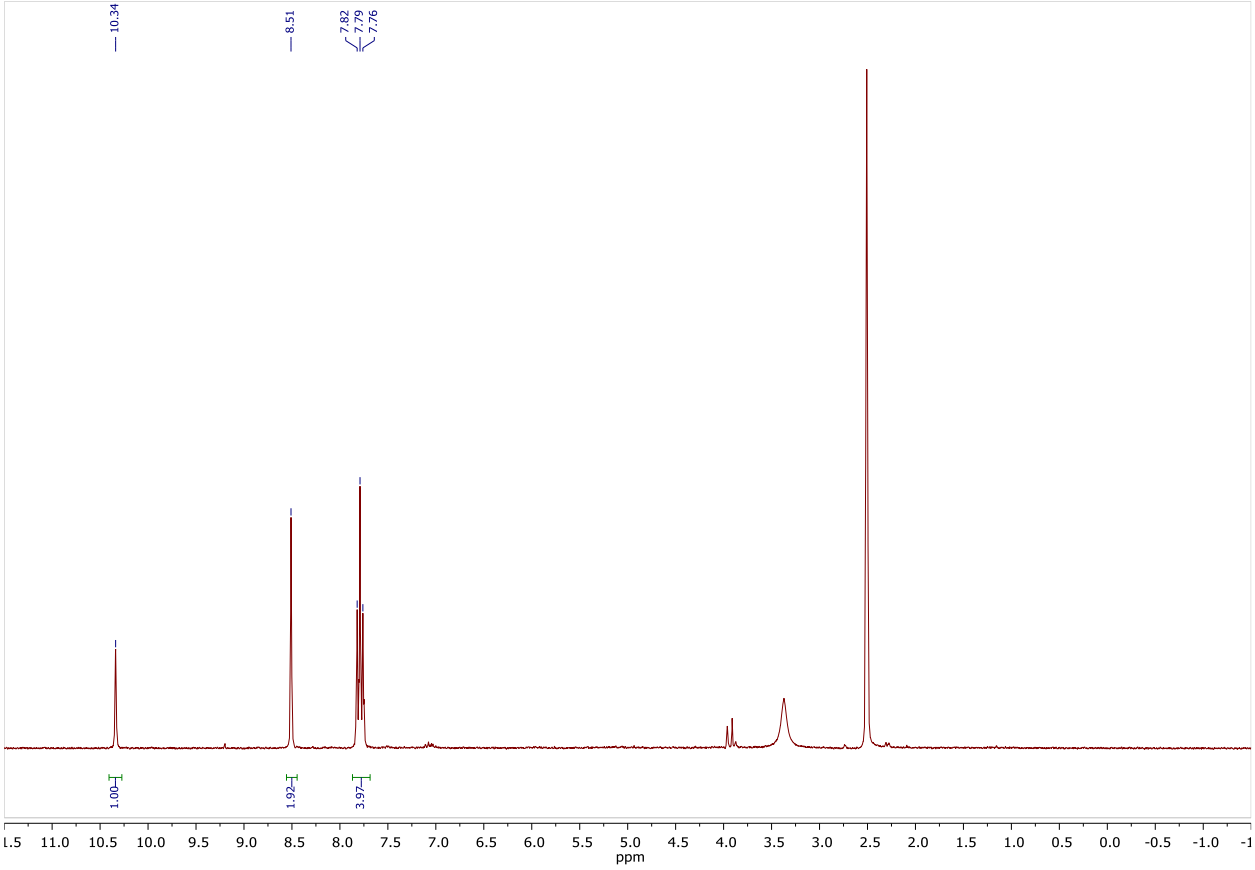

Figure S16. ^{1}H NMR spectrum of **2j**. Solvent: DMSO-d_6, 300 MHz.

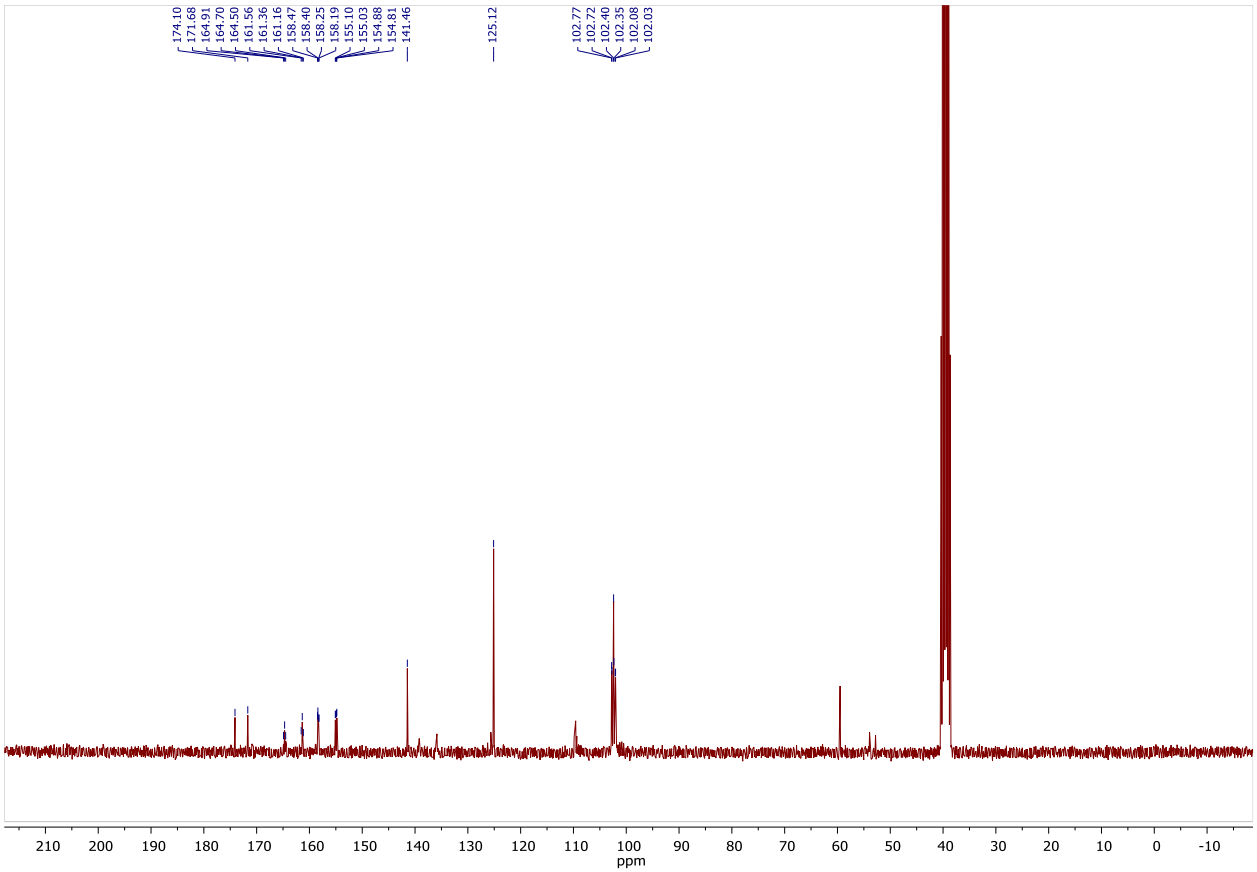

Figure S17. ^{13}C{^{1}H} NMR spectrum of **2j**. Solvent: DMSO-d_6, 75 MHz.

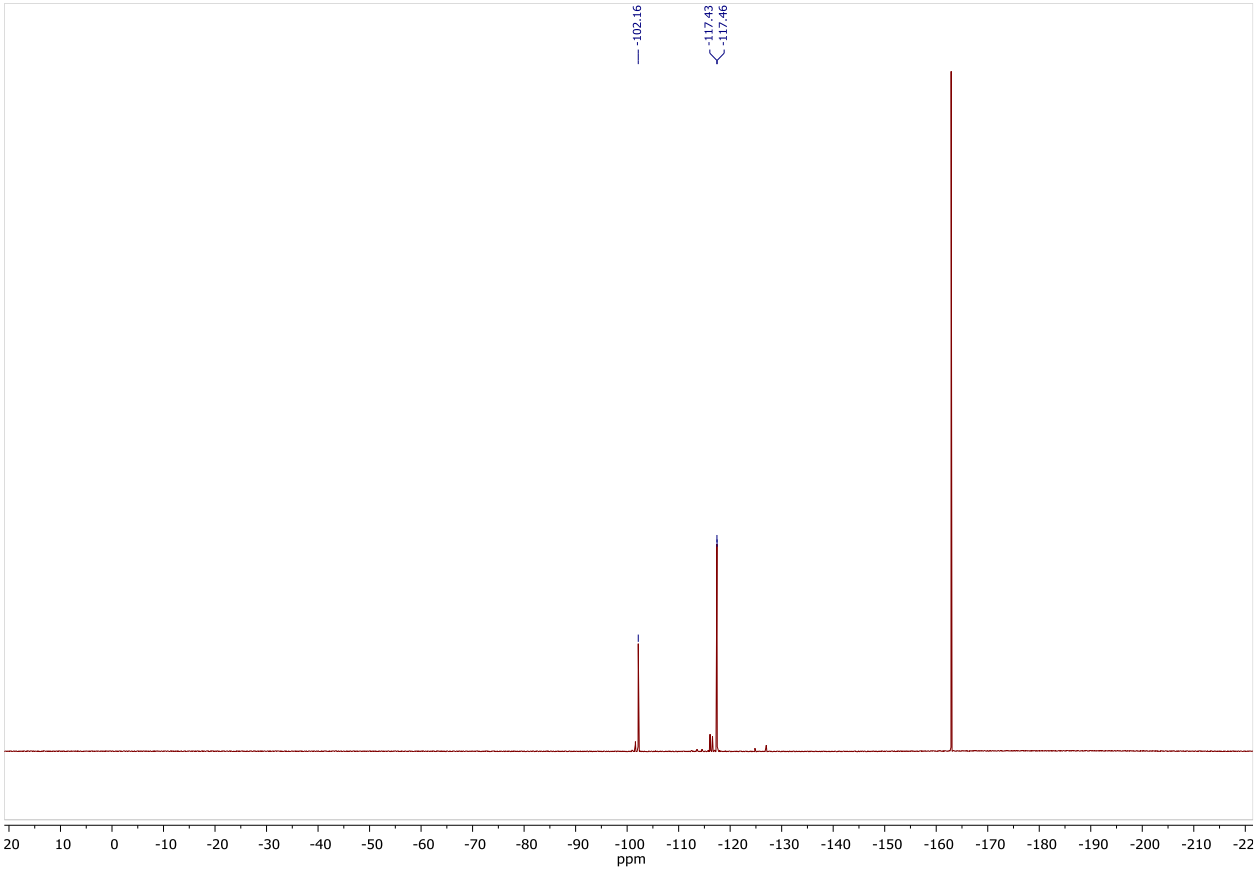

Figure S18. $^{19}F\{^{1}H\}$ NMR spectrum of **2j**. Solvent: DMSO-d_6, 282.4 MHz. Standard: C_6F_6 with respect to $CFCl_3$.

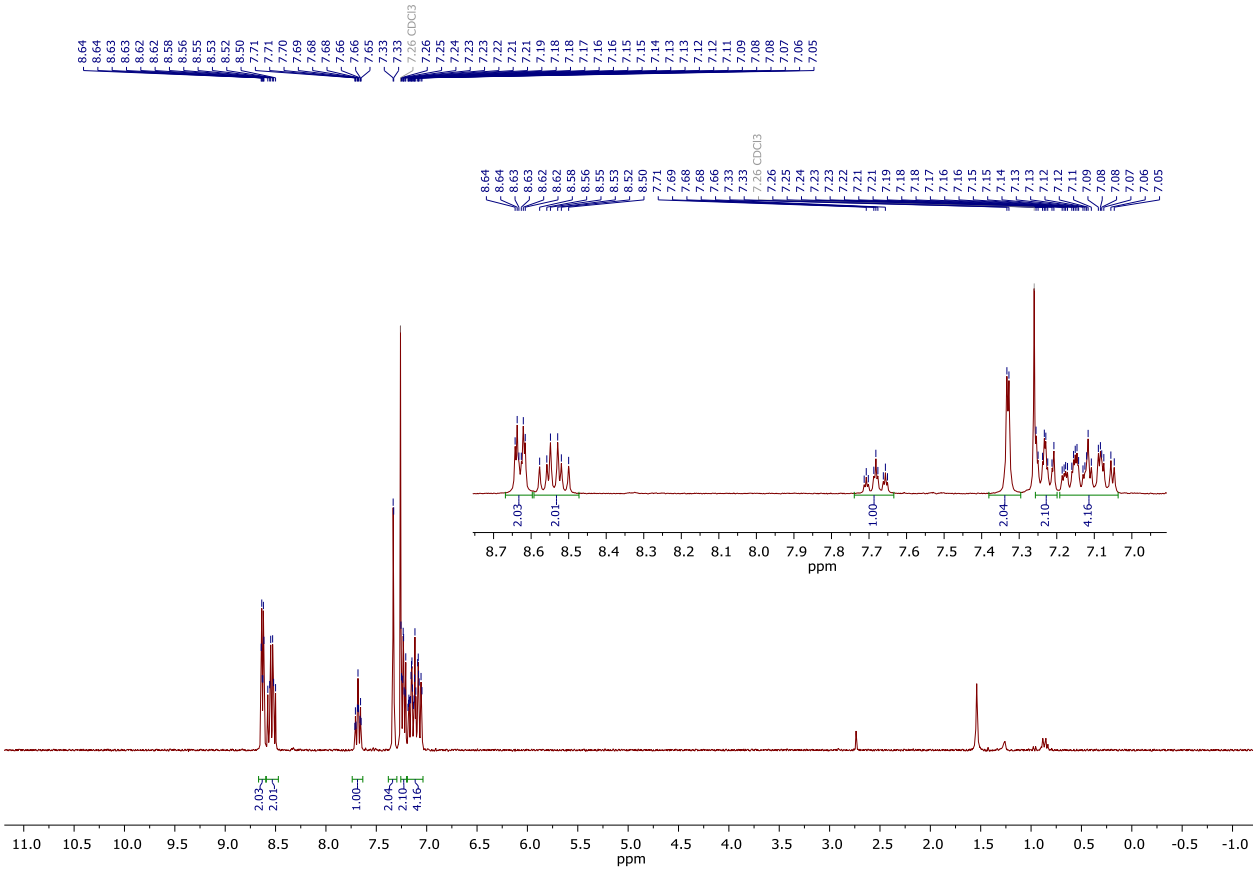

Figure S19. ^{1}H NMR spectrum of **3c**. Solvent: $CDCl_3$, 300 MHz.

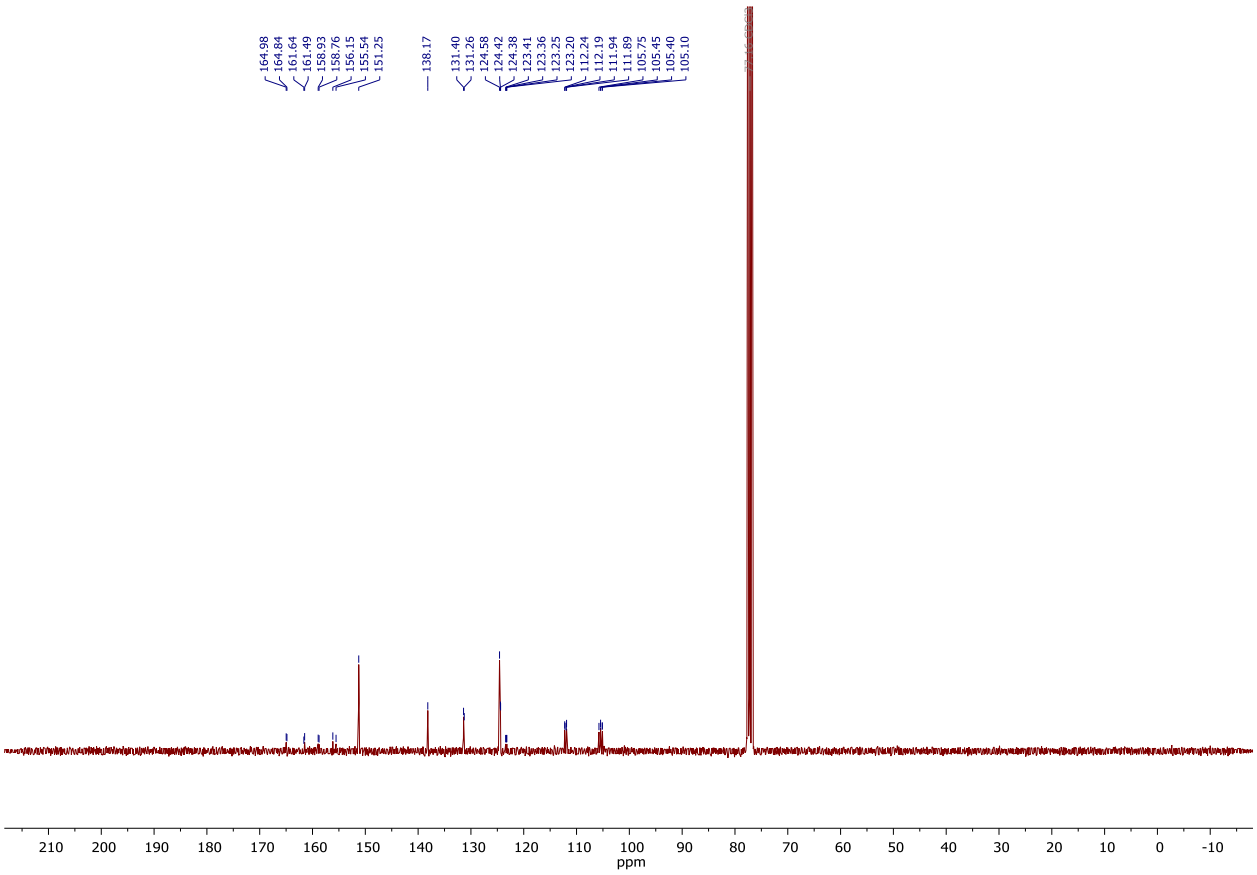

Figure S20. $^{13}C\{^{1}H\}$ NMR spectrum of **3c**. Solvent: $CDCl_3$, 75 MHz.

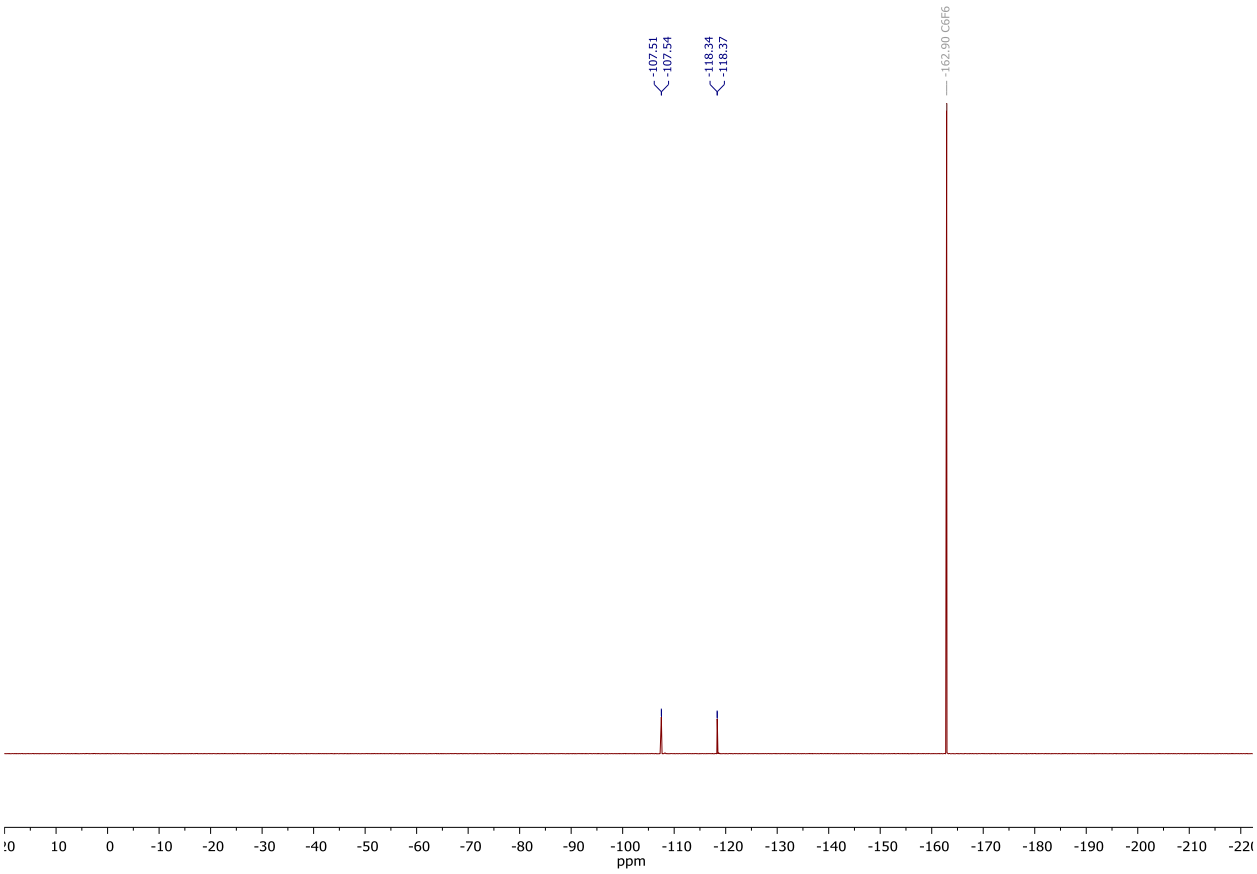

Figure S21. $^{19}F\{^{1}H\}$ NMR spectrum of **3c**. Solvent: $CDCl_3$, 282.4 MHz. Standard: C_6F_6 with respect to $CFCl_3$.

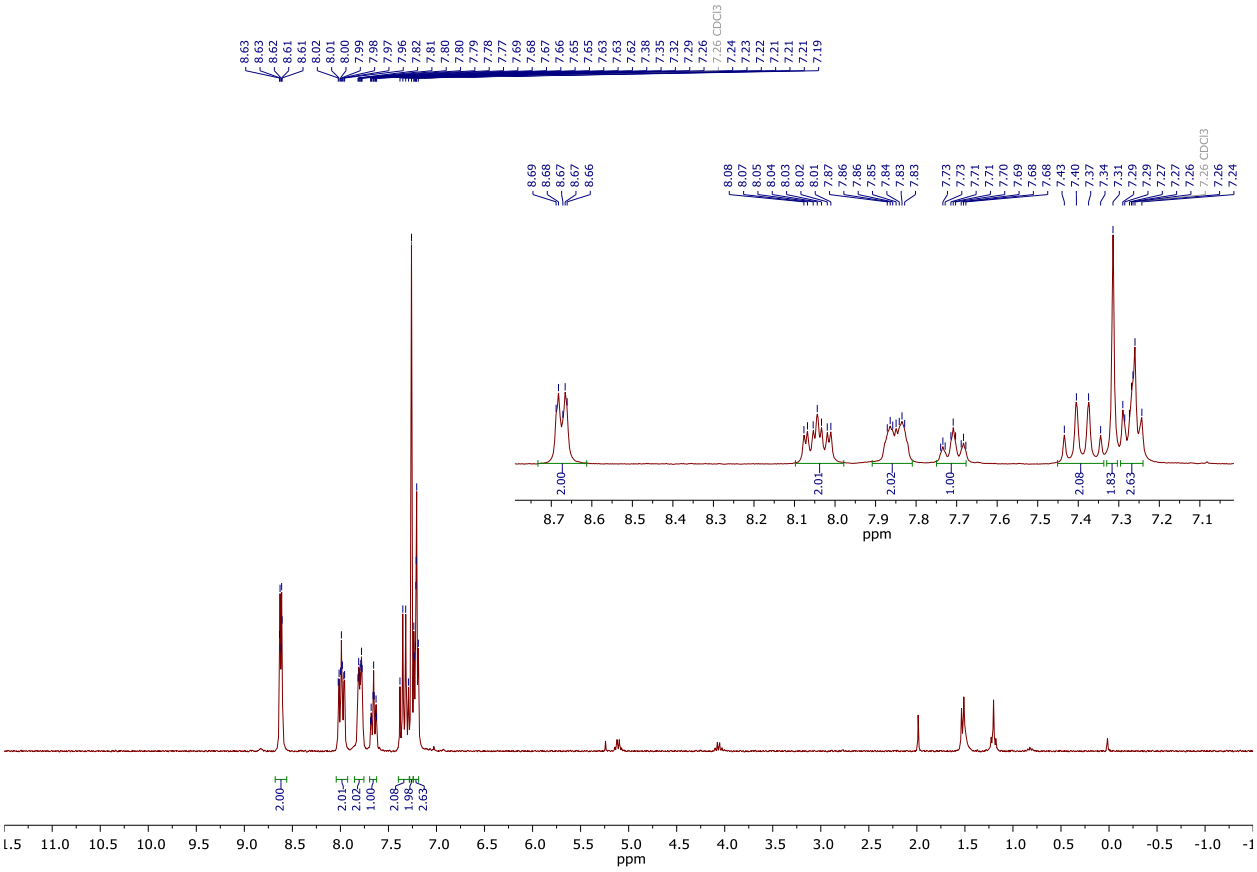

Figure S22. ^{1}H NMR spectrum of **3d**. Solvent: $CDCl_3$, 300 MHz.

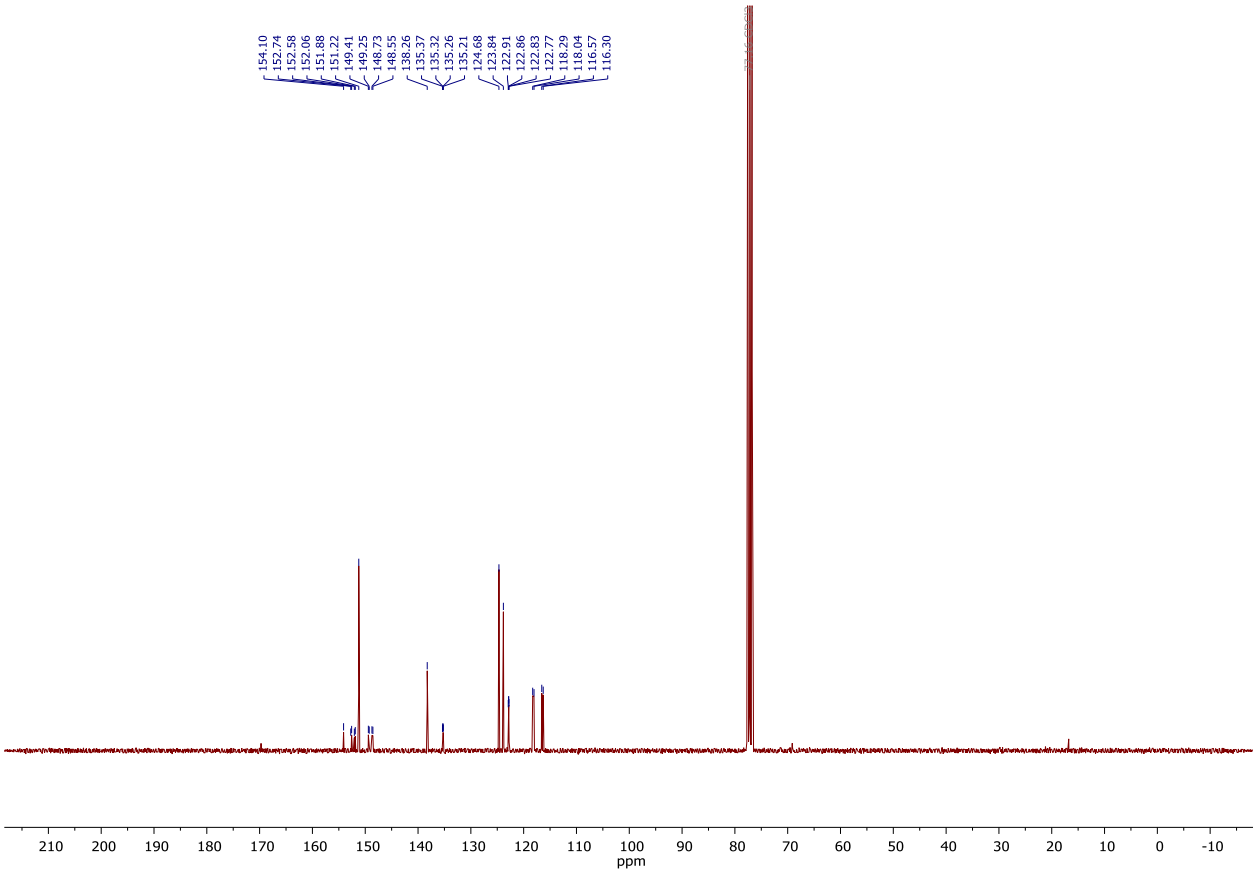

Figure S23. $^{13}C\{^{1}H\}$ NMR spectrum of **3d**. Solvent: $CDCl_3$, 75 MHz.

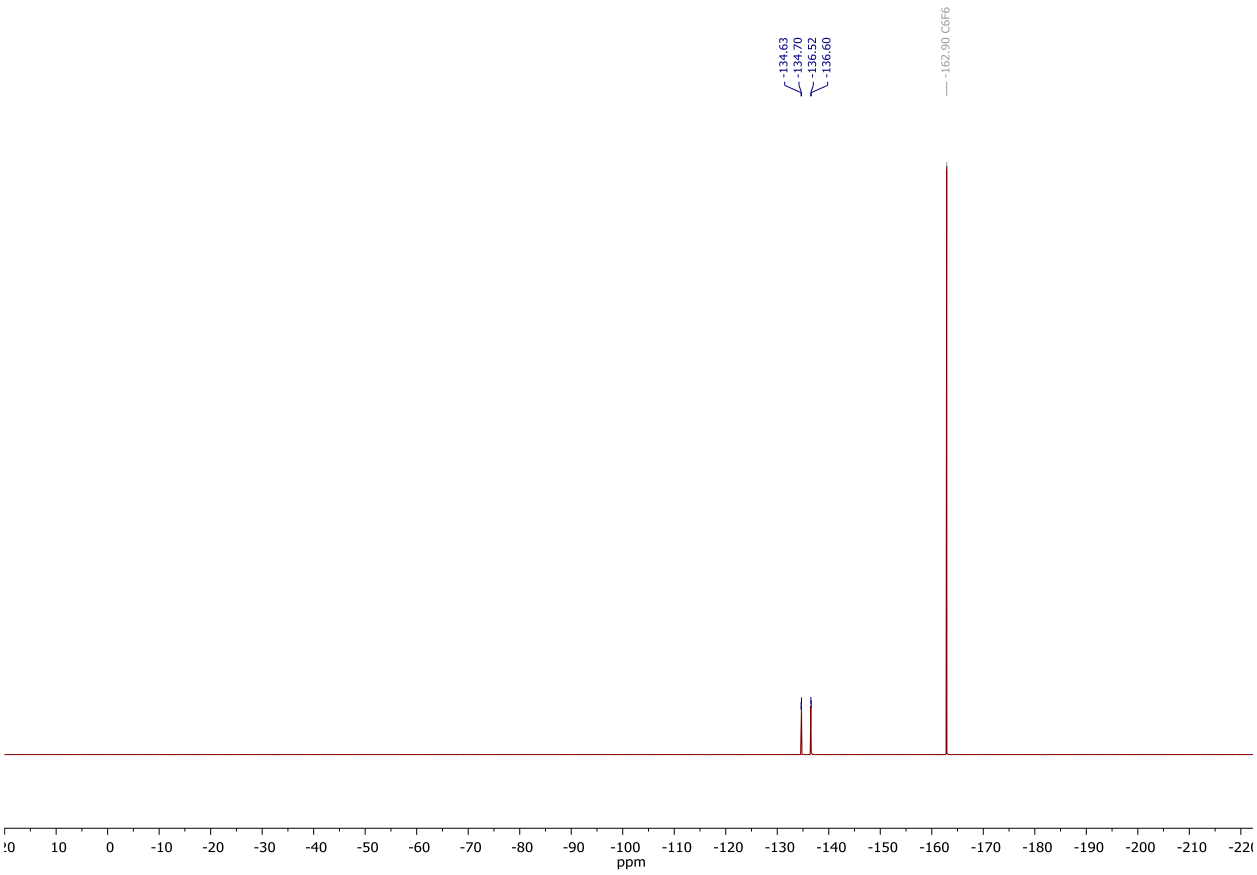

Figure S24. $^{19}F\{^{1}H\}$ NMR spectrum of **3d**. Solvent: $CDCl_3$, 282.4 MHz. Standard: C_6F_6 with respect to $CFCl_3$.

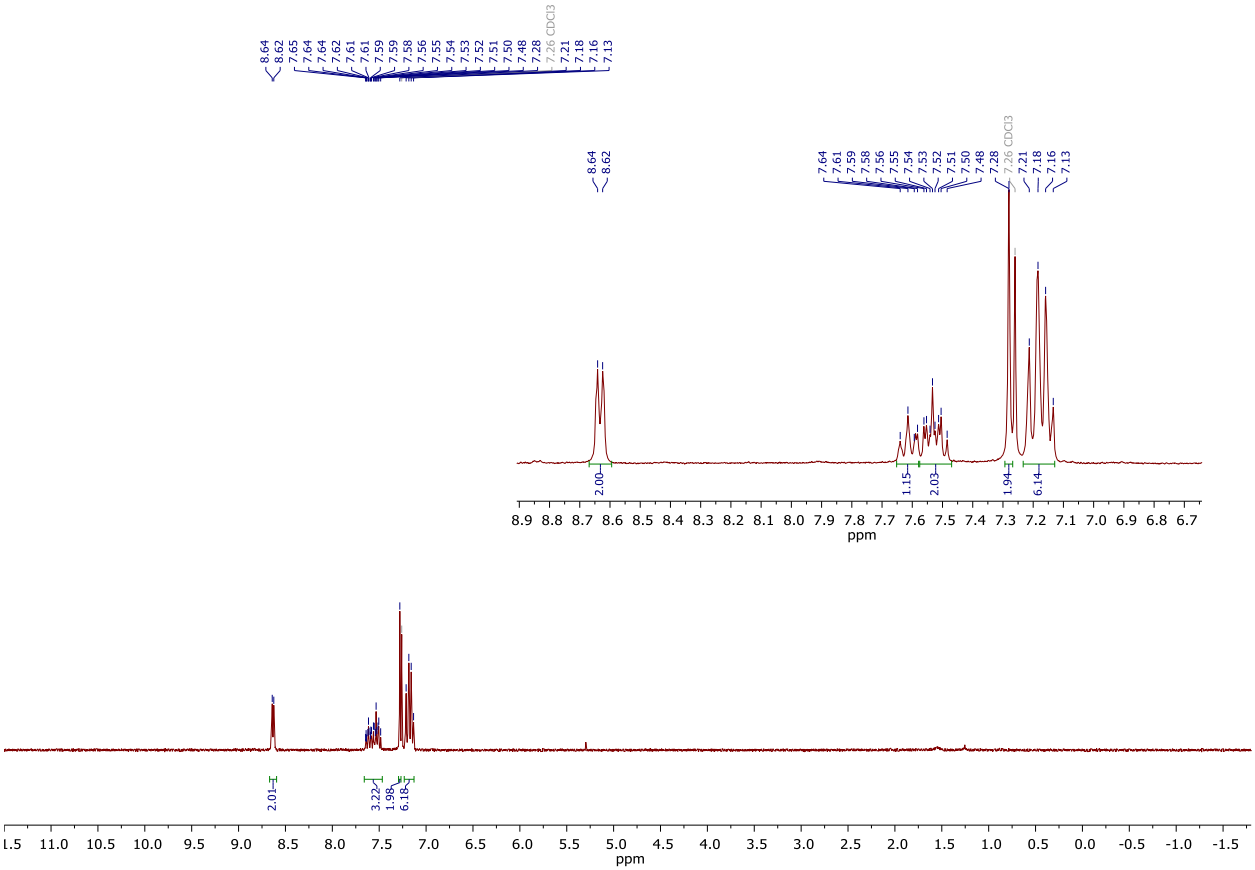

Figure S25. ^{1}H NMR spectrum of **3e**. Solvent: $CDCl_3$, 300 MHz.

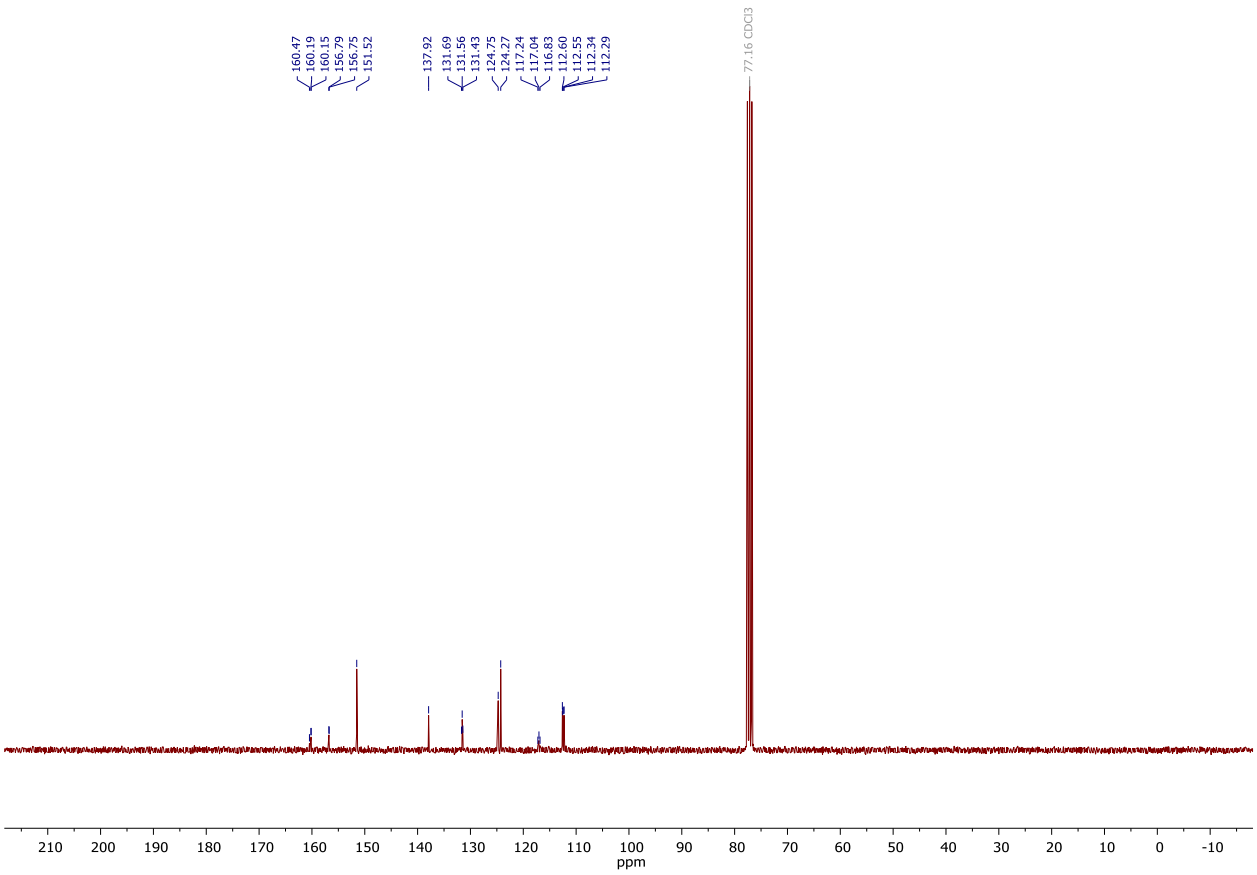

Figure S26. $^{13}C\{^{1}H\}$ NMR spectrum of **3e**. Solvent: $CDCl_3$, 75 MHz.

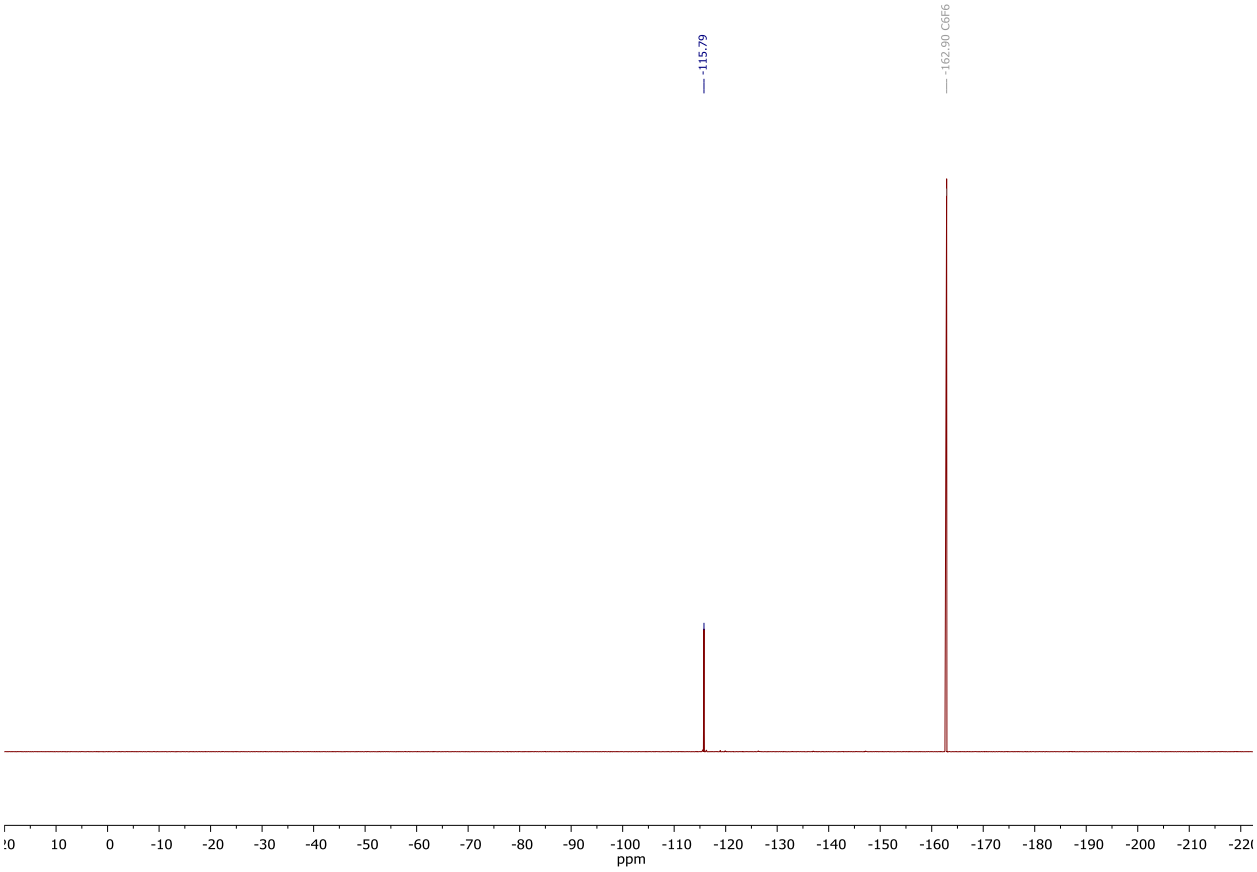

Figure S27. $^{19}F\{^{1}H\}$ NMR spectrum of **3e**. Solvent: $CDCl_3$, 282.4 MHz. Standard: C_6F_6 with respect to $CFCl_3$.

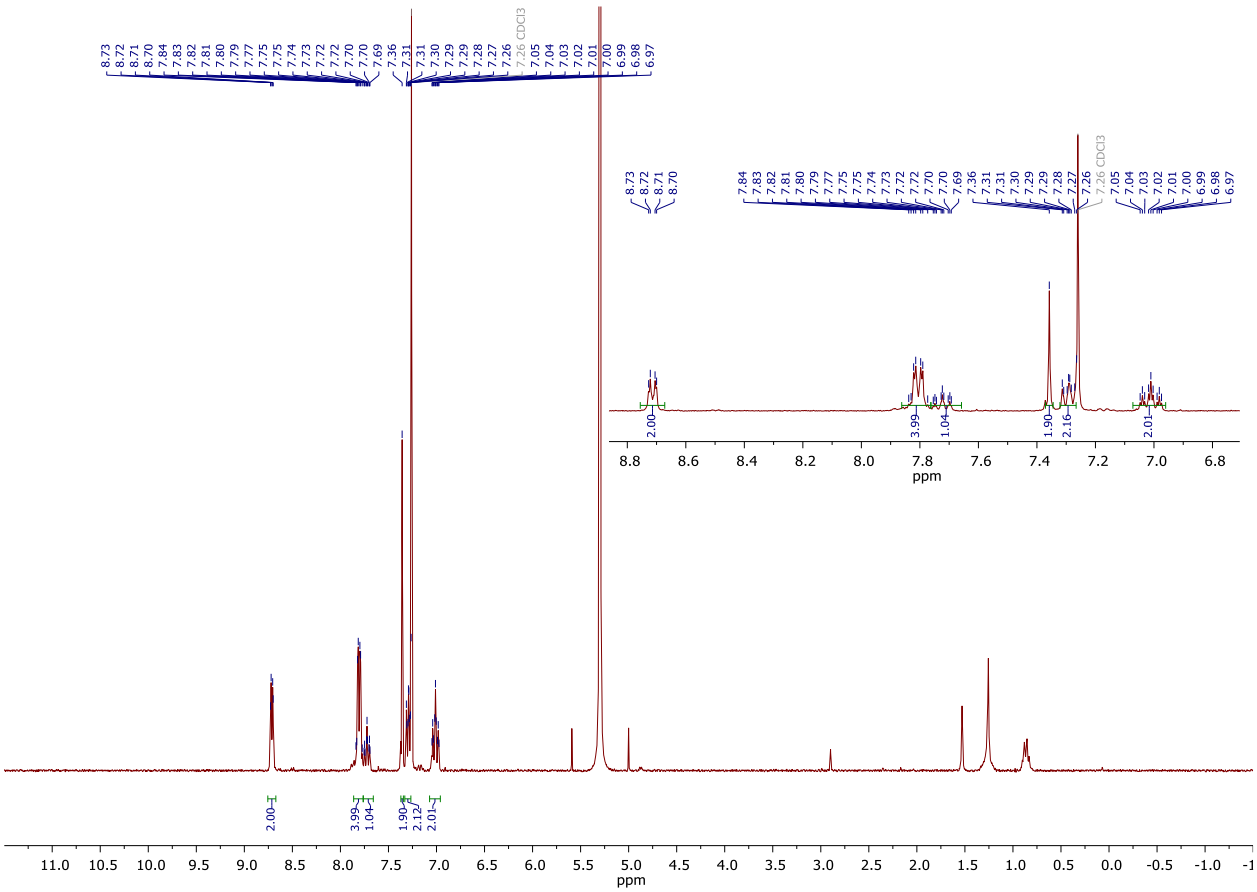

Figure S28. ^{1}H NMR spectrum of **3f**. Solvent: $CDCl_3$, 300 MHz.

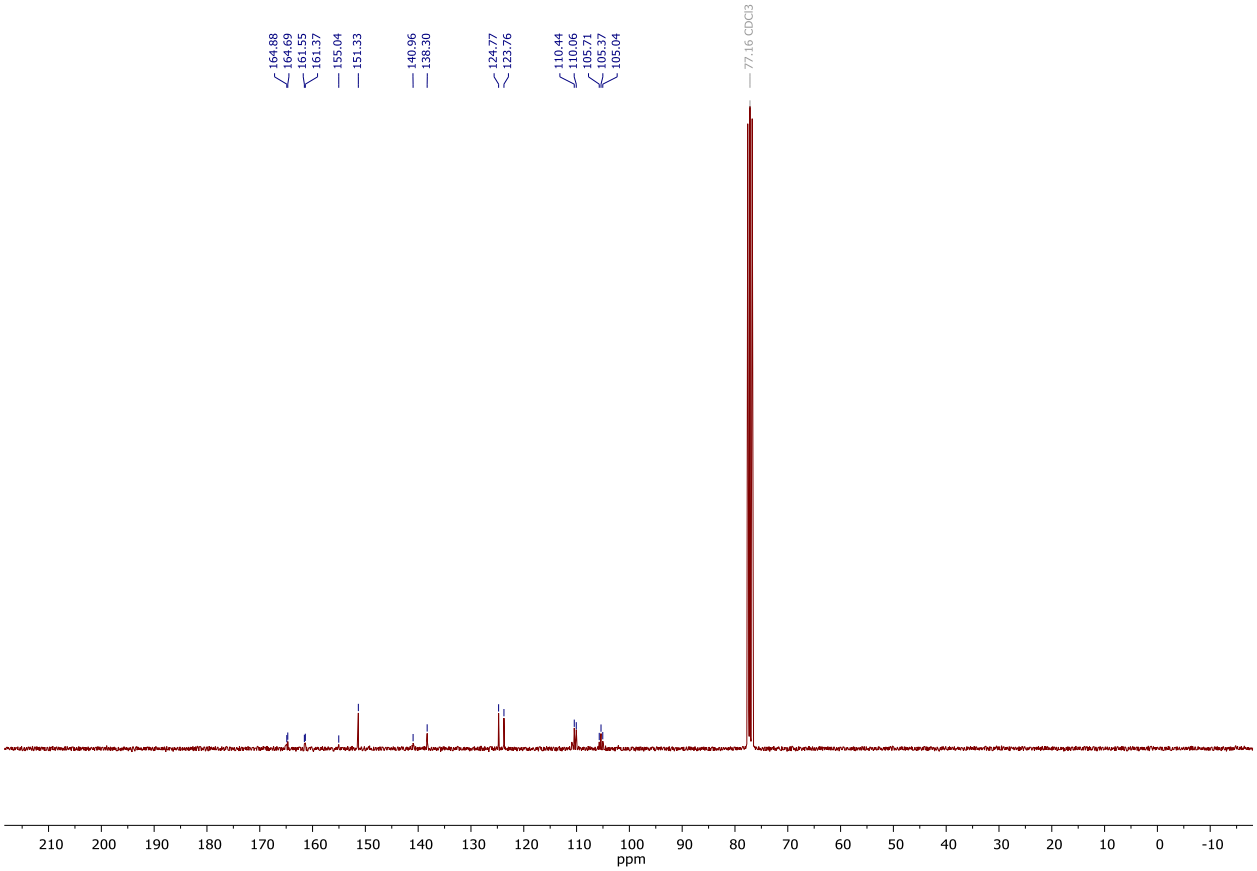

Figure S29. $^{13}C\{^{1}H\}$ NMR spectrum of **3f**. Solvent: $CDCl_3$, 75 MHz.

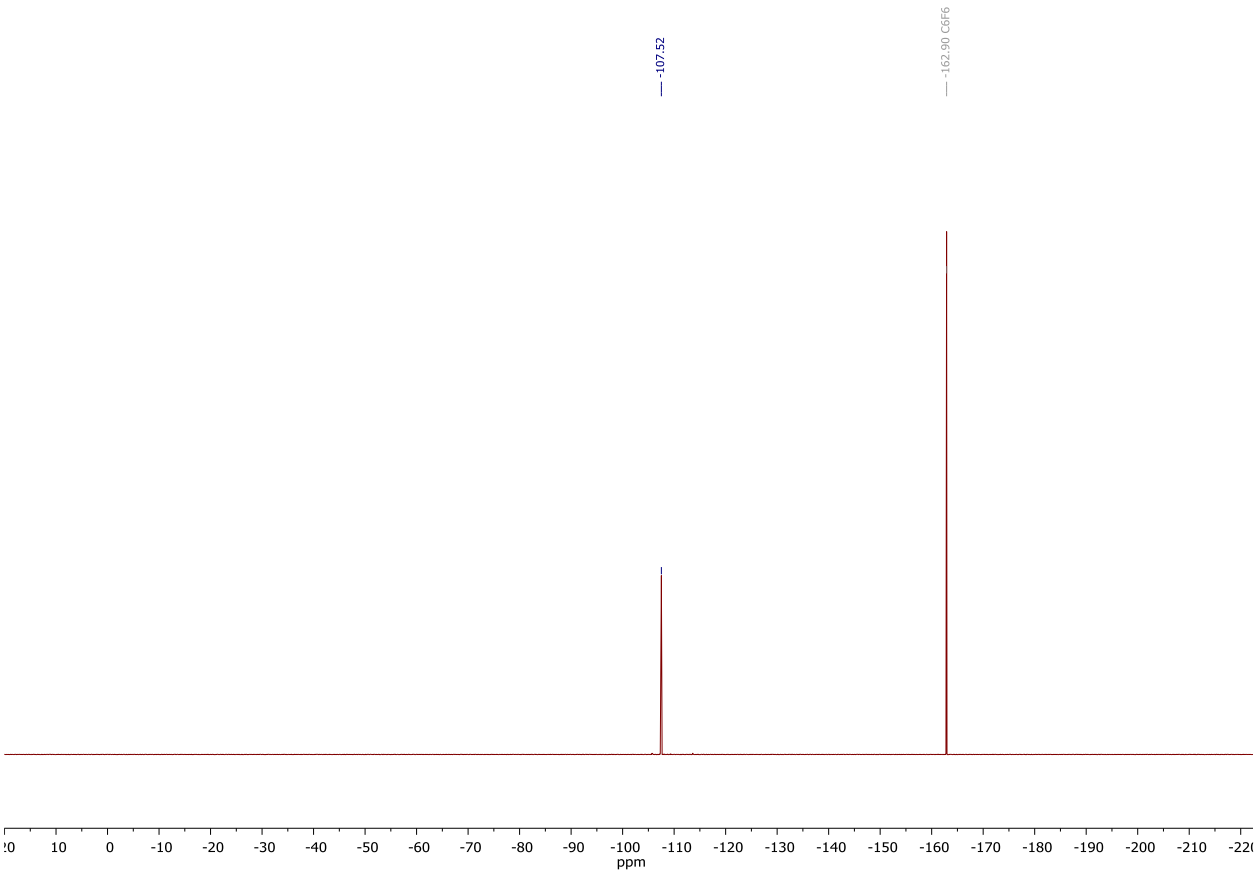

Figure S30. $^{19}F\{^{1}H\}$ NMR spectrum of **3f**. Solvent: $CDCl_3$, 282.4 MHz. Standard: C_6F_6 with respect to $CFCl_3$.

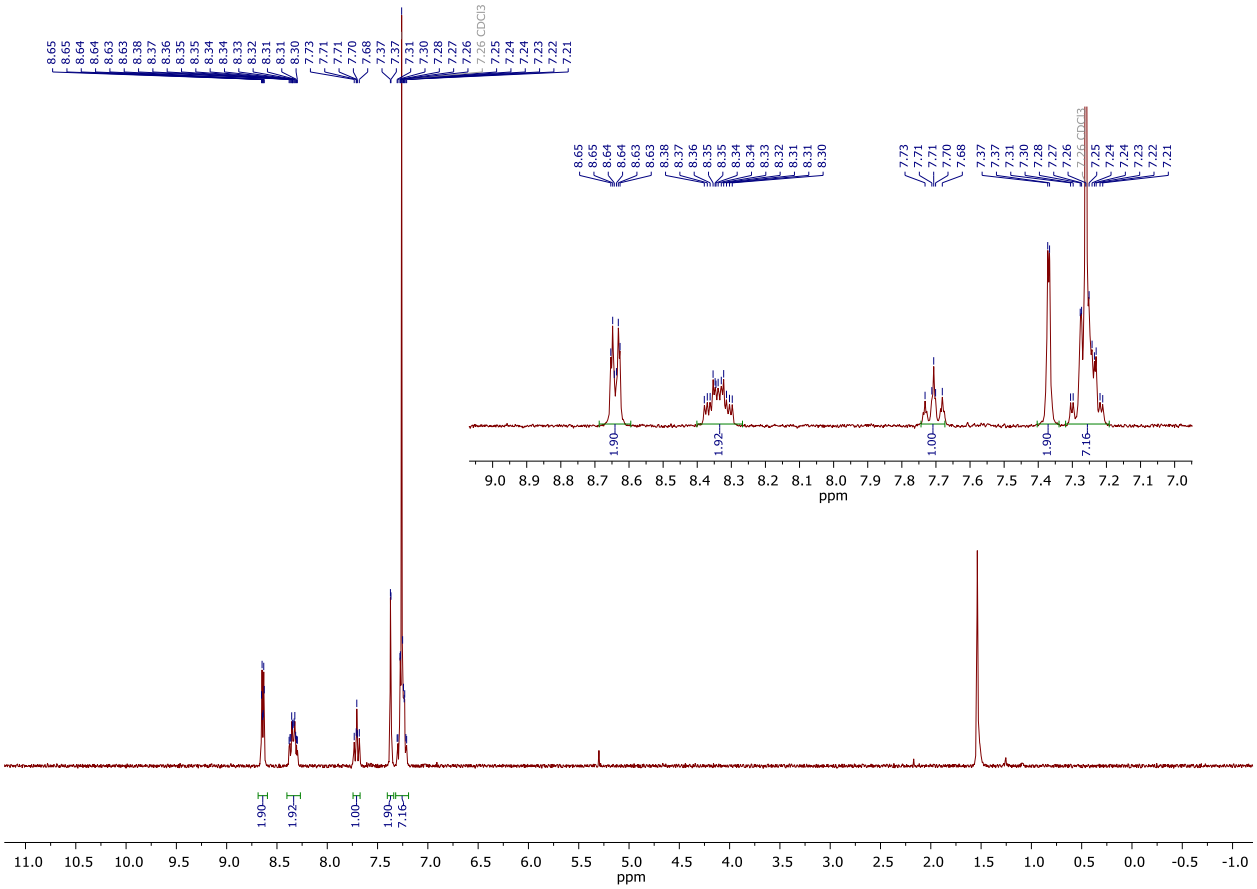

Figure S31. ^{1}H NMR spectrum of **3g**. Solvent: $CDCl_3$, 300 MHz.

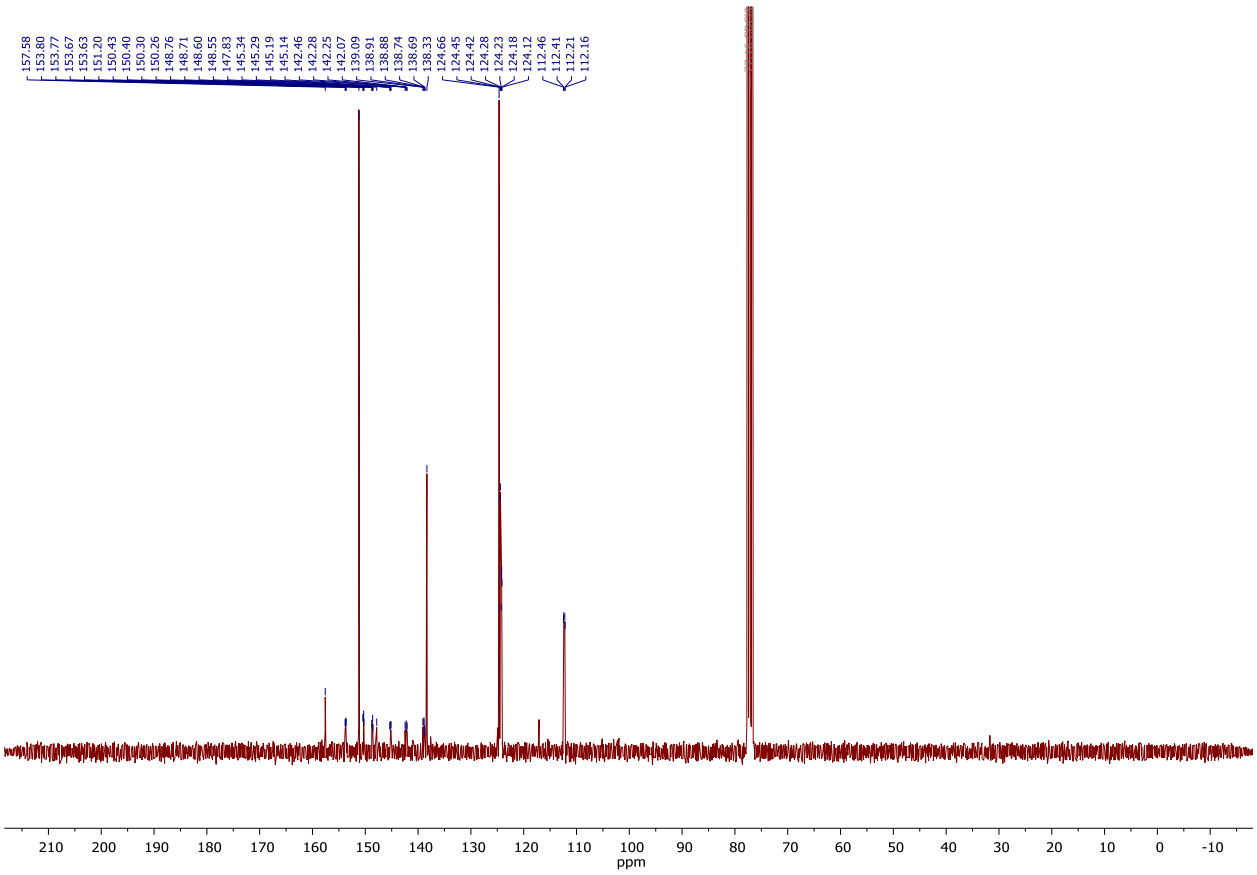

Figure S32. $^{13}C\{^{1}H\}$ NMR spectrum of **3g**. Solvent: $CDCl_3$, 75 MHz.

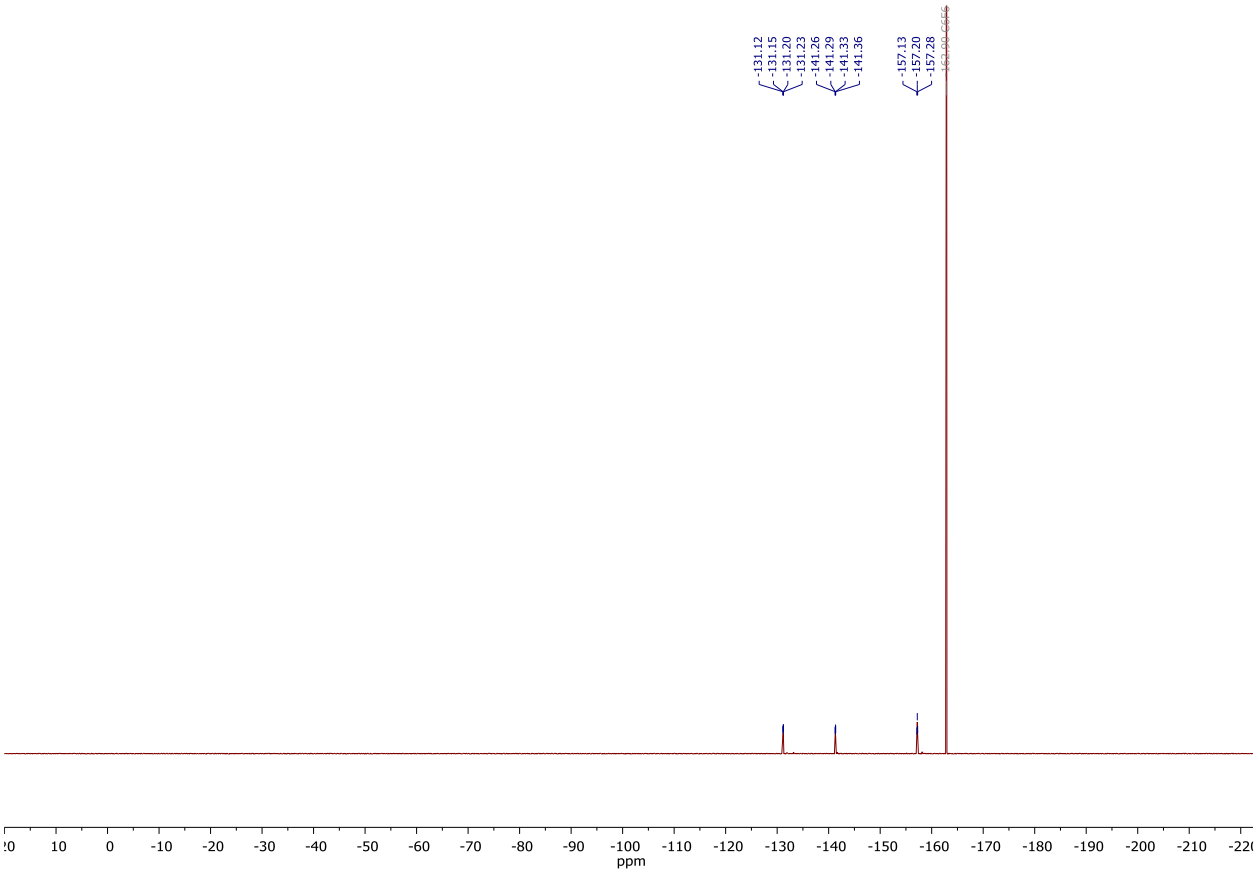

Figure S33. $^{19}F\{^{1}H\}$ NMR spectrum of **3g**. Solvent: $CDCl_3$, 282.4 MHz. Standard: C_6F_6 with respect to $CFCl_3$.

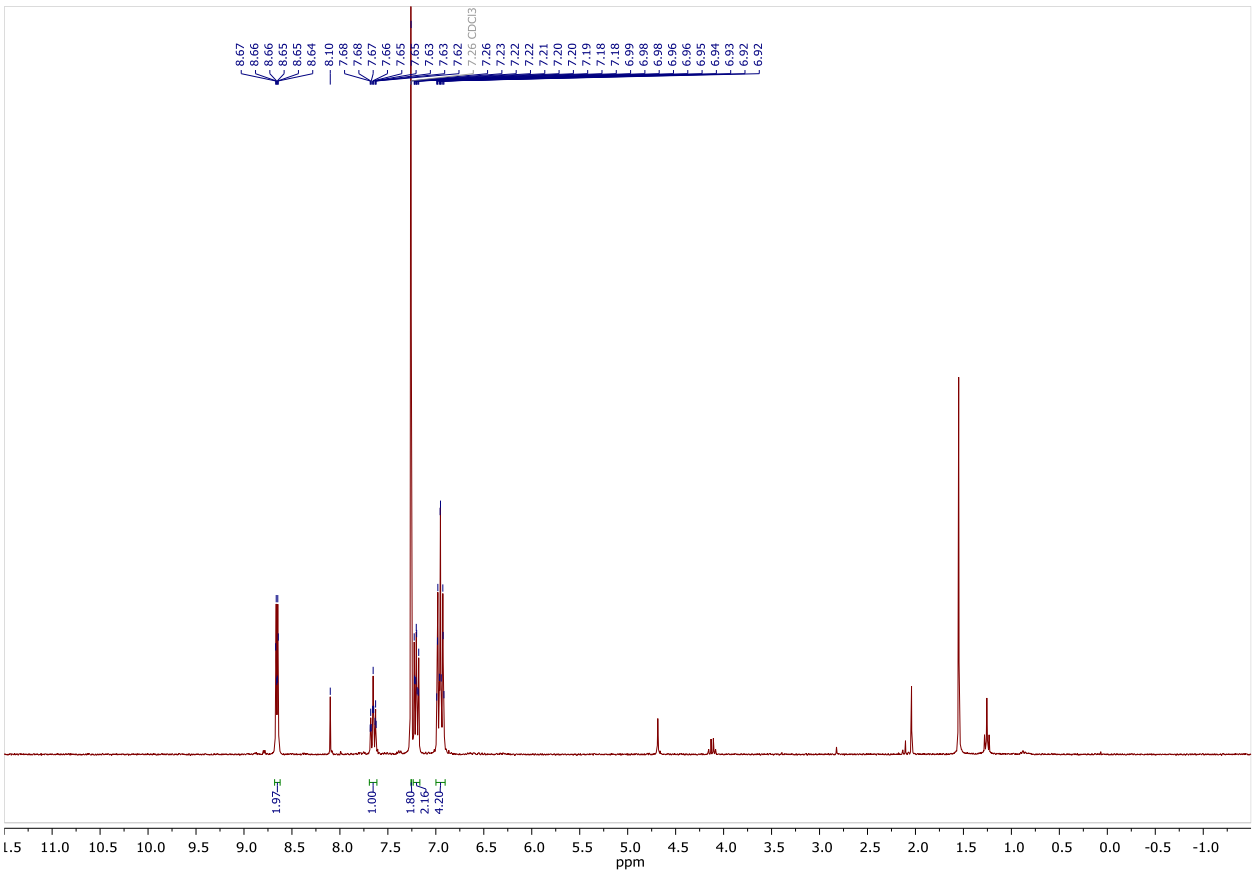

Figure S34. ^{1}H NMR spectrum of **3ja**. Solvent: $CDCl_3$, 300 MHz.

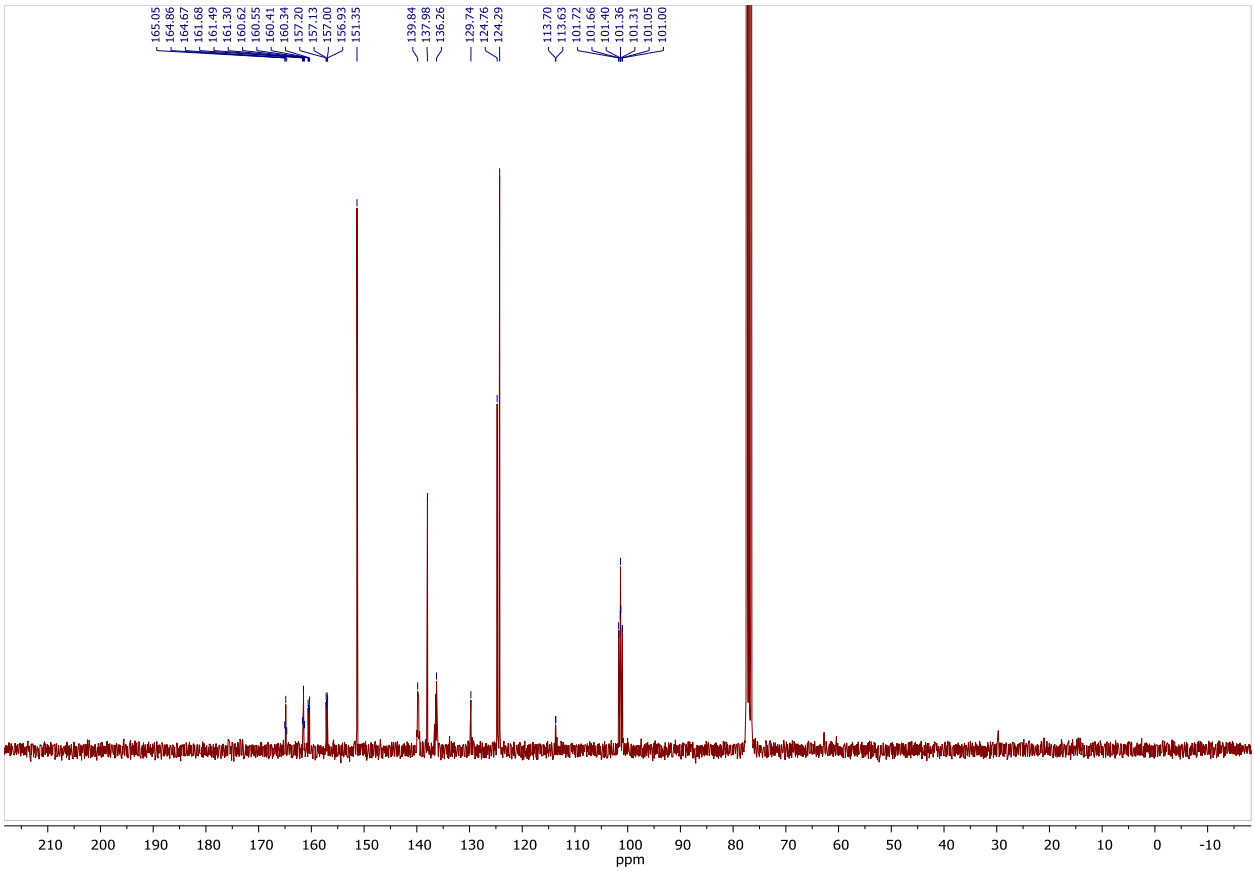

Figure S35. ^{13}C{^{1}H} NMR spectrum of **3ja**. Solvent: $CDCl_3$, 75 MHz.

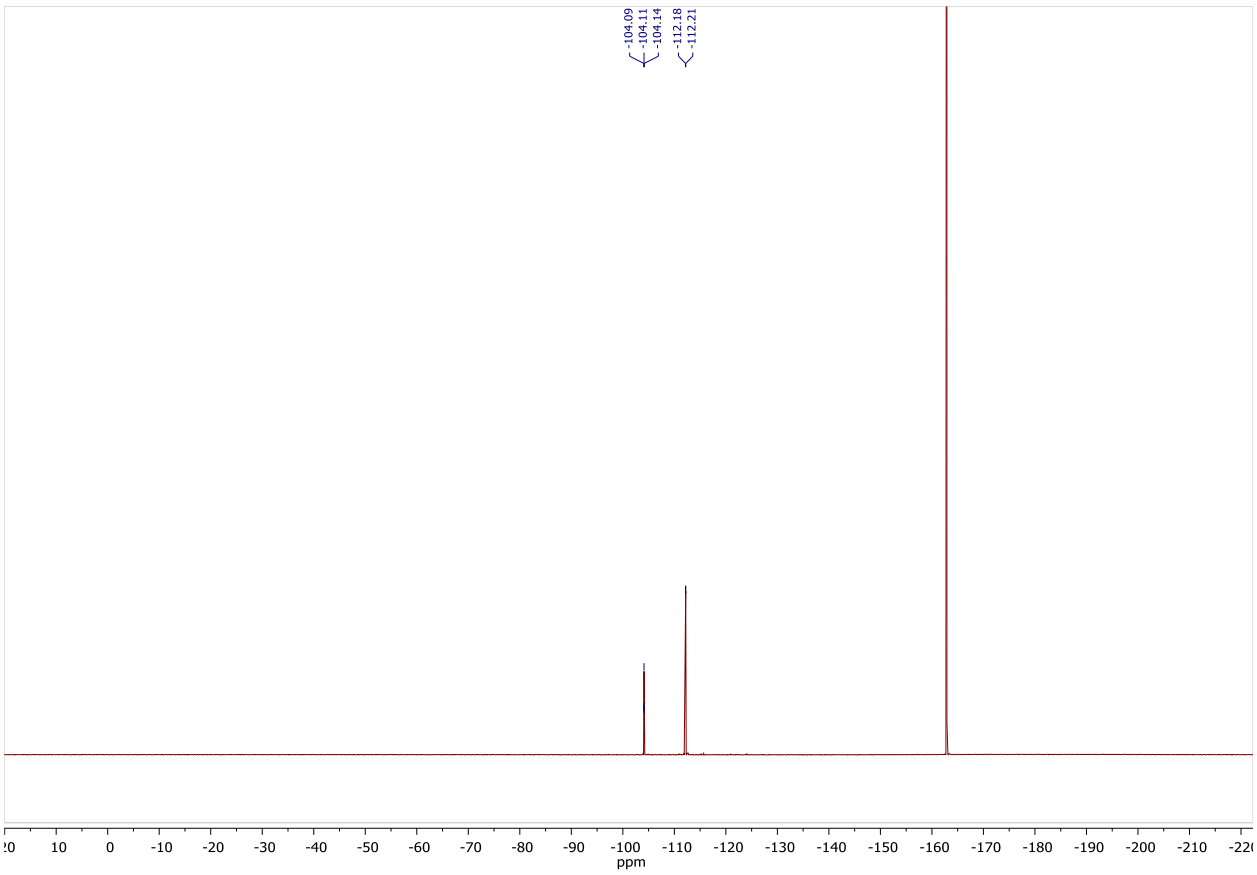

Figure S36. $^{19}F\{^{1}H\}$ NMR spectrum of **3ja**. Solvent: $CDCl_3$, 282.4 MHz. Standard: C_6F_6 with respect to $CFCl_3$.

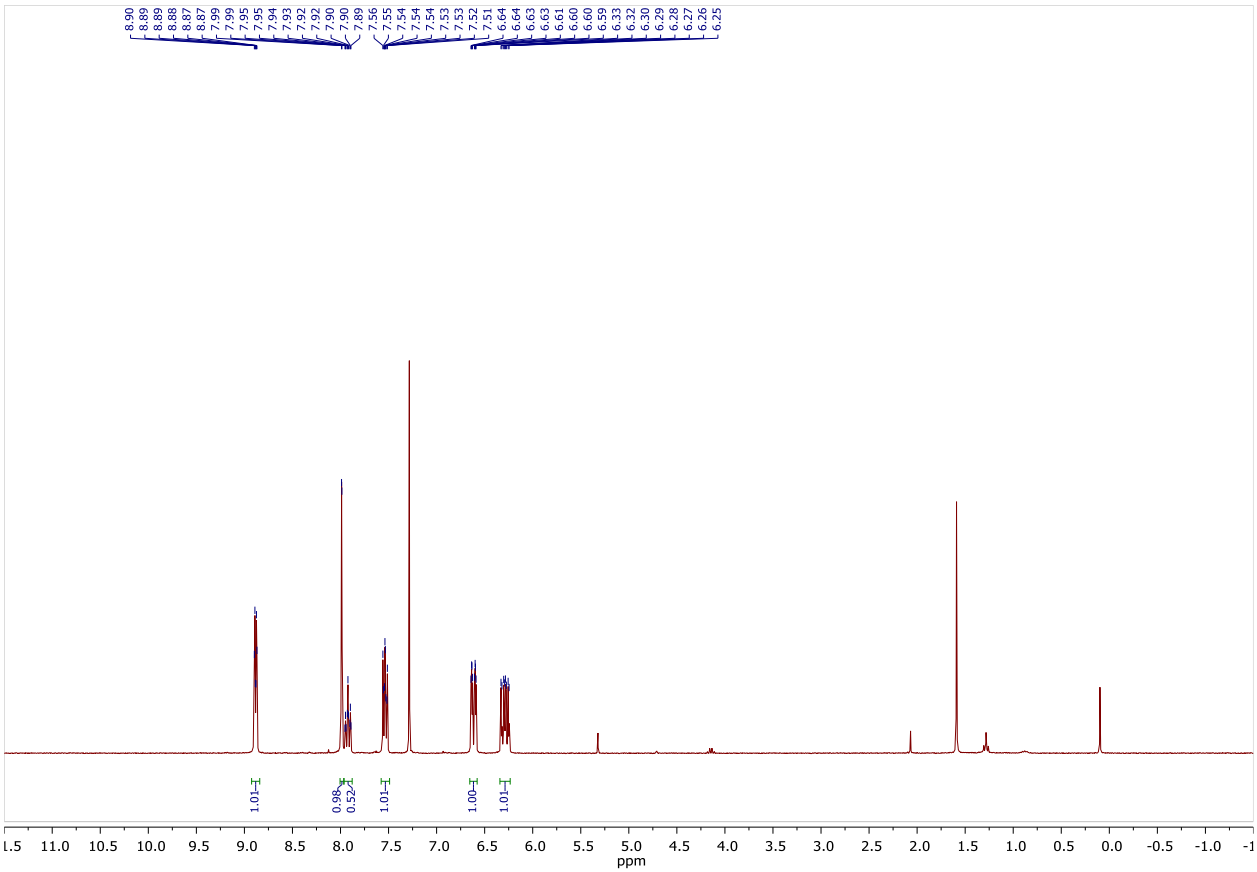

Figure S37. ^{1}H NMR spectrum of **3jb**. Solvent: $CDCl_3$, 300 MHz.

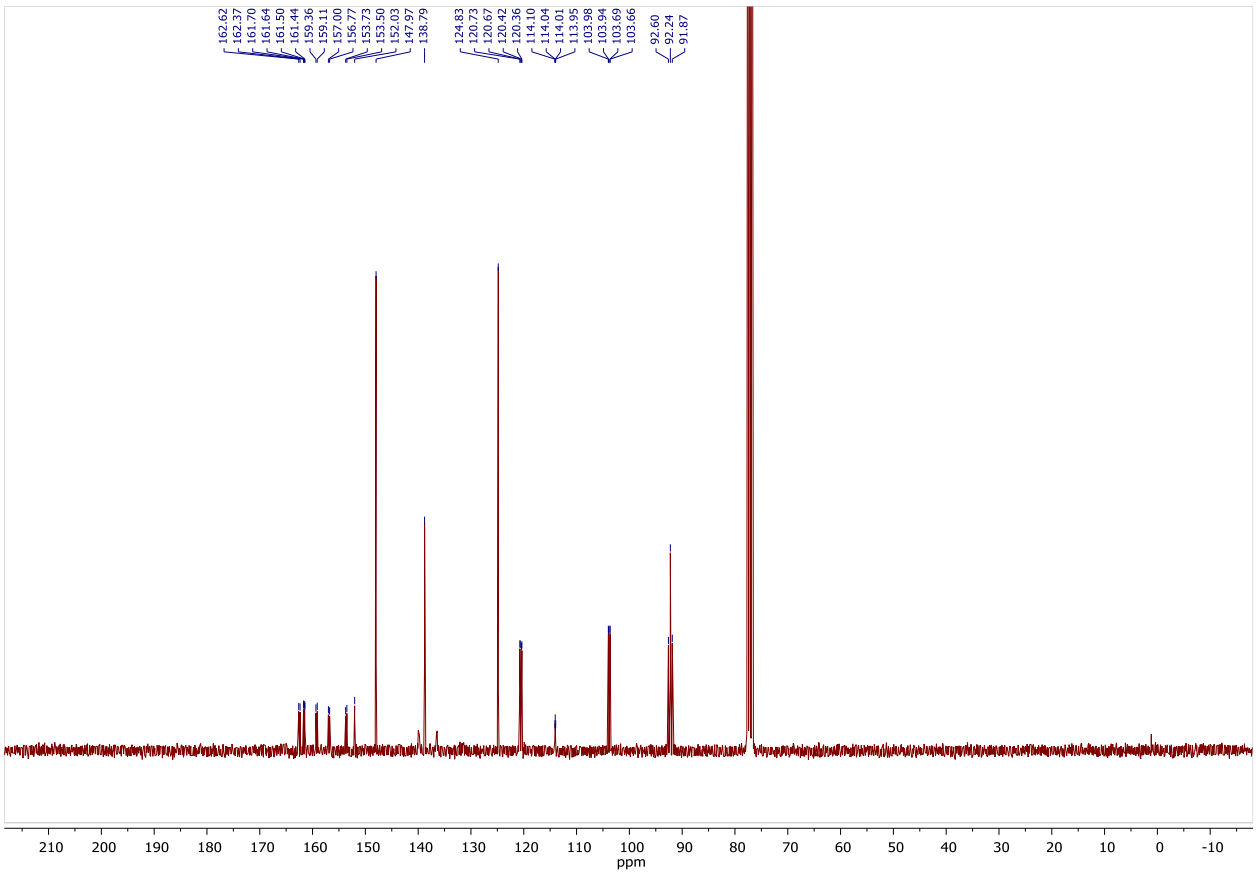

Figure S38. $^{13}C\{^{1}H\}$ NMR spectrum of **3jb**. Solvent: $CDCl_3$, 75 MHz.

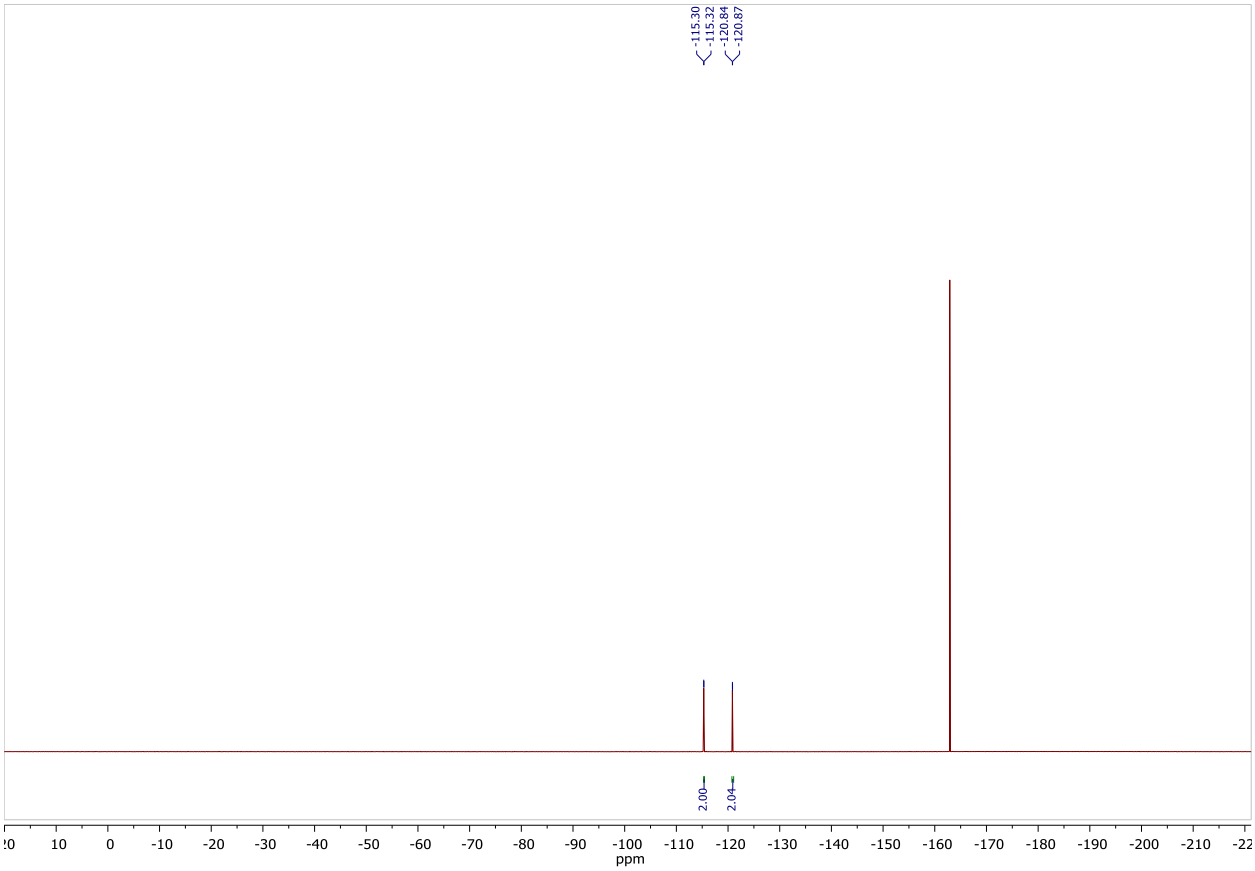

Figure S39. $^{19}F\{^{1}H\}$ NMR spectrum of **3jb**. Solvent: $CDCl_3$, 282.4 MHz. Standard: C_6F_6 with respect to $CFCl_3$.

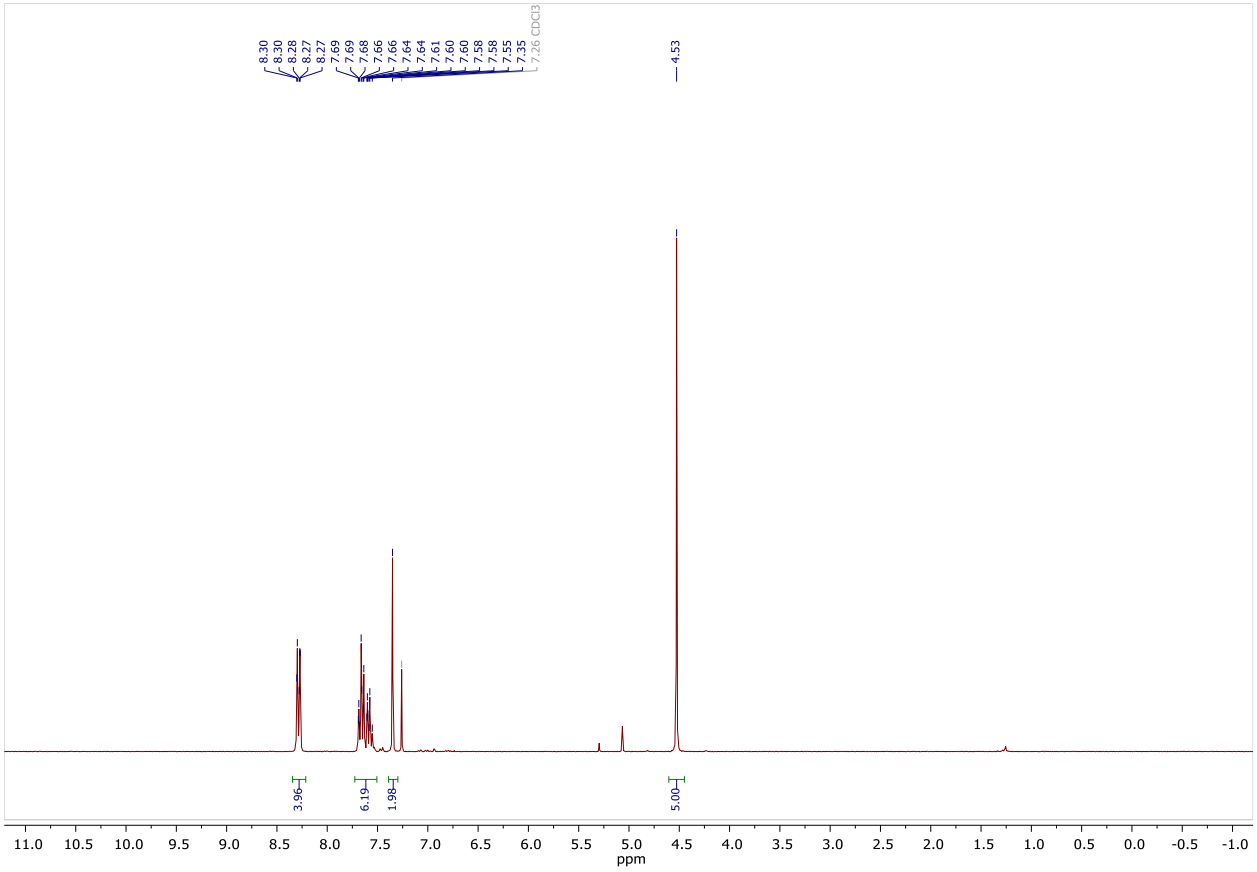

Figure S40. ^{1}H NMR spectrum of **4a**. Solvent: $CDCl_3$, 300 MHz.

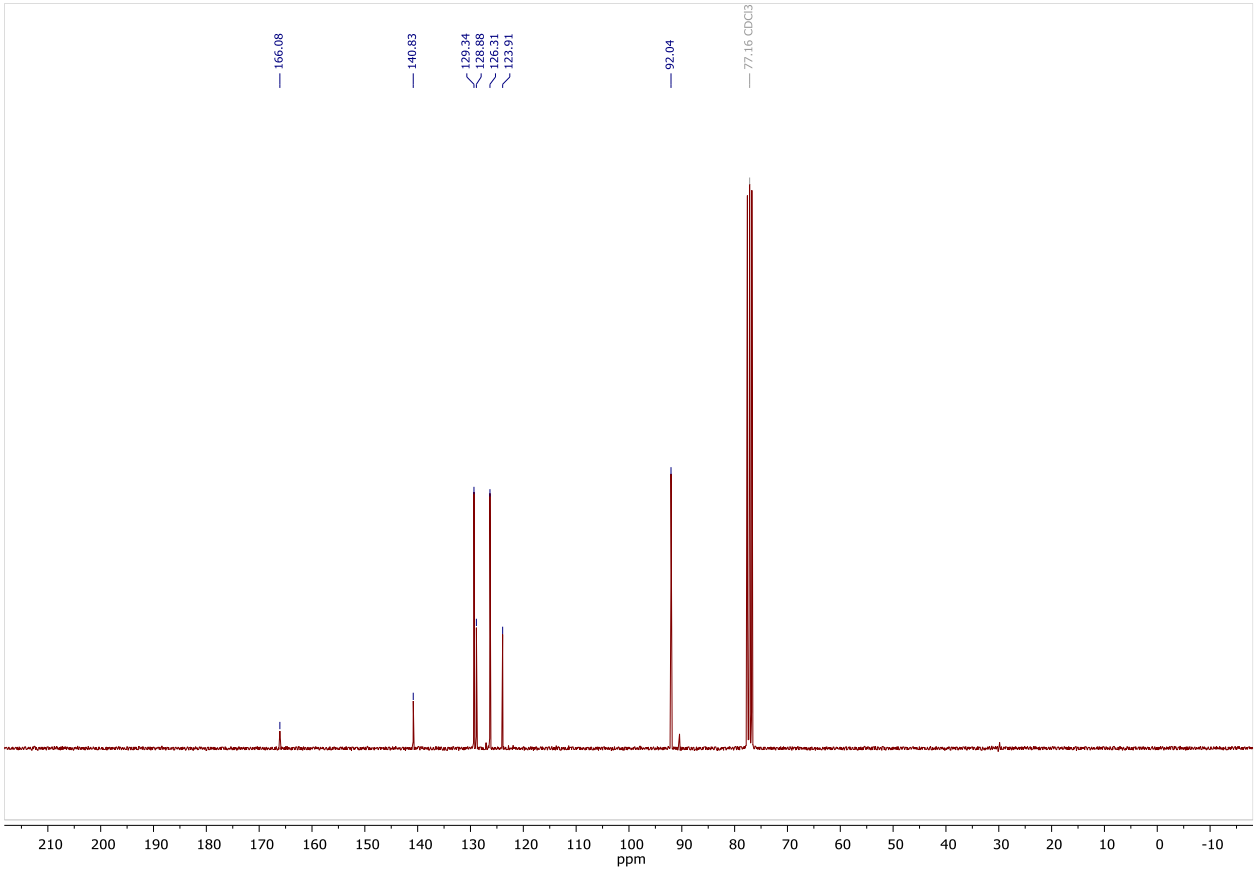

Figure S41. ^{13}C{^{1}H} NMR spectrum of **4a** Solvent: $CDCl_3$, 75 MHz.

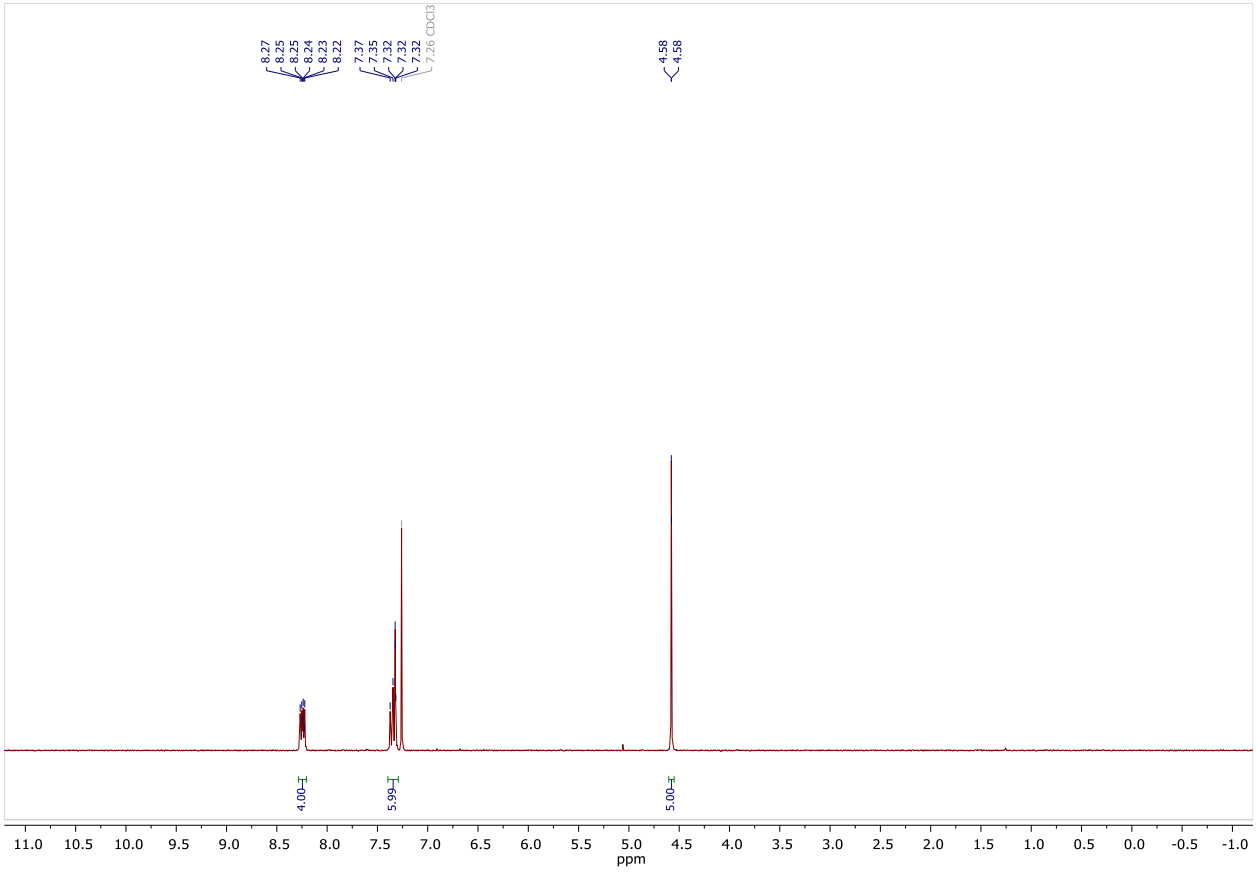

Figure S42. ^{1}H NMR spectrum of **4b**. Solvent: $CDCl_3$, 300 MHz.

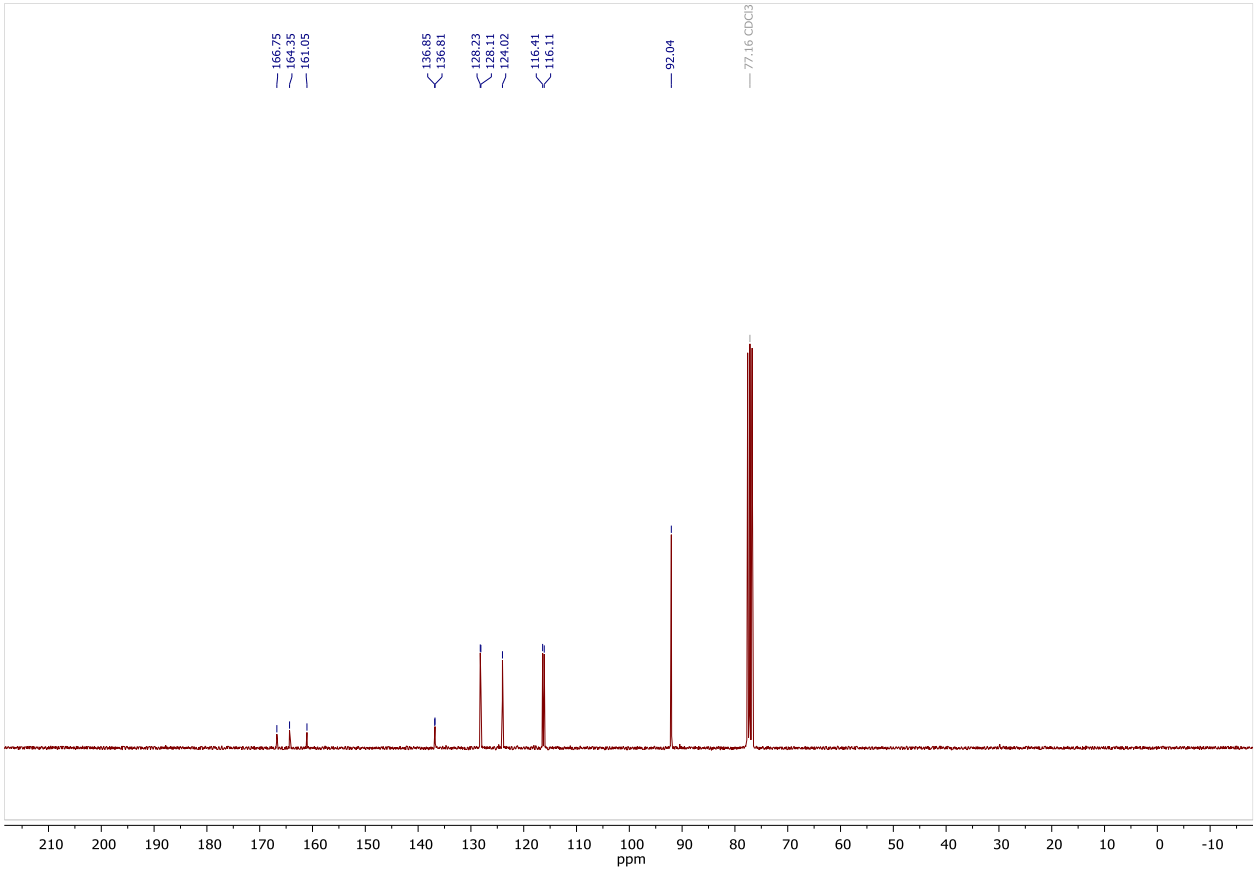

Figure S43. ^{13}C{^{1}H} NMR spectrum of **4b**. Solvent: $CDCl_3$, 75 MHz.

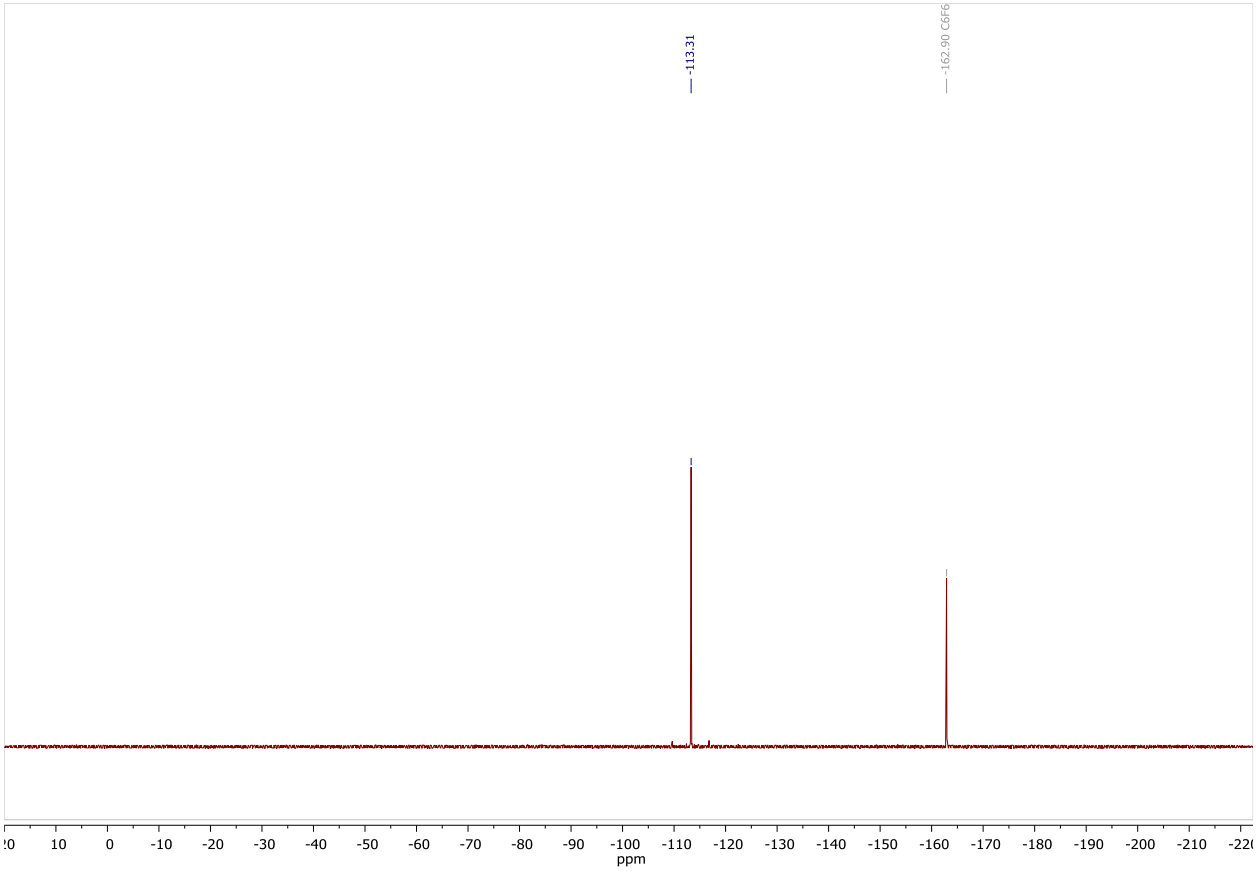

Figure S44. $^{19}F\{^{1}H\}$ NMR spectrum of **4b**. Solvent: $CDCl_3$, 282.4 MHz. Standard: C_6F_6 with respect to $CFCl_3$.

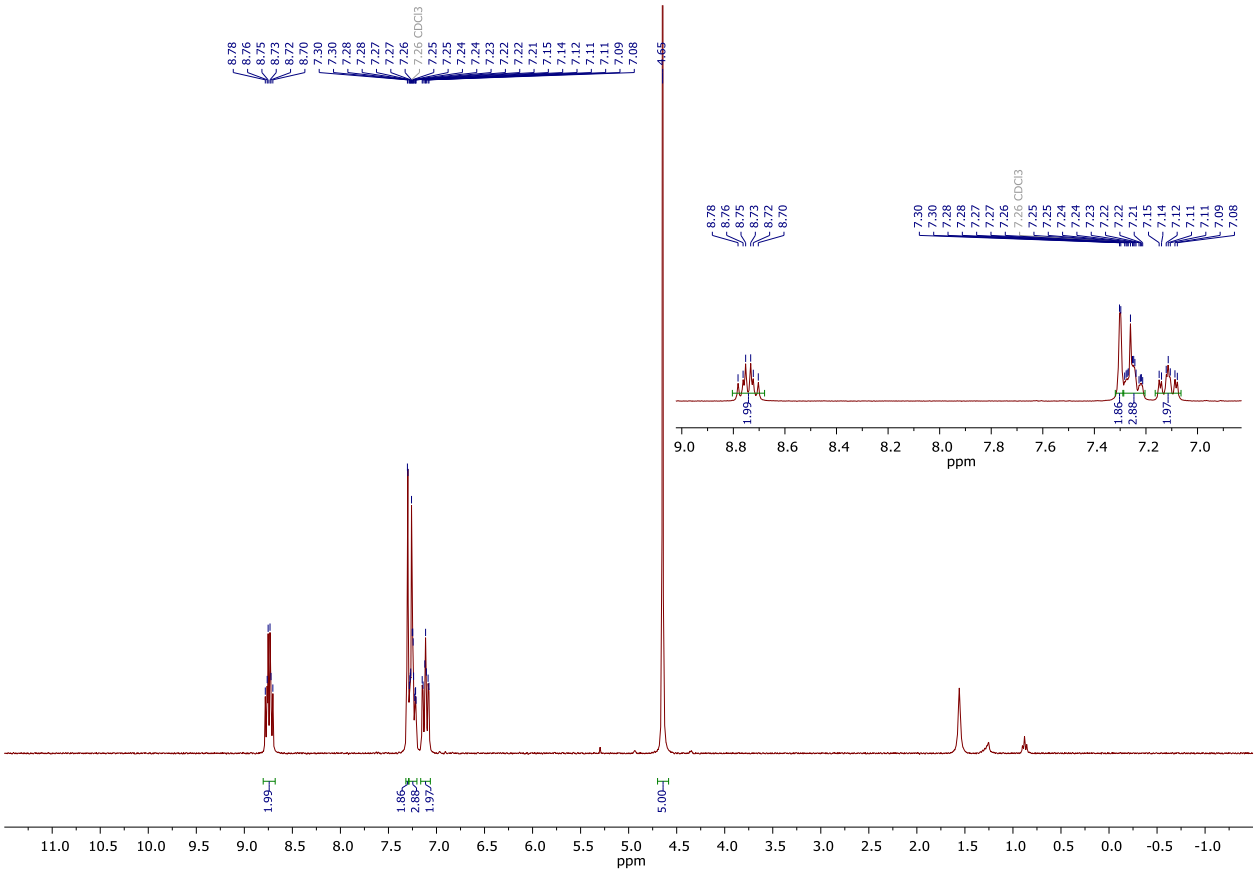

Figure S45. ^{1}H NMR spectrum of **4c**. Solvent: $CDCl_3$, 300 MHz.

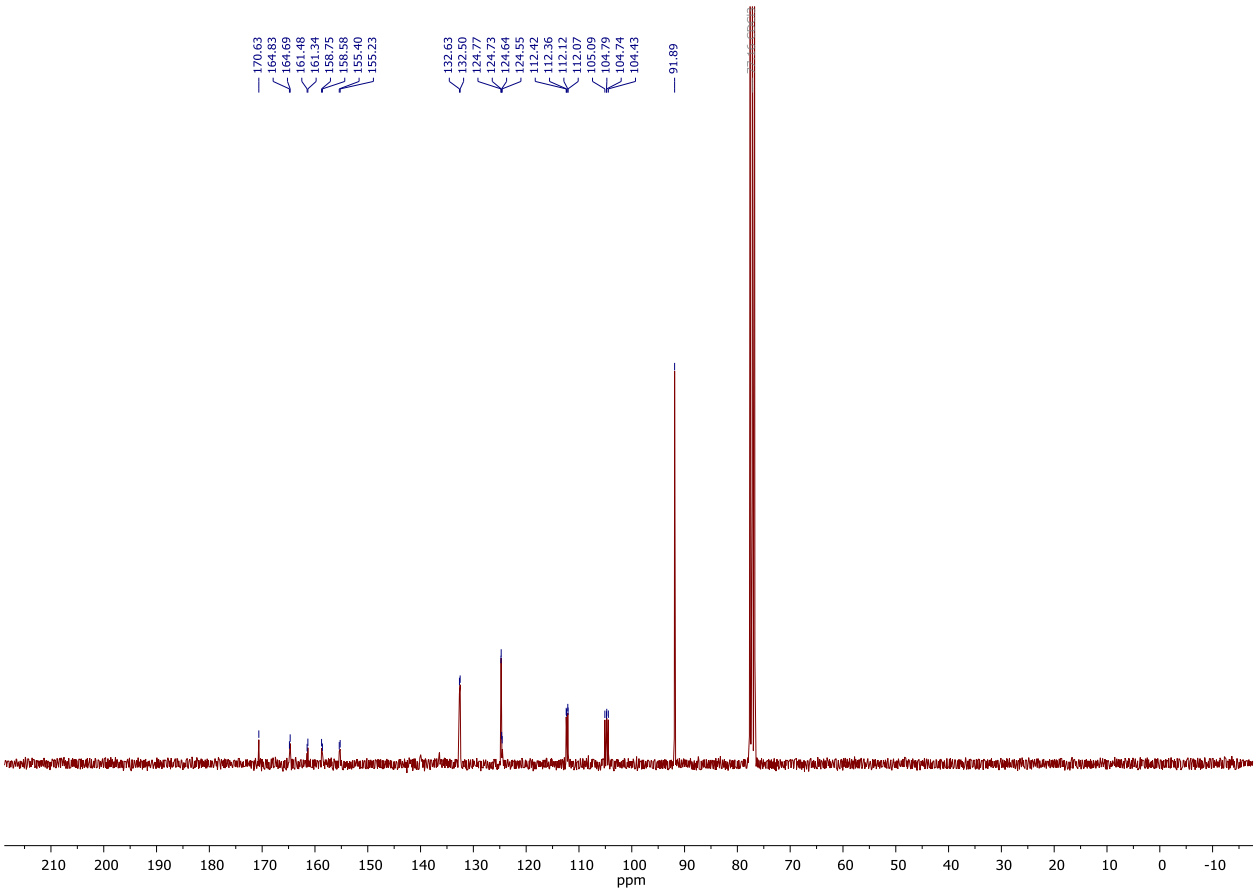

Figure S46. $^{13}C\{^{1}H\}$ NMR spectrum of **4c**. Solvent: $CDCl_3$, 75 MHz.

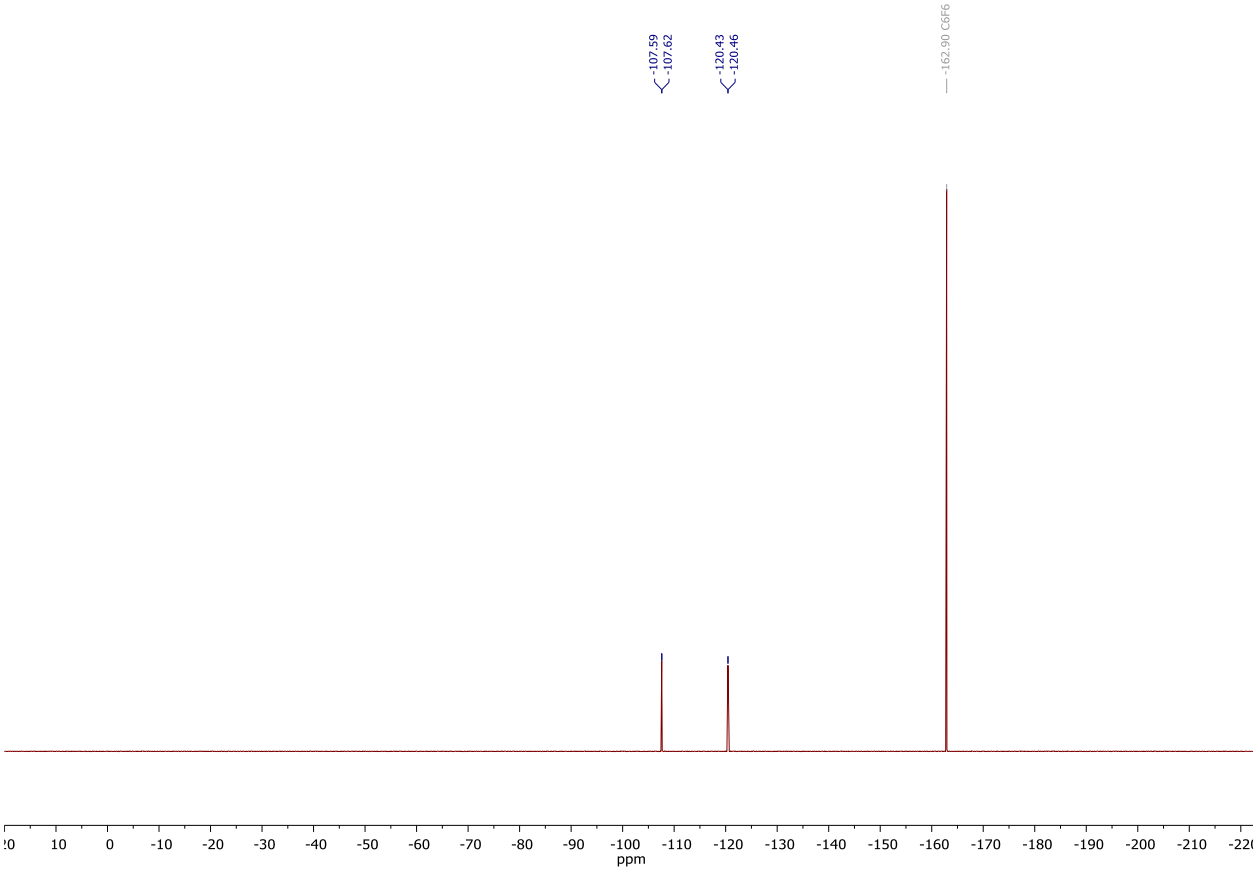

Figure S47. $^{19}F\{^{1}H\}$ NMR spectrum of **4c**. Solvent: $CDCl_3$, 282.4 MHz. Standard: C_6F_6 with respect to $CFCl_3$.

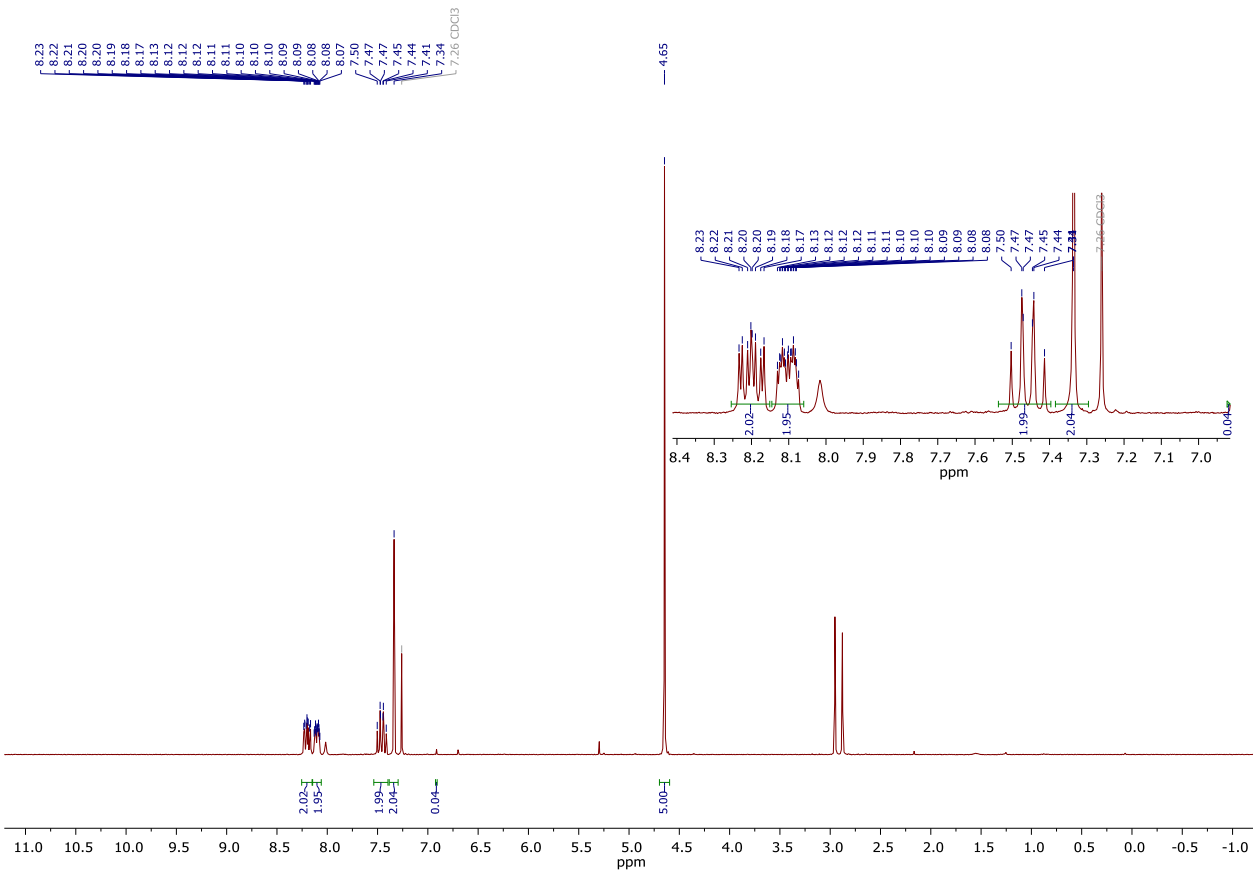

Figure S48. ^{1}H NMR spectrum of **4d**. Solvent: $CDCl_3$, 300 MHz.

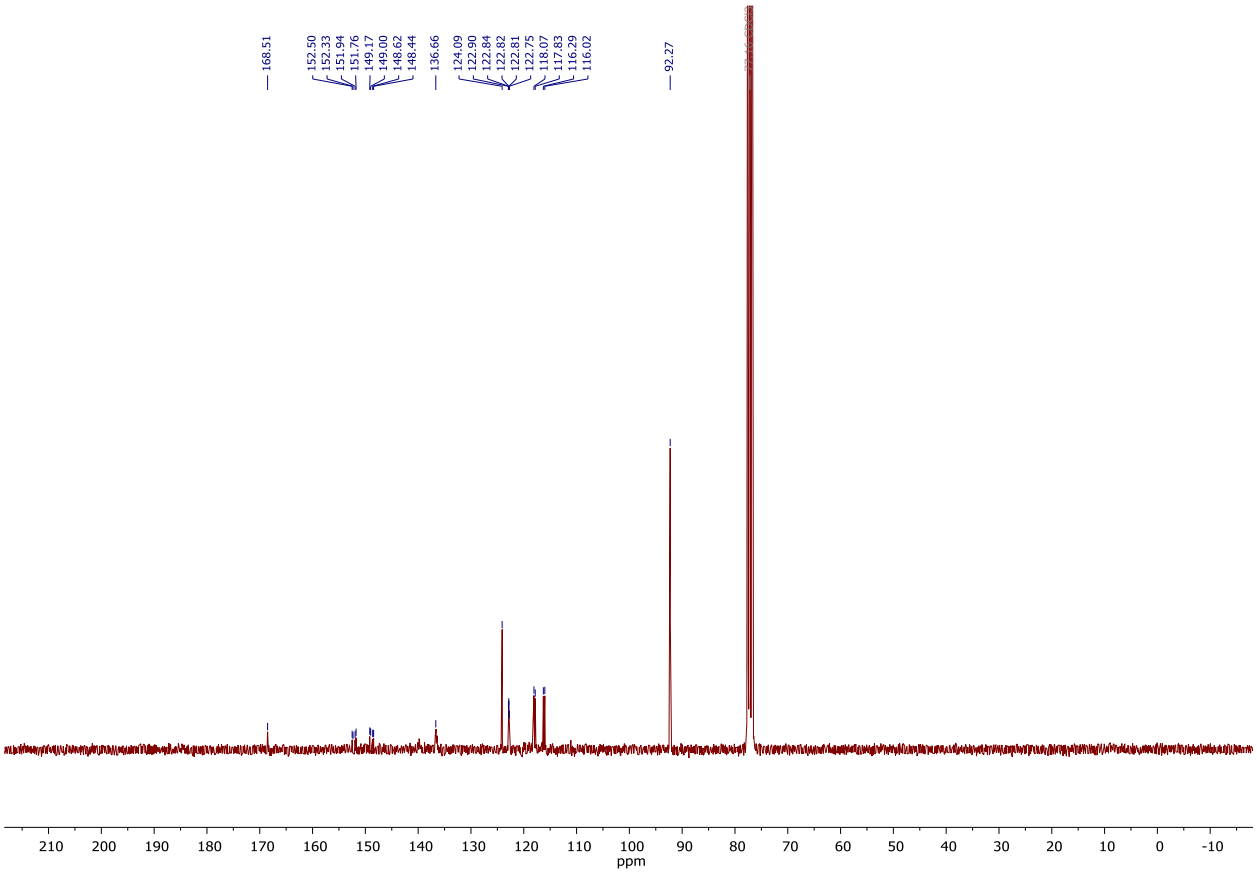

Figure S49. $^{13}C\{^{1}H\}$ NMR spectrum of **4d**. Solvent: $CDCl_3$, 75 MHz.

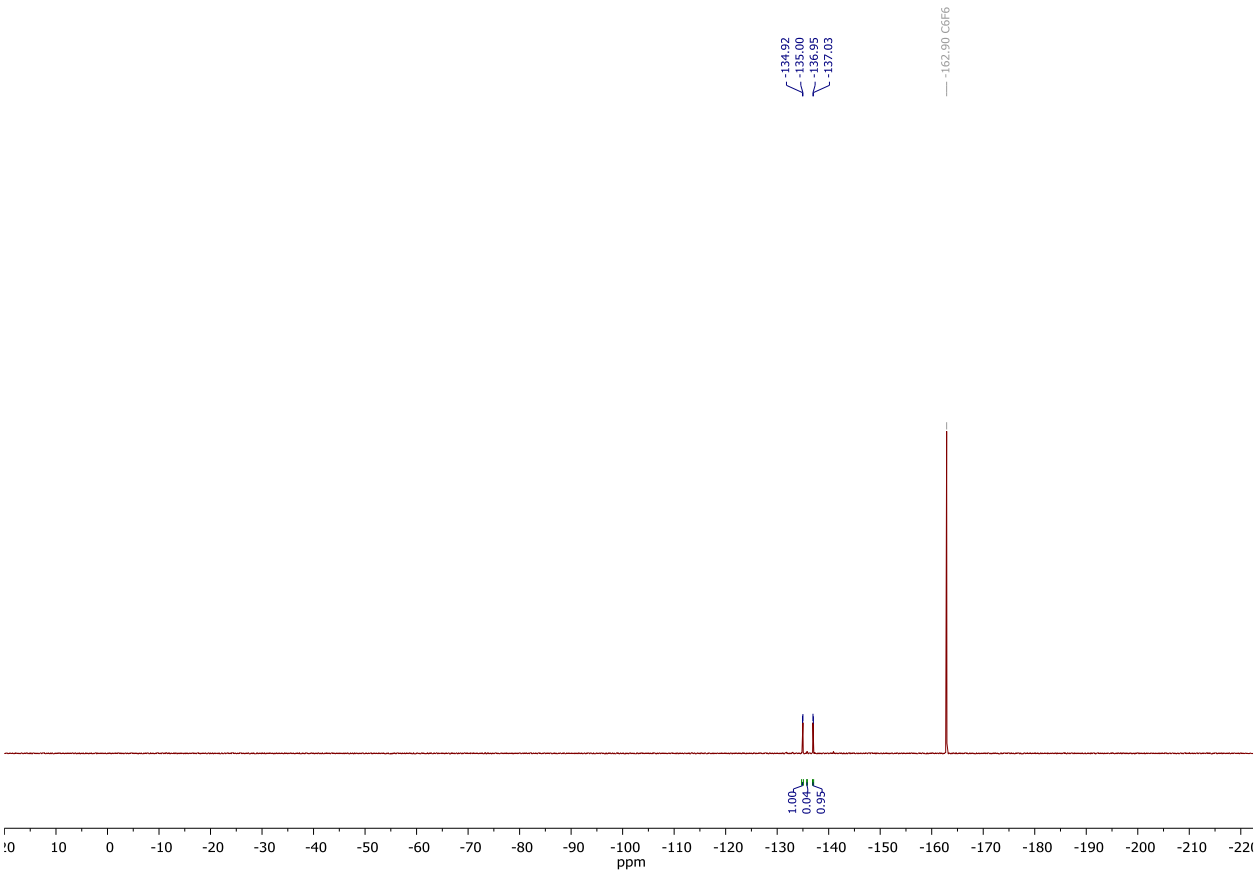

Figure S50. $^{19}F\{^{1}H\}$ NMR spectrum of **4d**. Solvent: $CDCl_3$, 282.4 MHz. Standard: C_6F_6 with respect to $CFCl_3$.

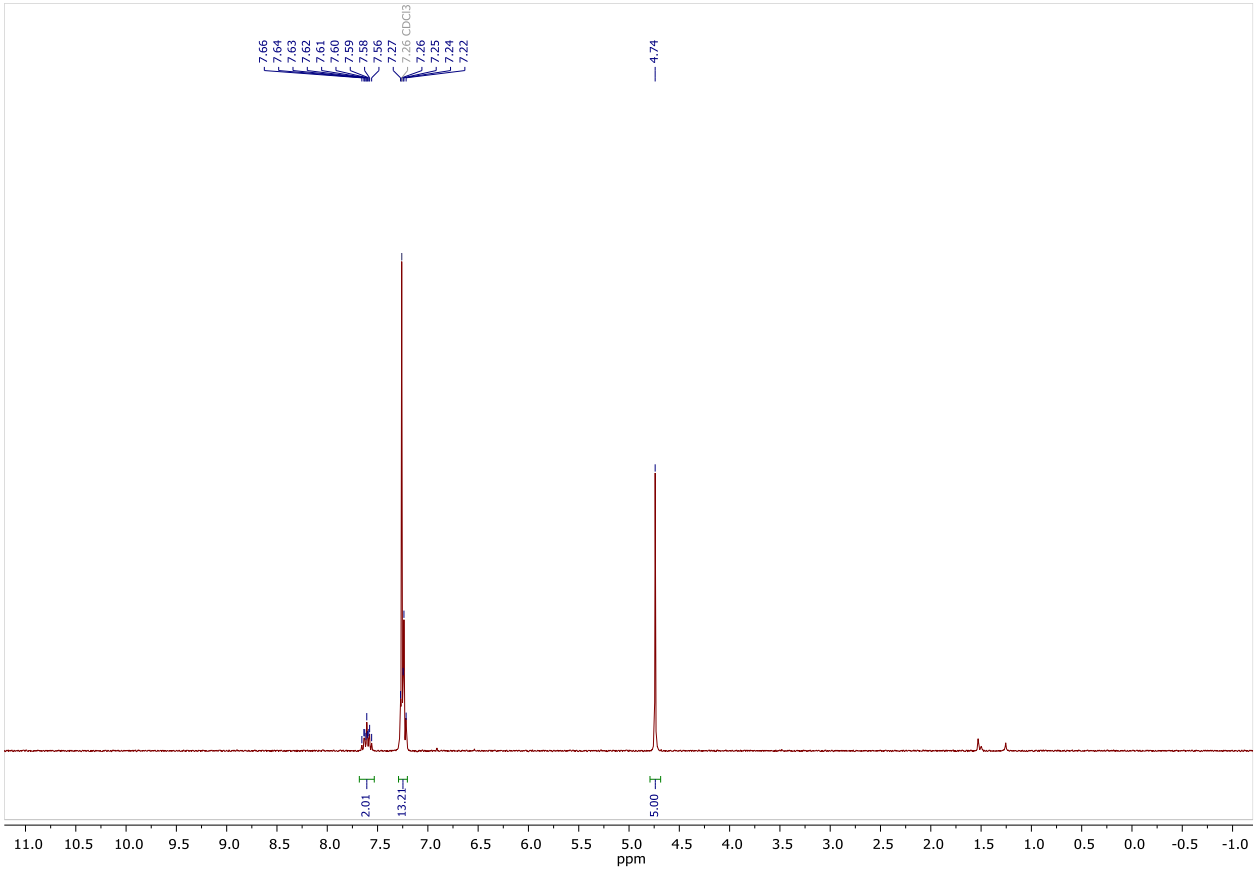

Figure S51. ^{1}H NMR spectrum of **4e**. Solvent: $CDCl_3$, 300 MHz.

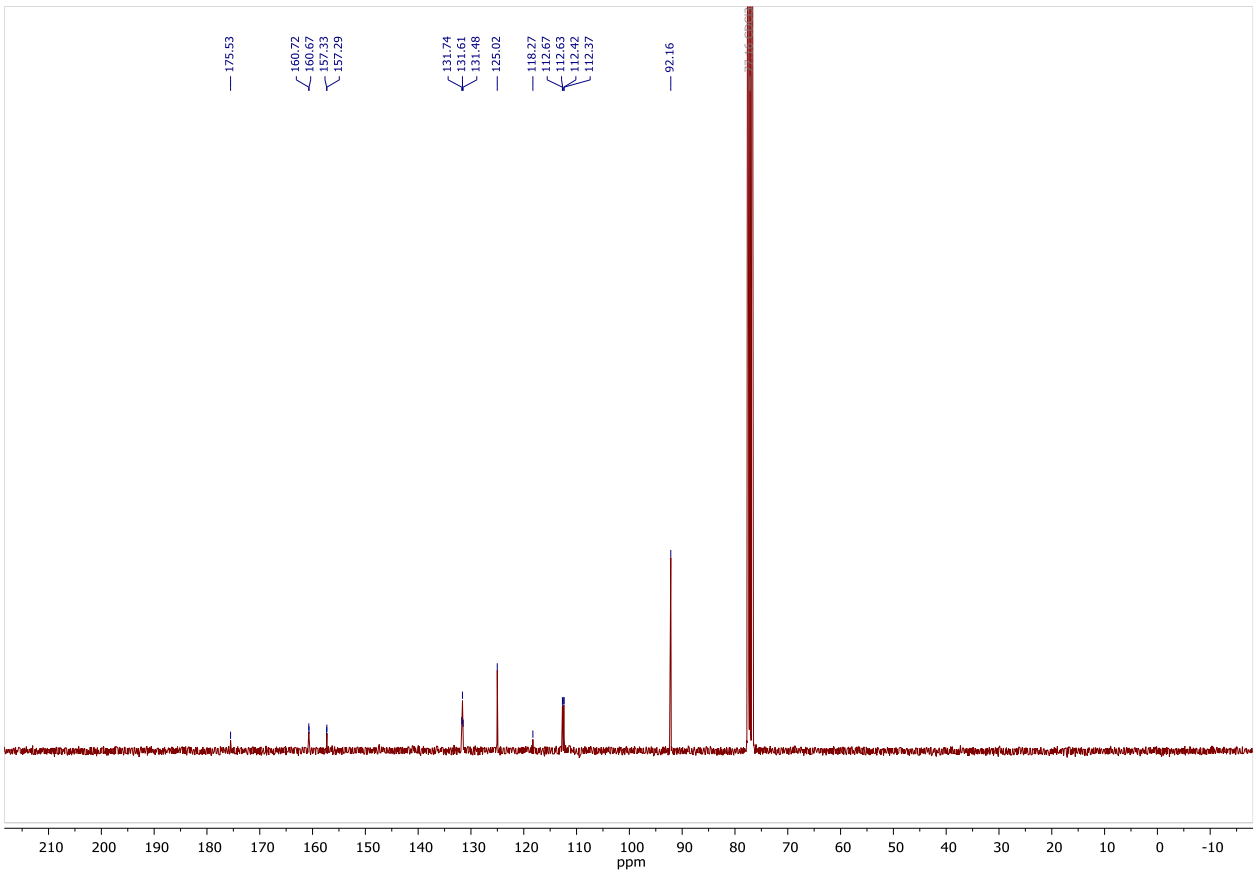

Figure S52. $^{13}C\{^{1}H\}$ NMR spectrum of **4e**. Solvent: $CDCl_3$, 75 MHz.

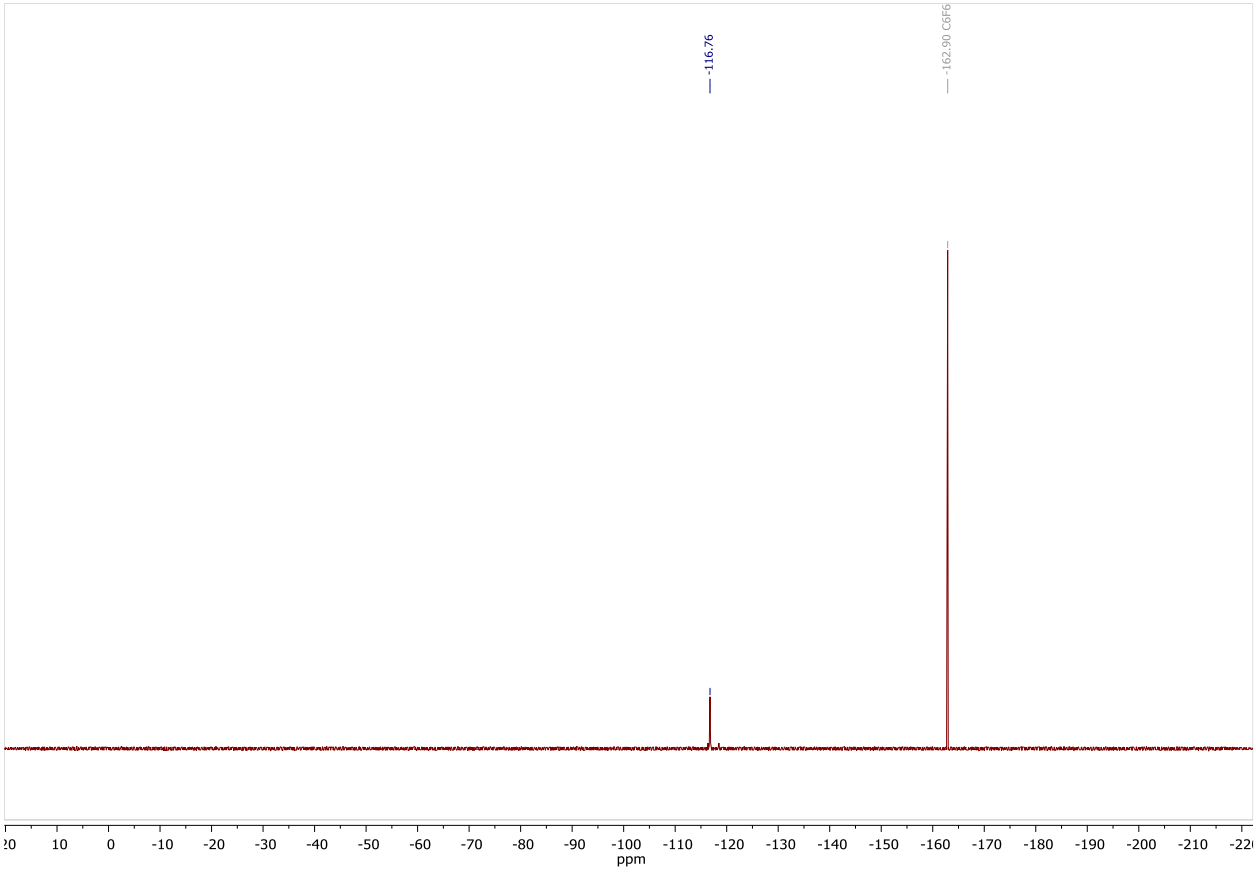

Figure S53. $^{19}F\{^{1}H\}$ NMR spectrum of **4e**. Solvent: $CDCl_3$, 282.4 MHz. Standard: C_6F_6 with respect to $CFCl_3$.

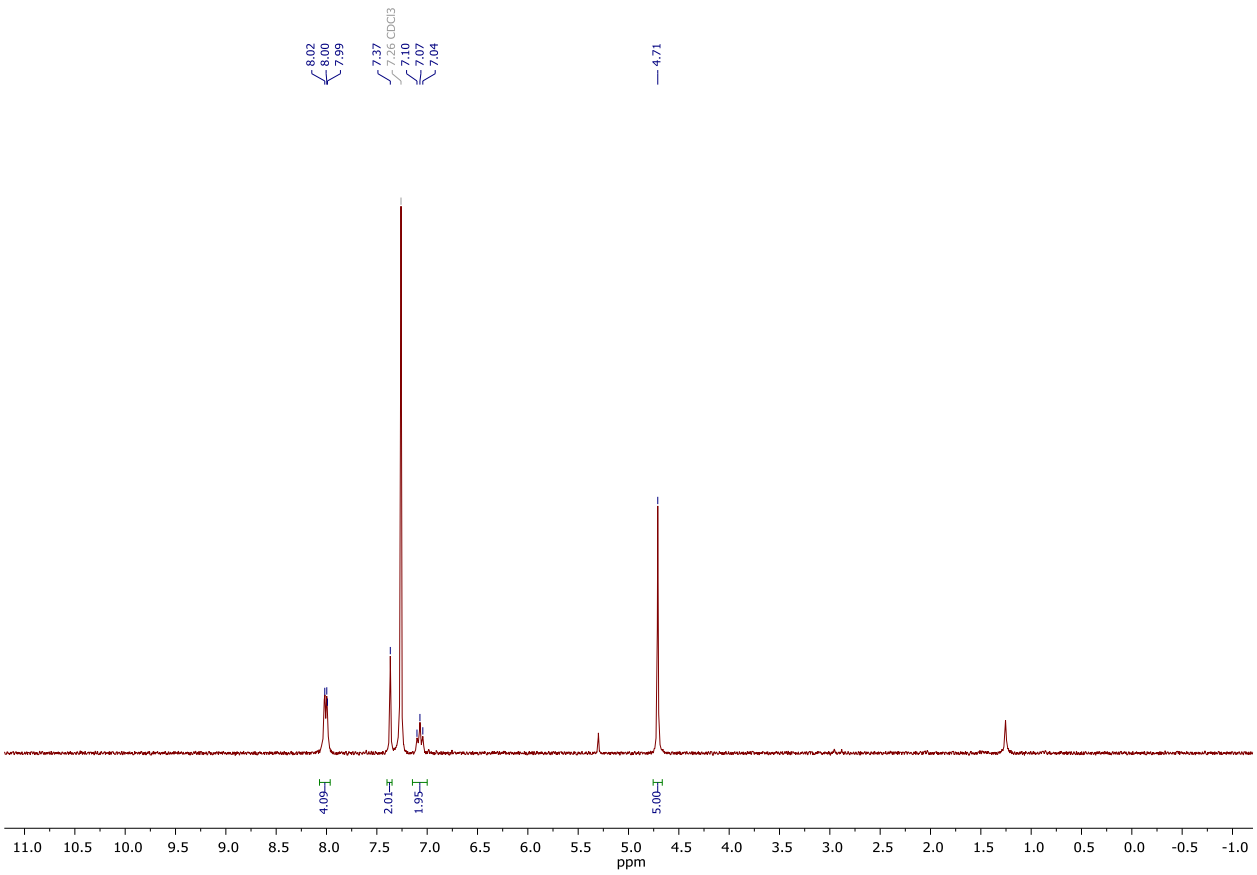

Figure S54. ^{1}H NMR spectrum of **4f**. Solvent: $CDCl_3$, 300 MHz.

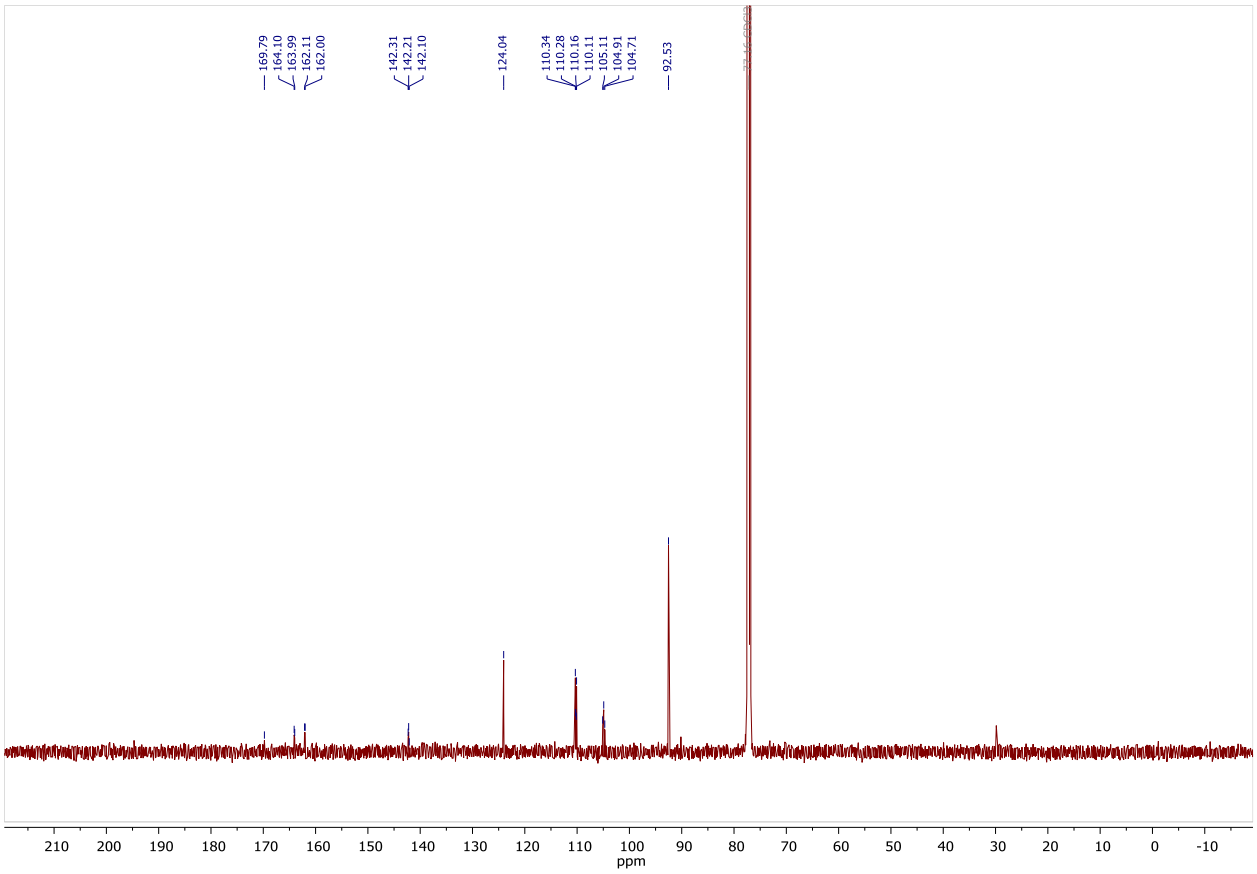

Figure S55. ^{13}C{^{1}H} NMR spectrum of **4f**. Solvent: $CDCl_3$, 75 MHz.

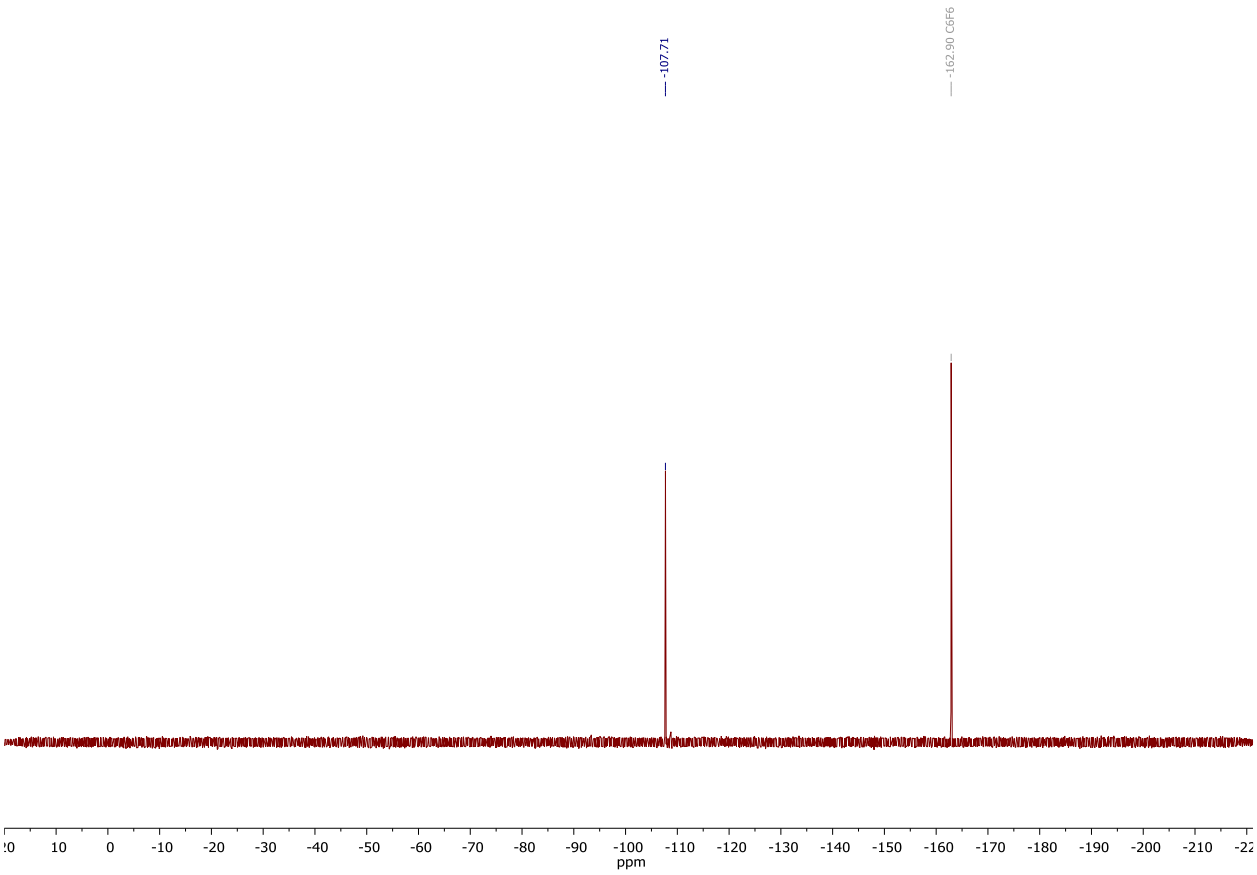

Figure S56. $^{19}F\{^{1}H\}$ NMR spectrum of **4f**. Solvent: $CDCl_3$, 282.4 MHz. Standard: C_6F_6 with respect to $CFCl_3$.

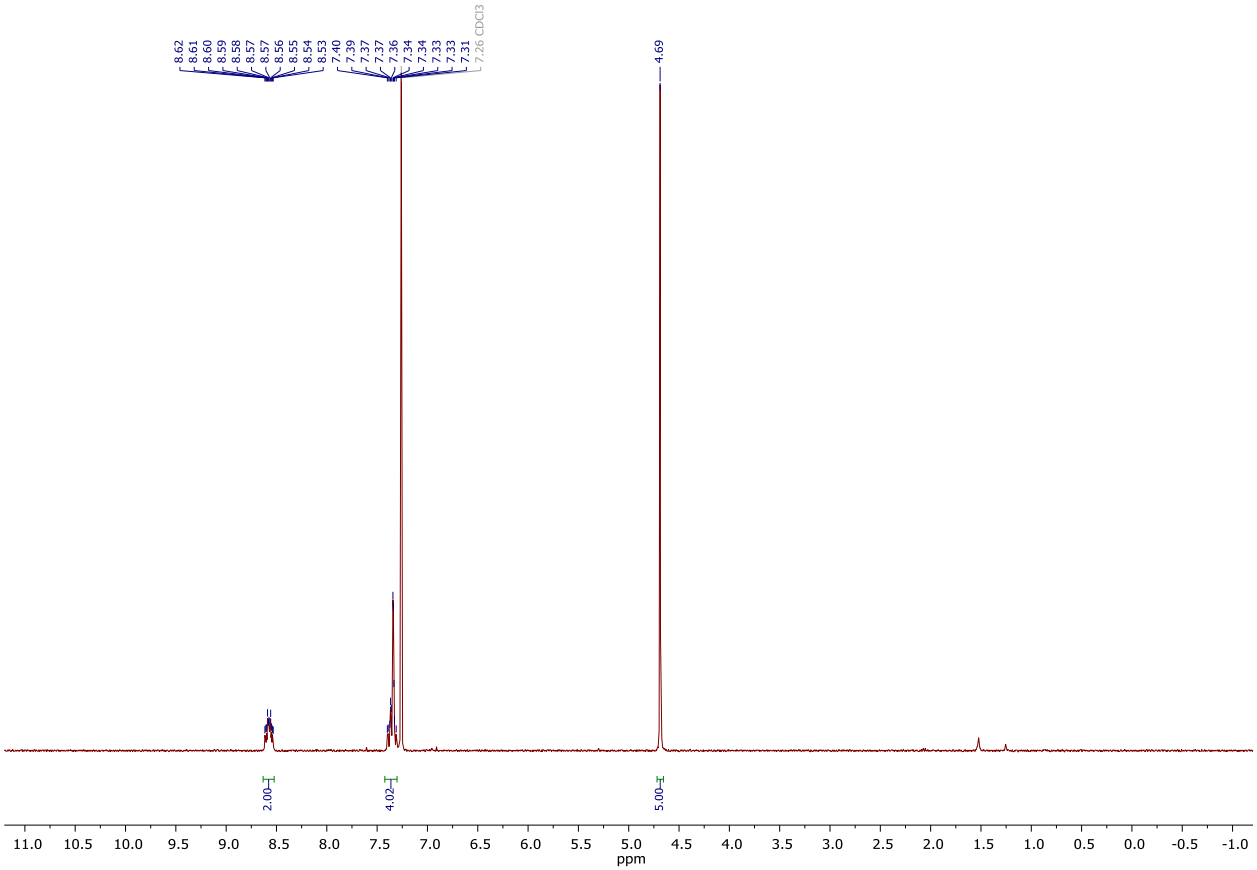

Figure S57. ^{1}H NMR spectrum of **4g**. Solvent: $CDCl_3$, 300 MHz.

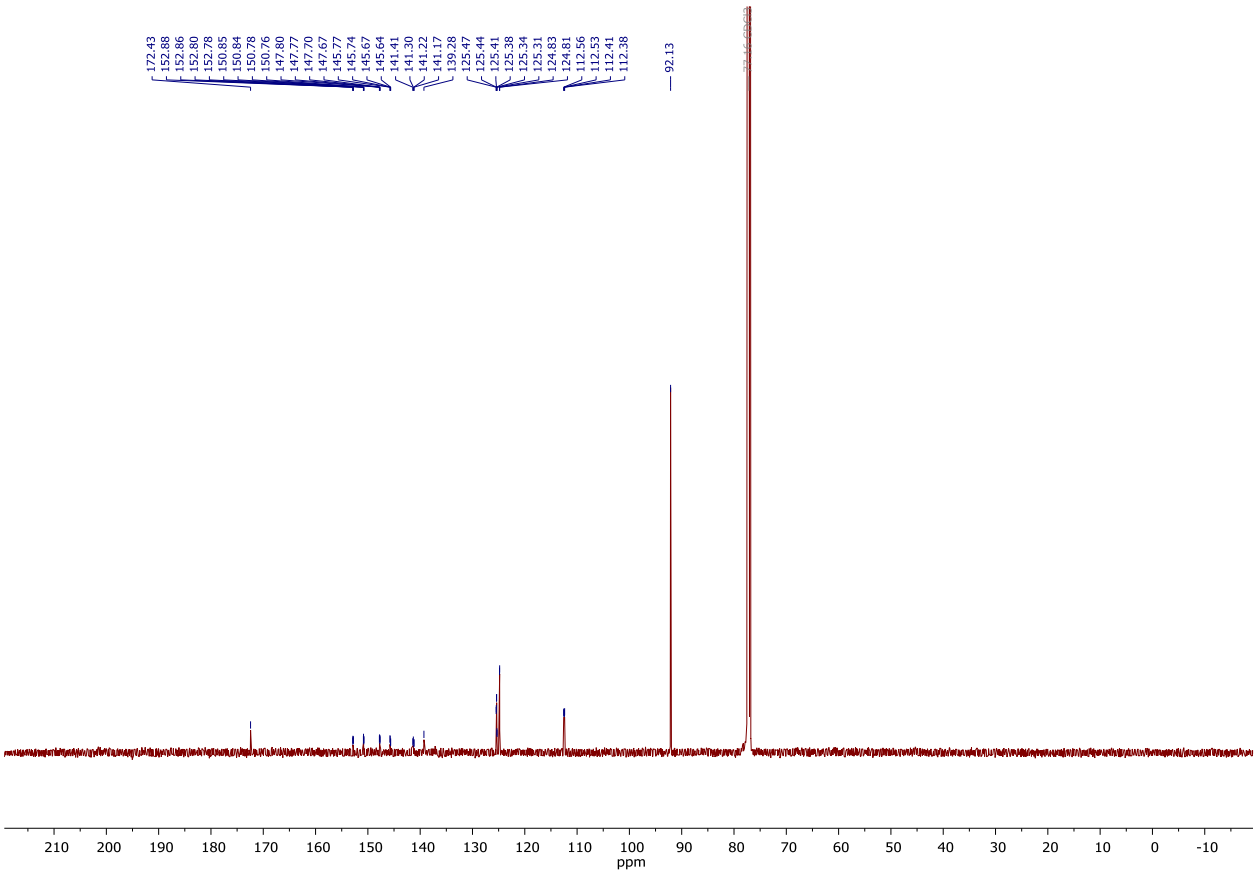

Figure S58. $^{13}C\{^{1}H\}$ NMR spectrum of **4g**. Solvent: $CDCl_3$, 75 MHz.

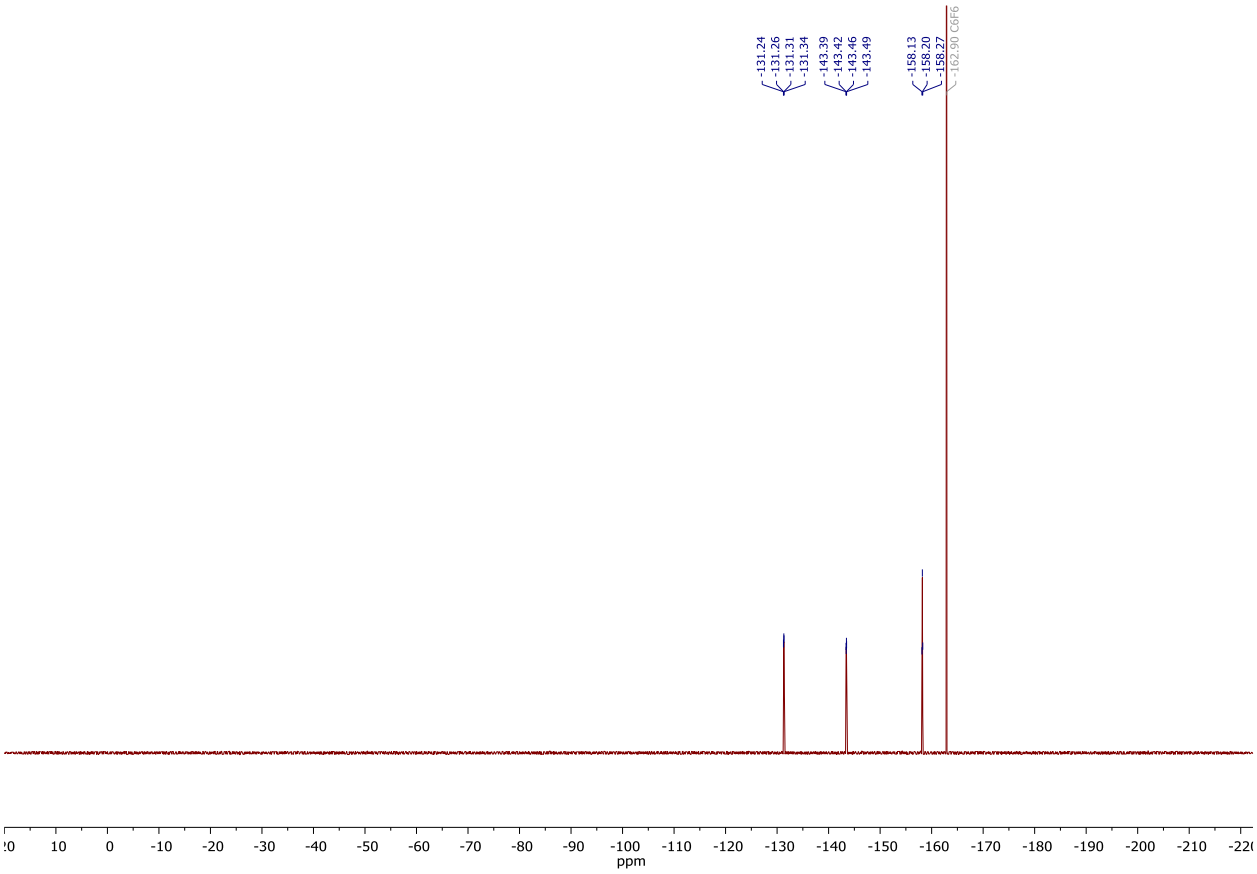

Figure S59. $^{19}F\{^{1}H\}$ NMR spectrum of **4g**. Solvent: $CDCl_3$, 282.4 MHz. Standard: C_6F_6 with respect to $CFCl_3$.

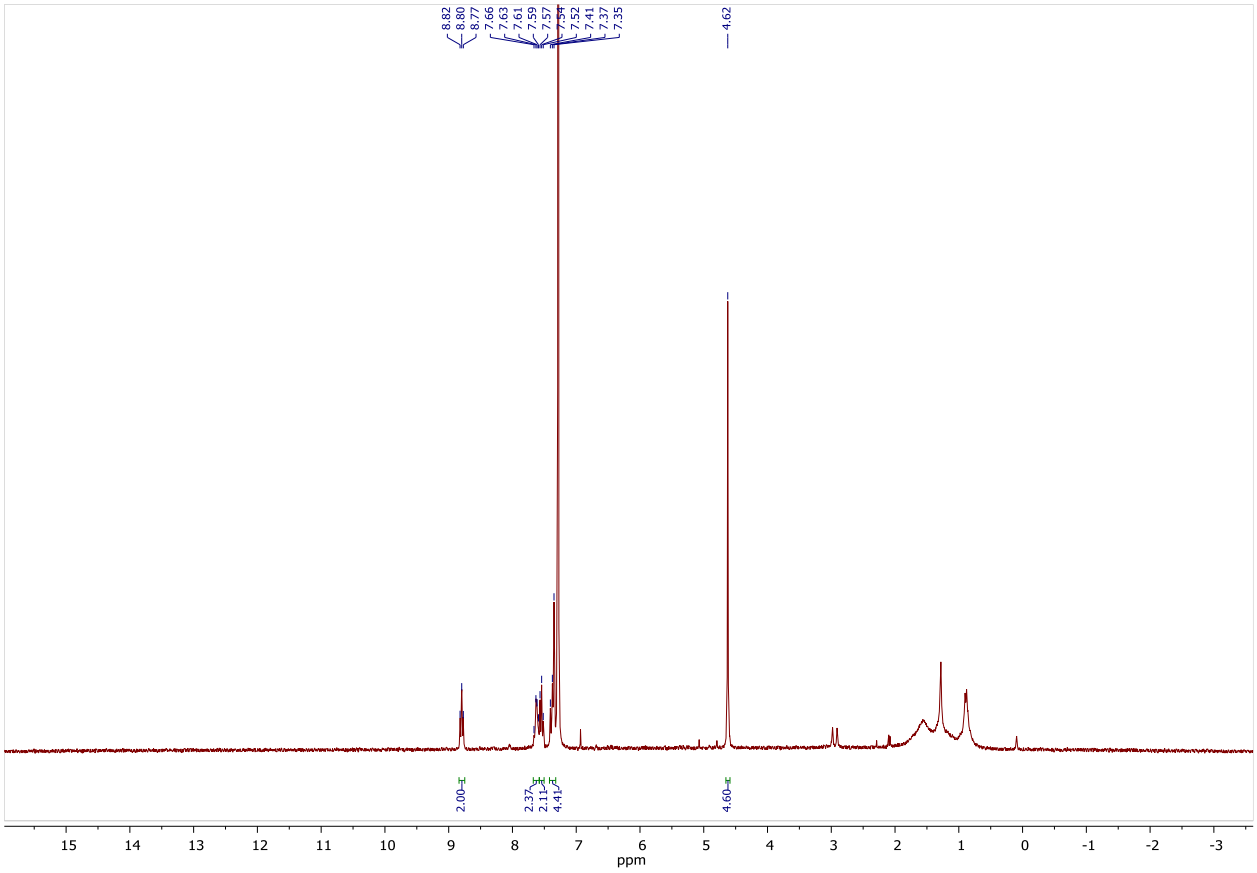

Figure S60. ^{1}H NMR spectrum of **4h**. Solvent: $CDCl_3$, 300 MHz.

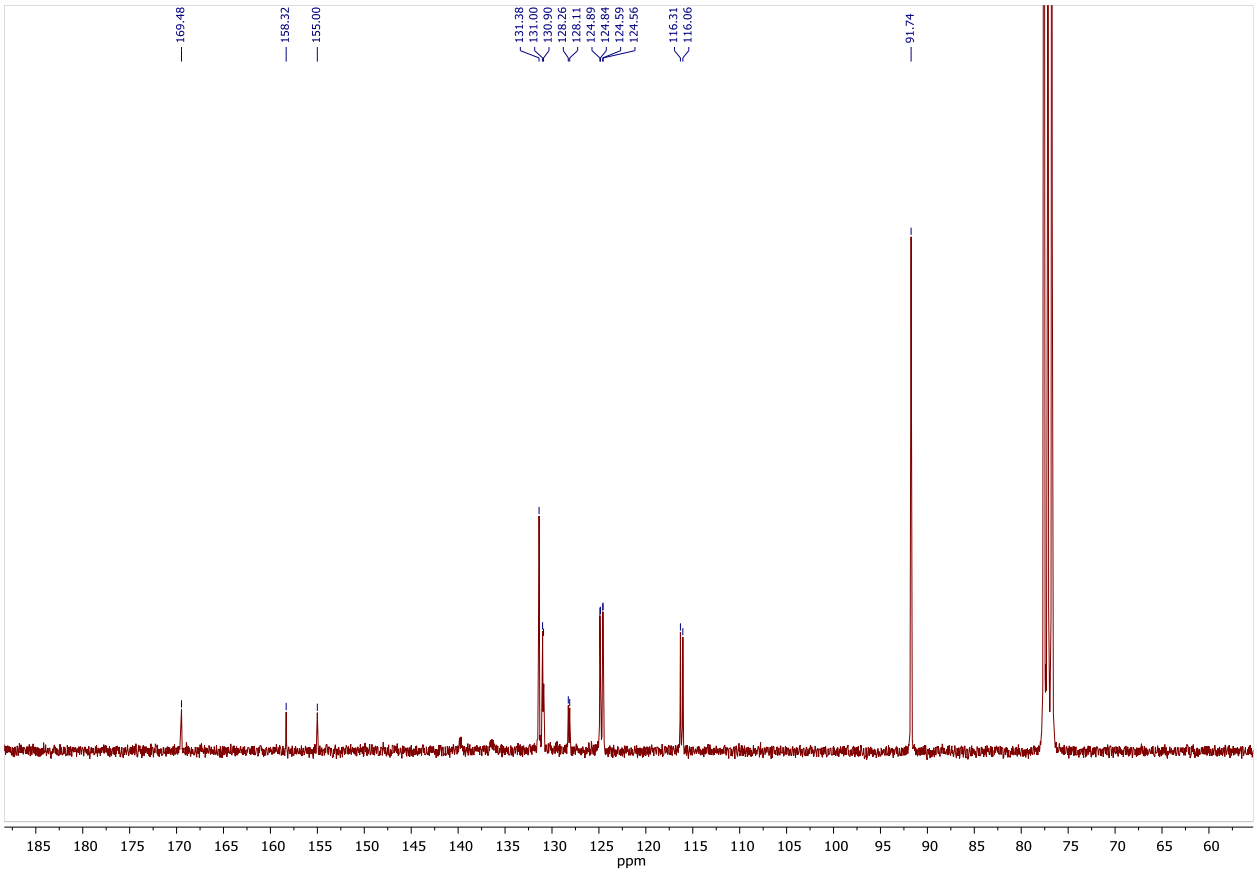

Figure S61. ^{13}C{^{1}H} NMR spectrum of **4h**. Solvent: $CDCl_3$, 75 MHz.

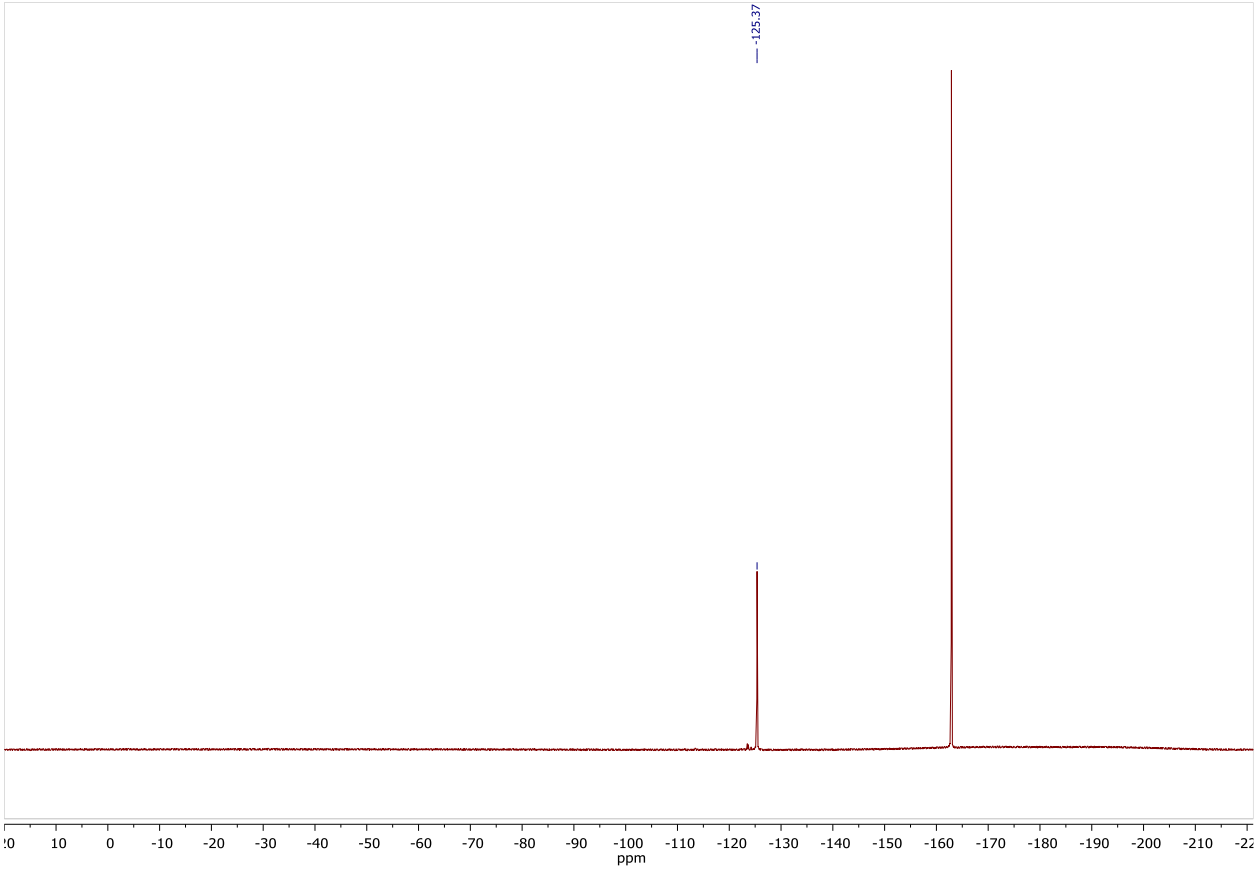

Figure S62. $^{19}F\{^{1}H\}$ NMR spectrum of **4h**. Solvent: $CDCl_3$, 282.4 MHz. Standard: C_6F_6 with respect to $CFCl_3$.

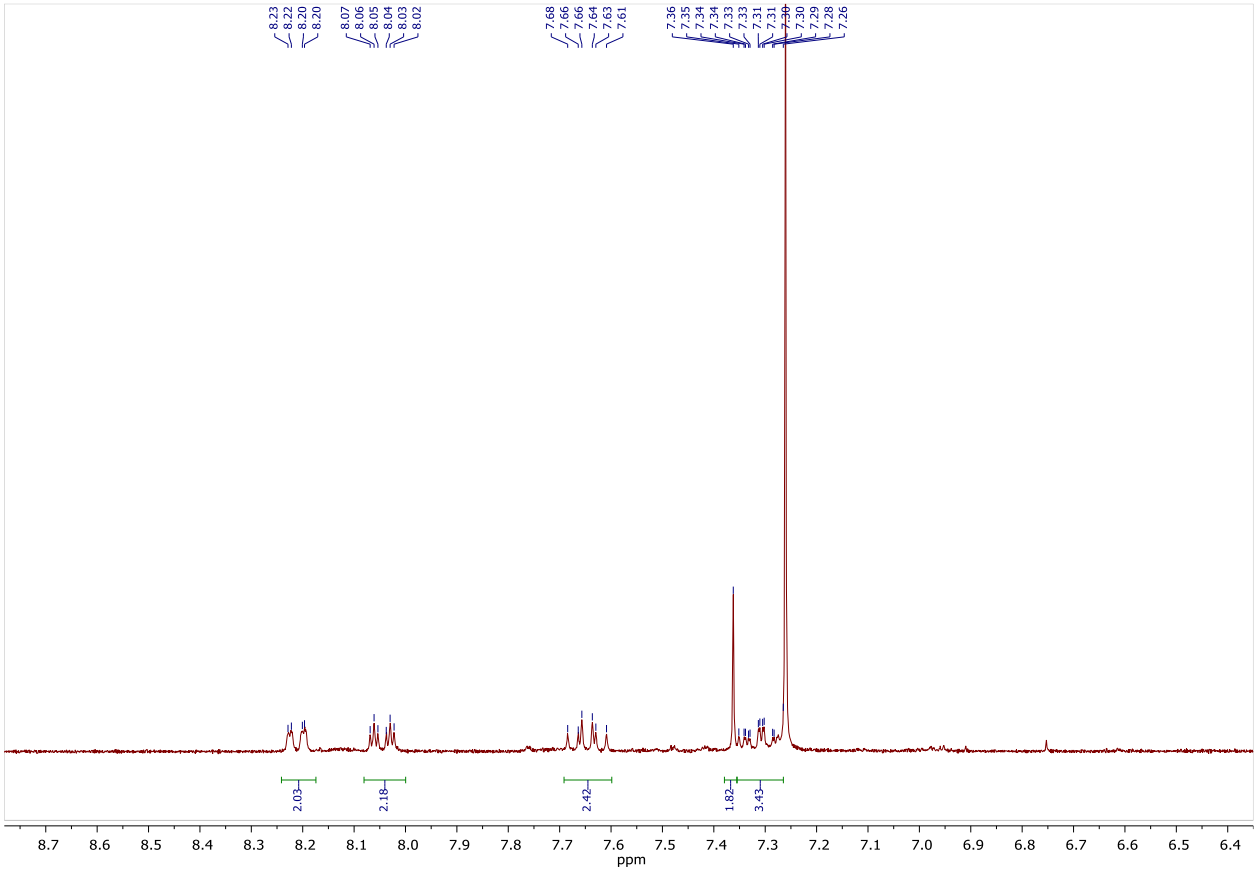

Figure S63. ^{1}H NMR spectrum of **4i**. Solvent: $CDCl_3$, 300 MHz.

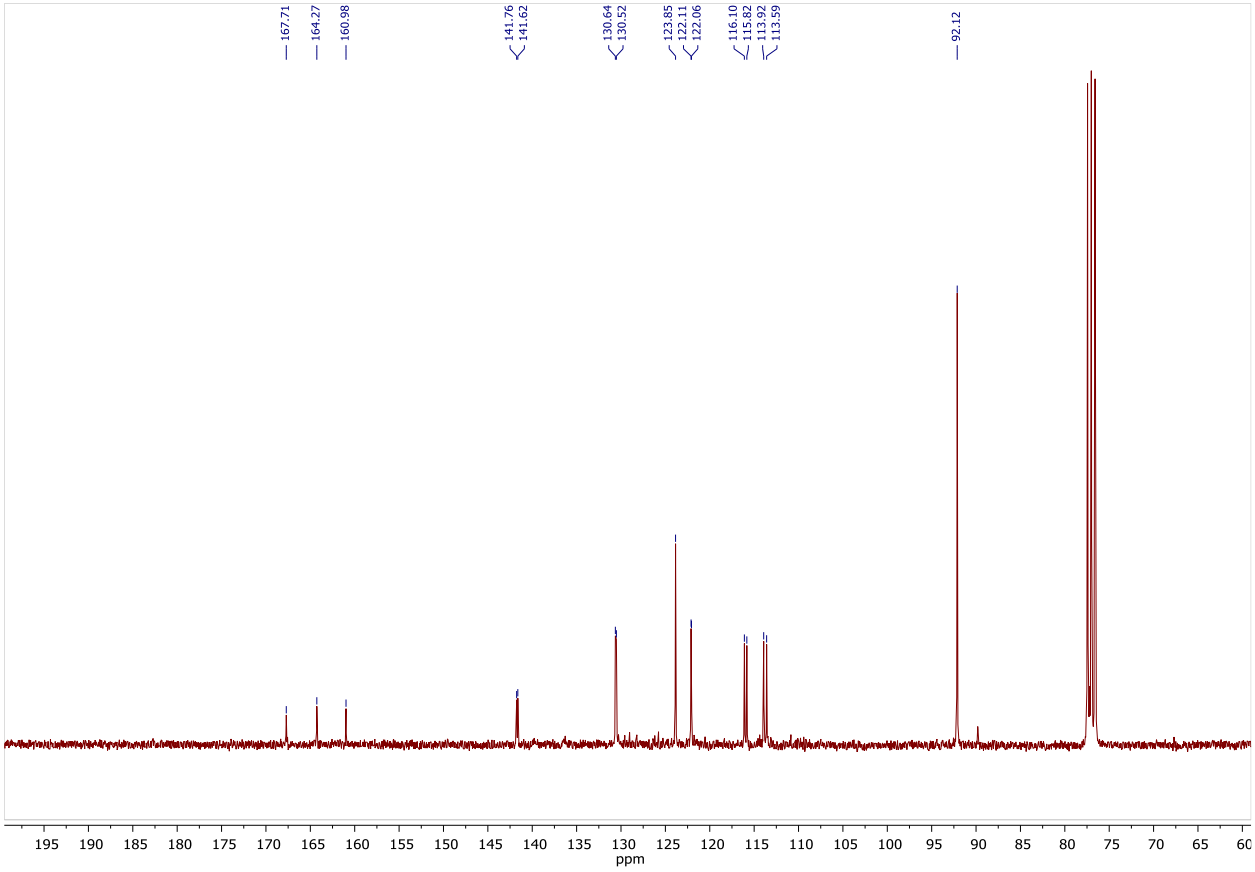

Figure S64. $^{13}C\{^{1}H\}$ NMR spectrum of **4i**. Solvent: $CDCl_3$, 75 MHz.

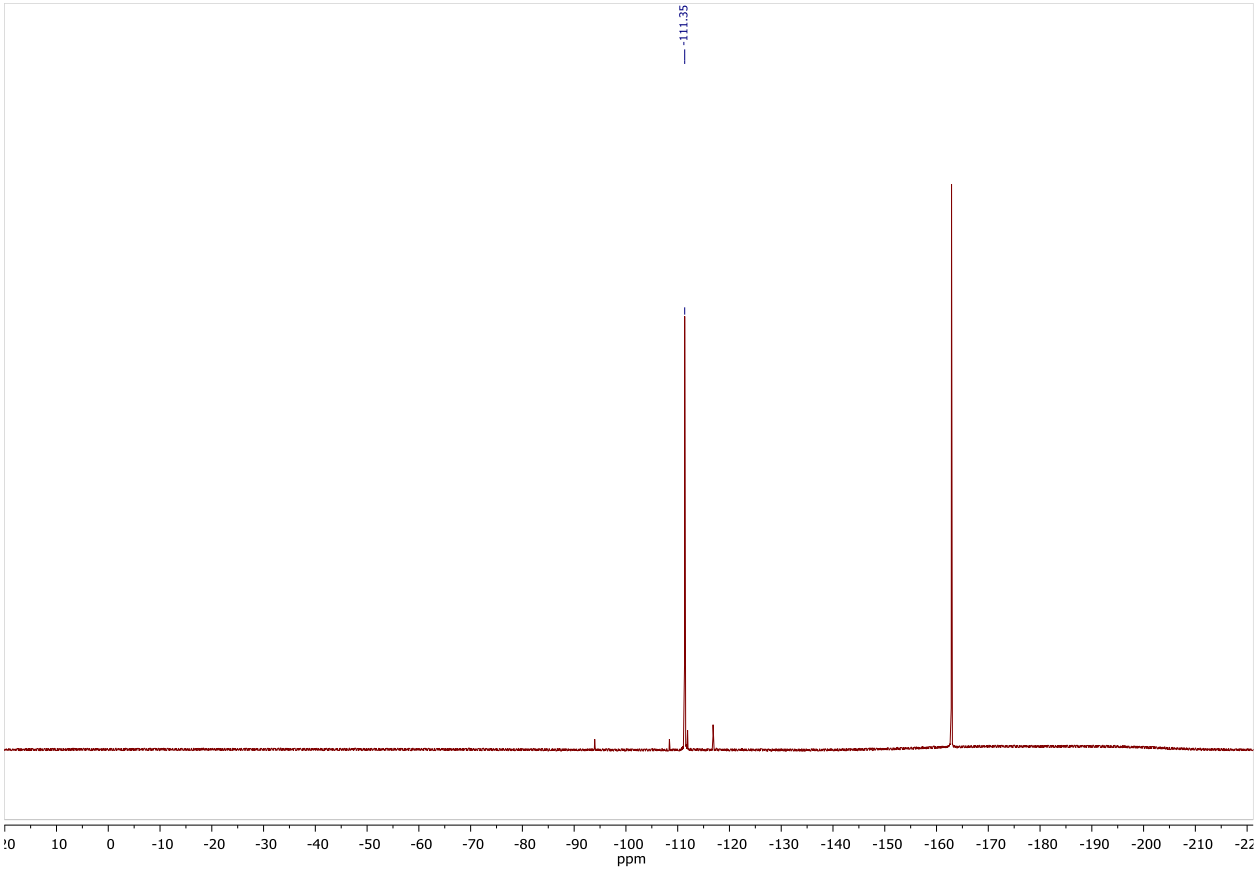

Figure S65. $^{19}F\{^{1}H\}$ NMR spectrum of **4i**. Solvent: $CDCl_3$, 282.4 MHz. Standard: C_6F_6 with respect to $CFCl_3$.

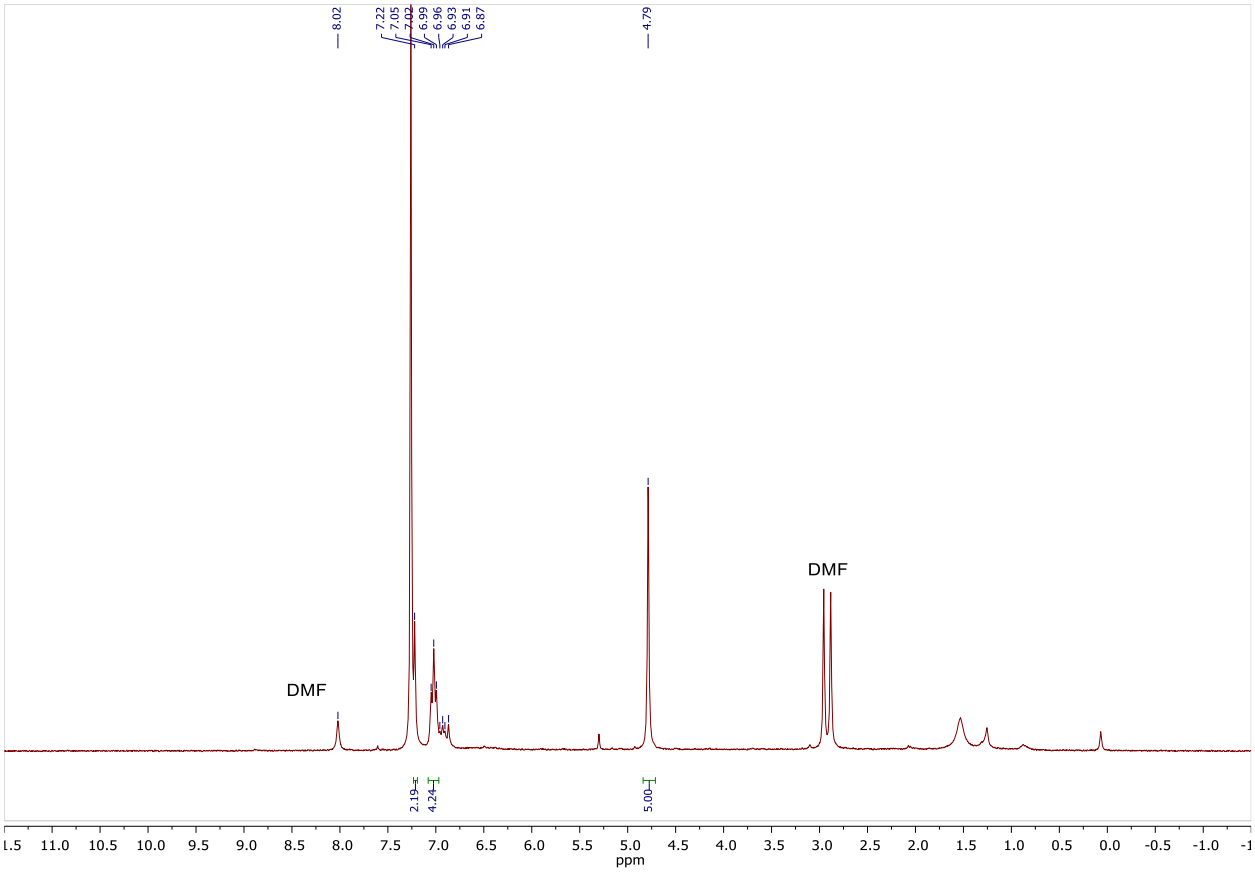

Figure S66. ^{1}H NMR spectrum of **4j**. Solvent: $CDCl_3$, 300 MHz.

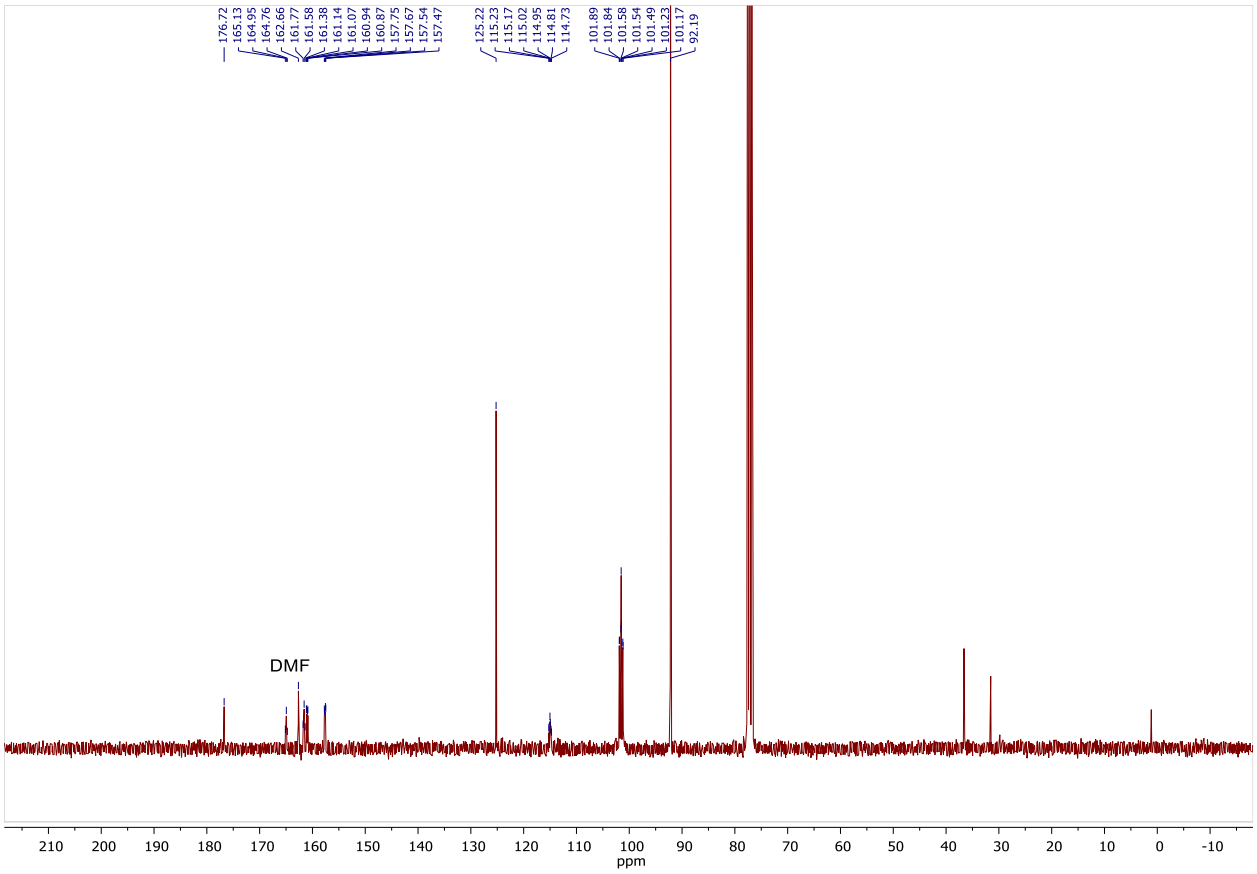

Figure S67. ^{13}C{^{1}H} NMR spectrum of **4j**. Solvent: $CDCl_3$, 75 MHz.

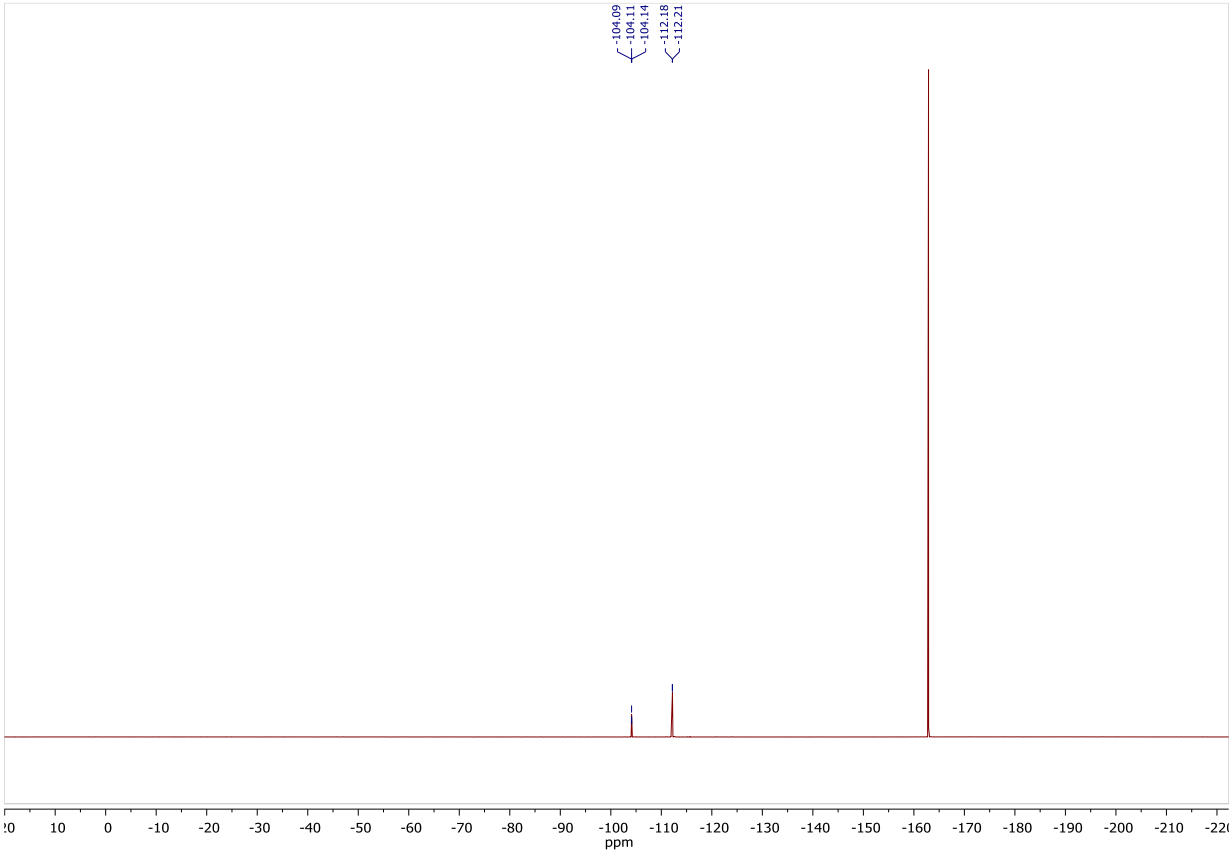

Figure S68. $^{19}F\{^{1}H\}$ NMR spectrum of **4j**. Solvent: $CDCl_3$, 282.4 MHz. Standard: C_6F_6 with respect to $CFCl_3$.

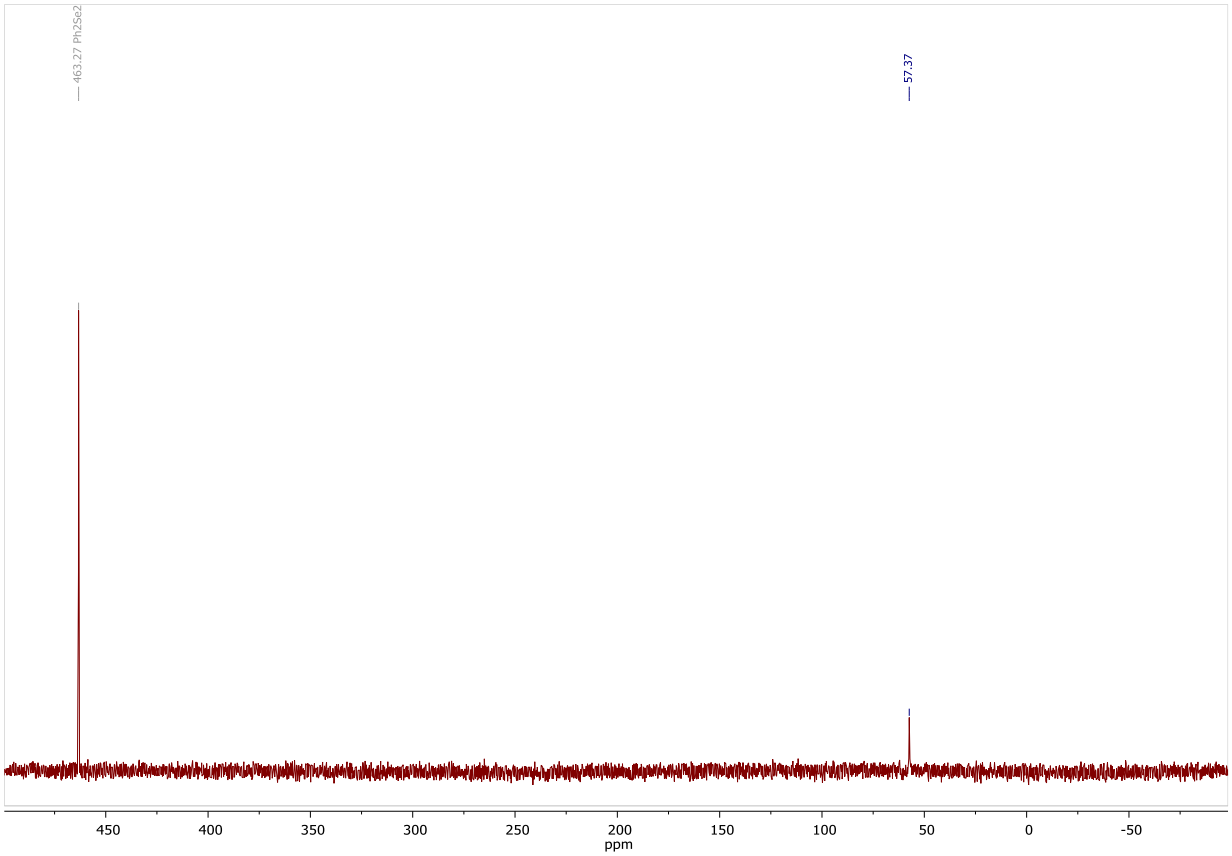

Figure S69. $^{77}Se\{^{1}H\}$ NMR spectrum of compound **5a**. Solvent: $CDCl_3$, 57 MHz. Standard: Ph_2Se_2.

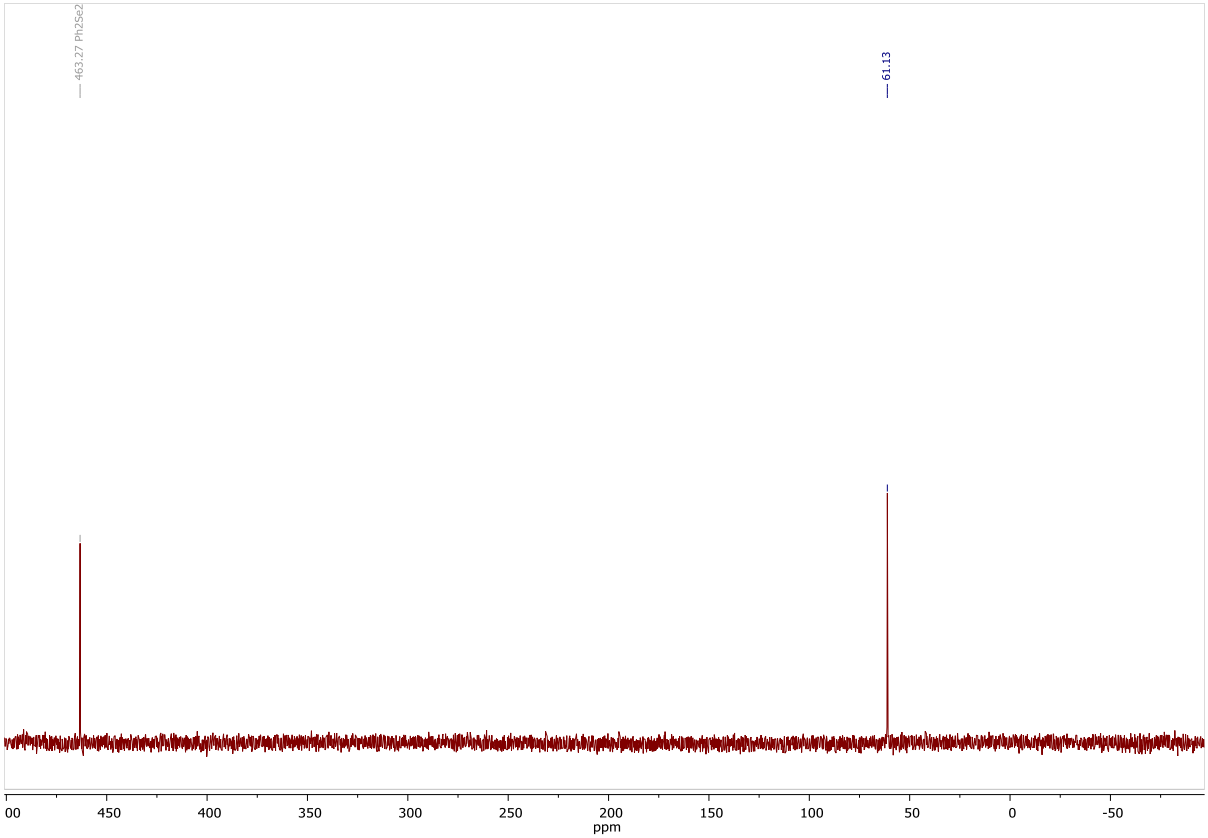

Figure S70. $^{77}Se\{^{1}H\}$ NMR spectrum of compound **5b**. Solvent: $CDCl_3$, 57 MHz. Standard: Ph_2Se_2.

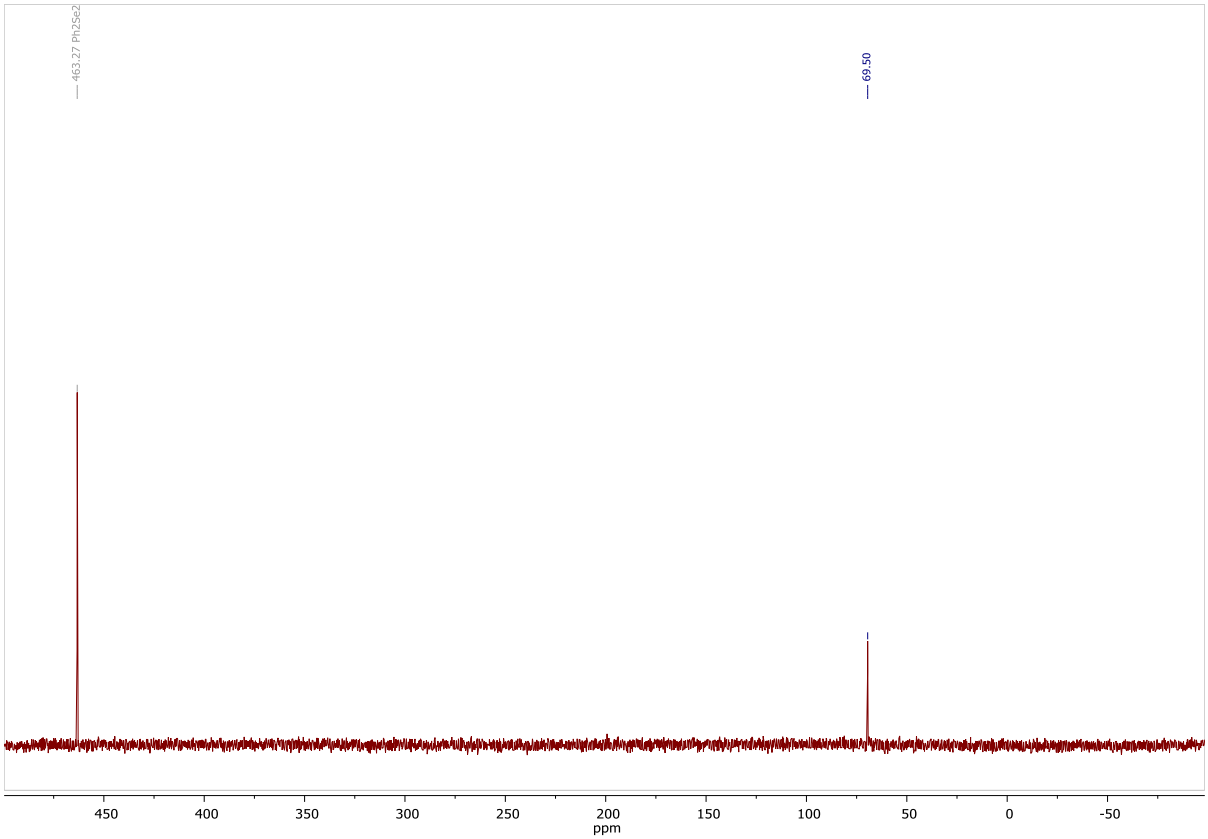

Figure S71. $^{77}Se\{^{1}H\}$ NMR spectrum of compound **5c**. Solvent: $CDCl_3$, 57 MHz. Standard: Ph_2Se_2.

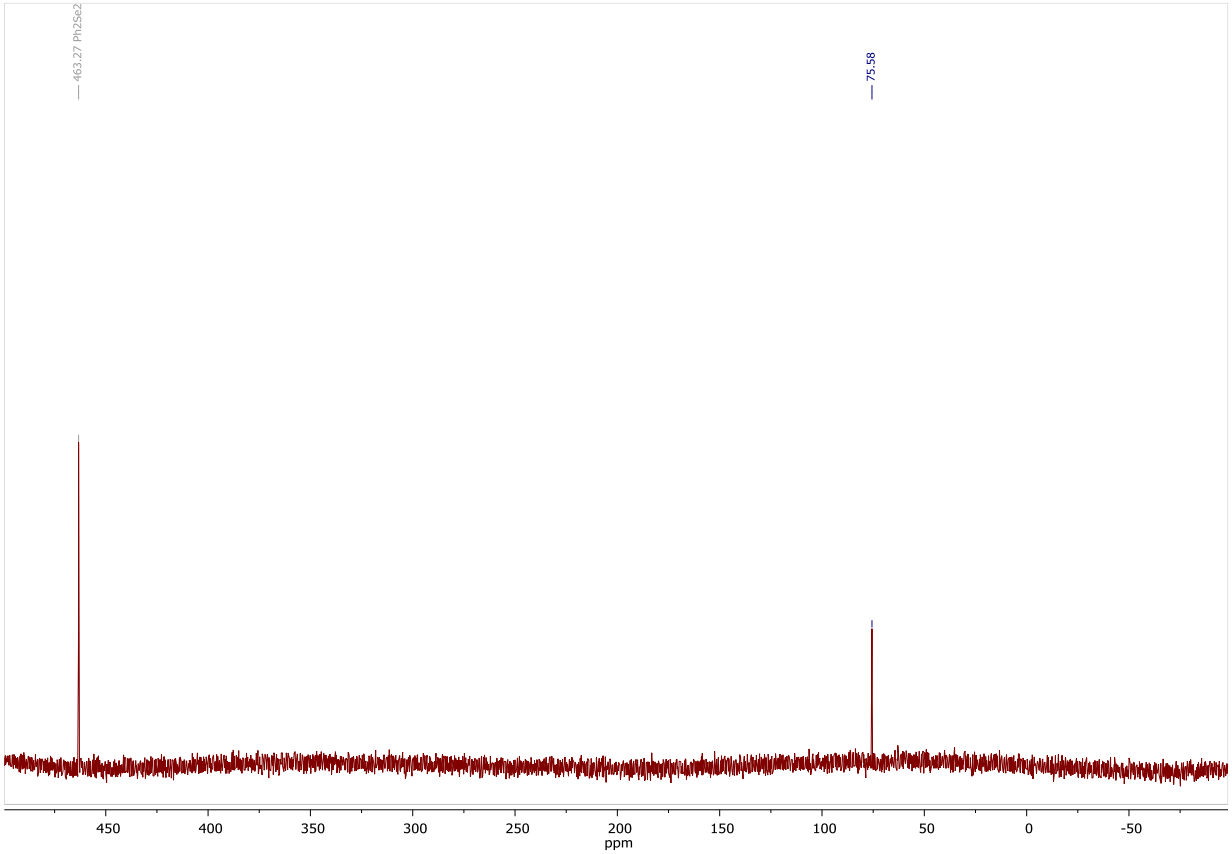

Figure S72. $^{77}Se\{^{1}H\}$ NMR spectrum of compound **5d**. Solvent: $CDCl_3$, 57 MHz. Standard: Ph_2Se_2.

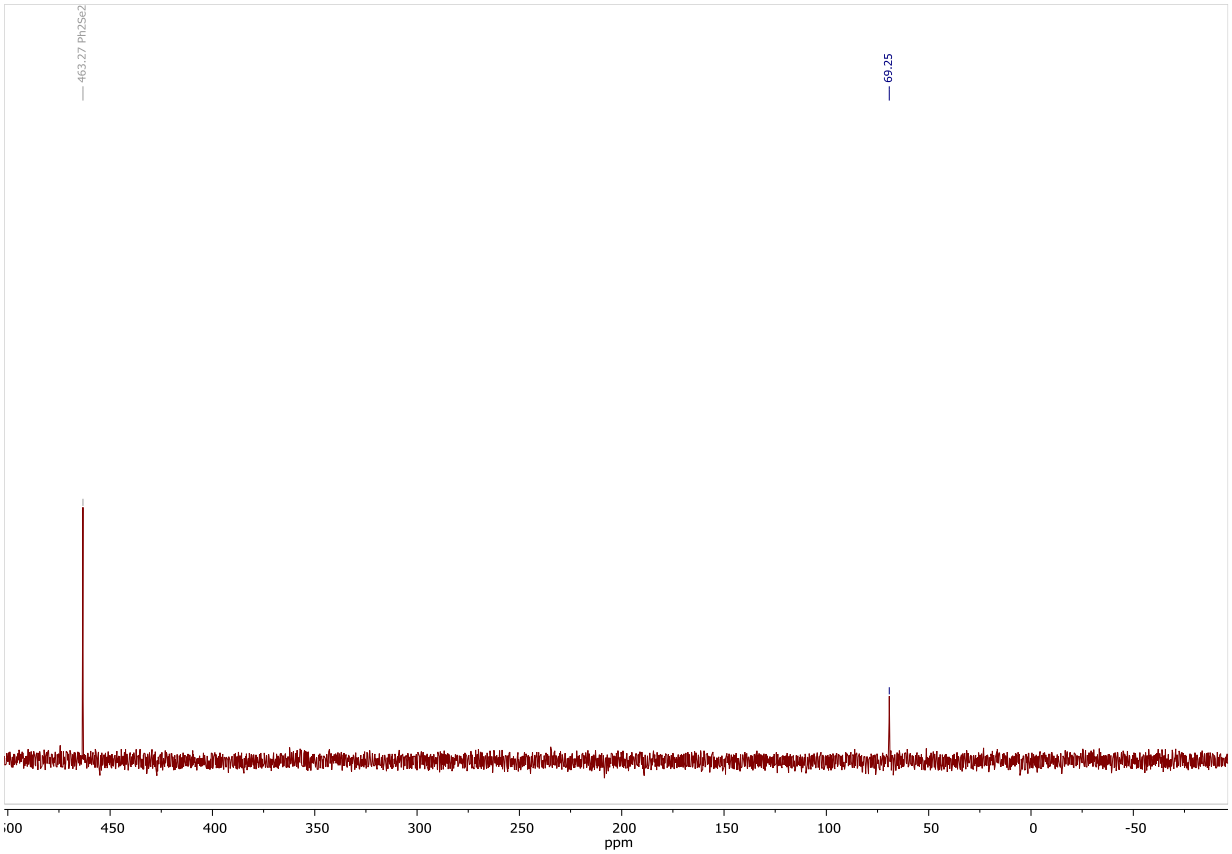

Figure S73. $^{77}Se\{^{1}H\}$ NMR spectrum of compound **5e**. Solvent: $CDCl_3$, 57 MHz. Standard: Ph_2Se_2.

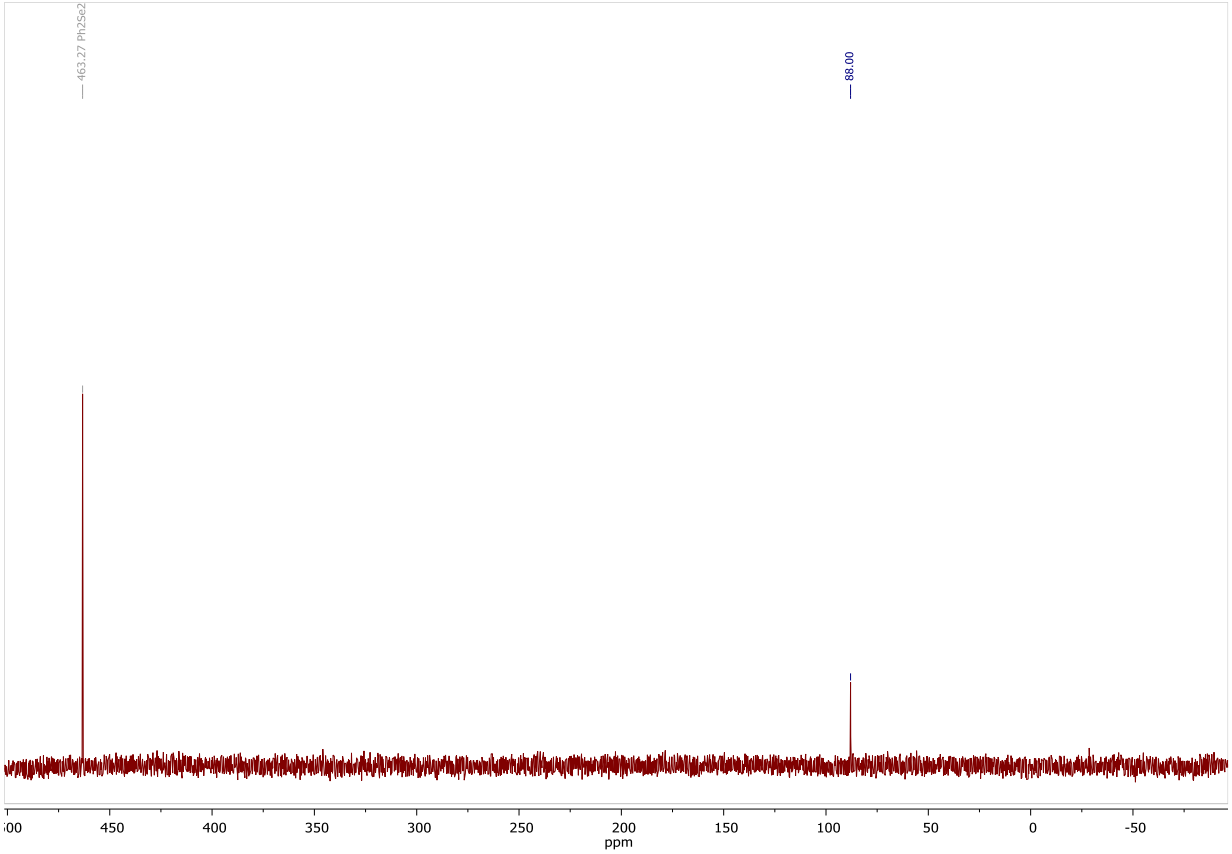

Figure S74. $^{77}Se\{^{1}H\}$ NMR spectrum of compound **5f**. Solvent: $CDCl_3$, 57 MHz. Standard: Ph_2Se_2.

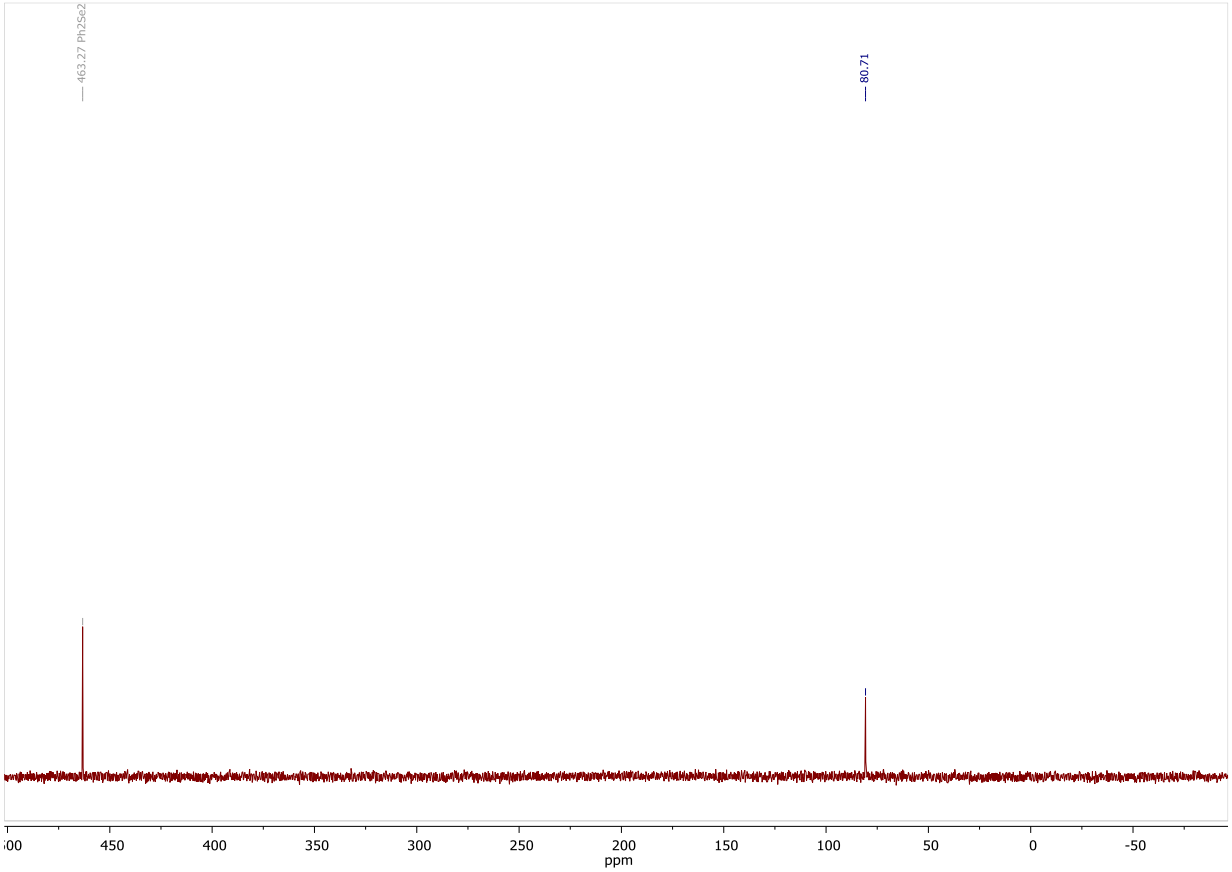

Figure S75. $^{77}Se\{^{1}H\}$ NMR spectrum of compound **5g**. Solvent: $CDCl_3$, 57 MHz. Standard: Ph_2Se_2.

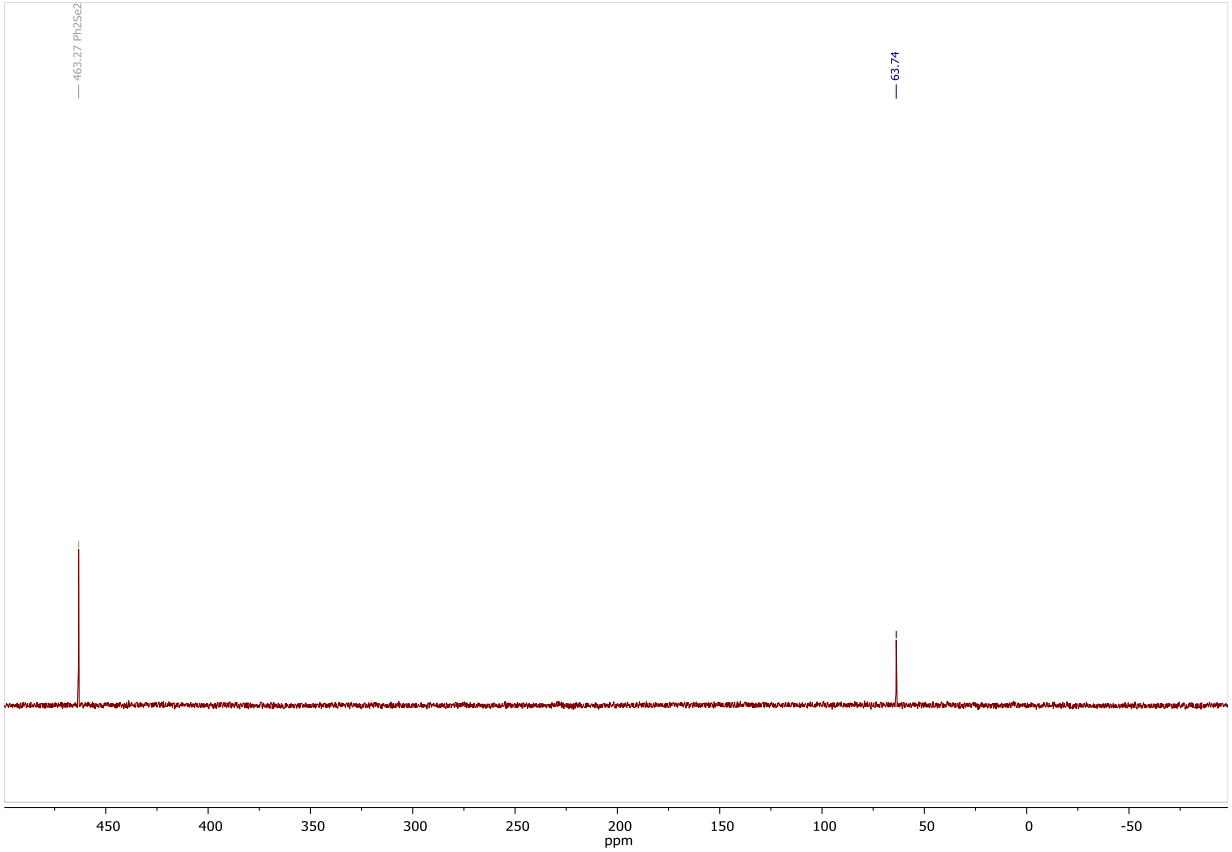

Figure S76. $^{77}Se\{^{1}H\}$ NMR spectrum of compound **5h**. Solvent: $CDCl_3$, 57 MHz. Standard: Ph_2Se_2.

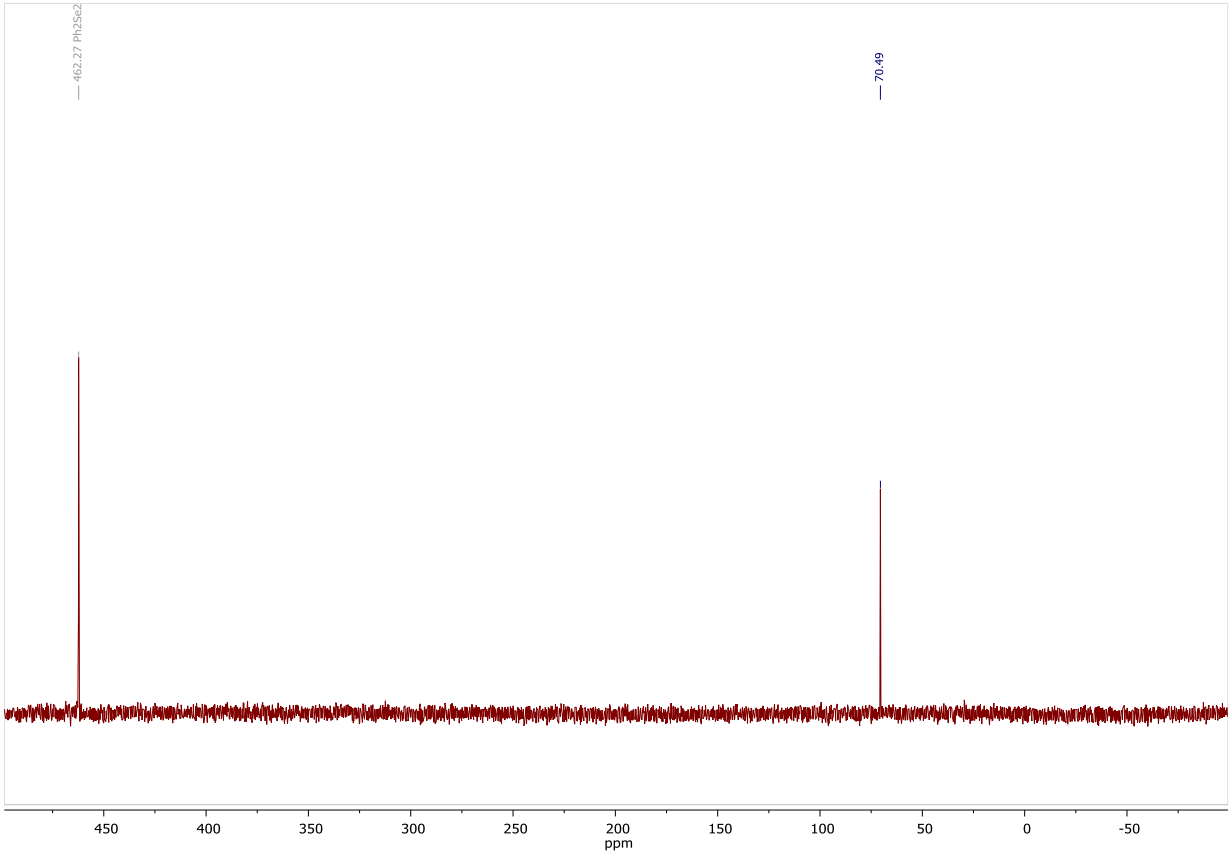

Figure S77. $^{77}Se\{^{1}H\}$ NMR spectrum of compound **5i**. Solvent: $CDCl_3$, 57 MHz. Standard: Ph_2Se_2.

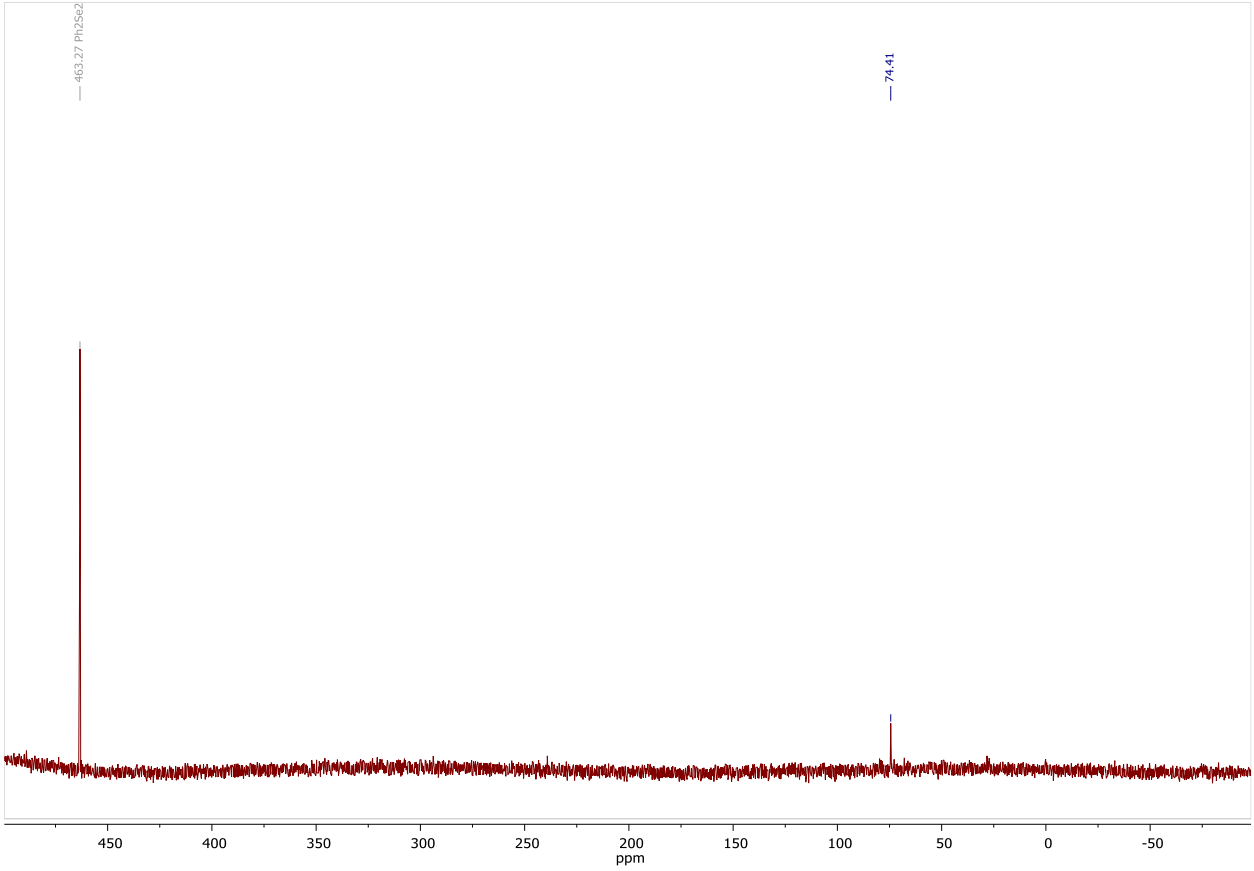

Figure S78. $^{77}Se\{^{1}H\}$ NMR spectrum of compound **5j**. Solvent: $CDCl_3$, 57 MHz. Standard: Ph_2Se_2.

3.2 ESI-HRMS spectra of the obtained compounds

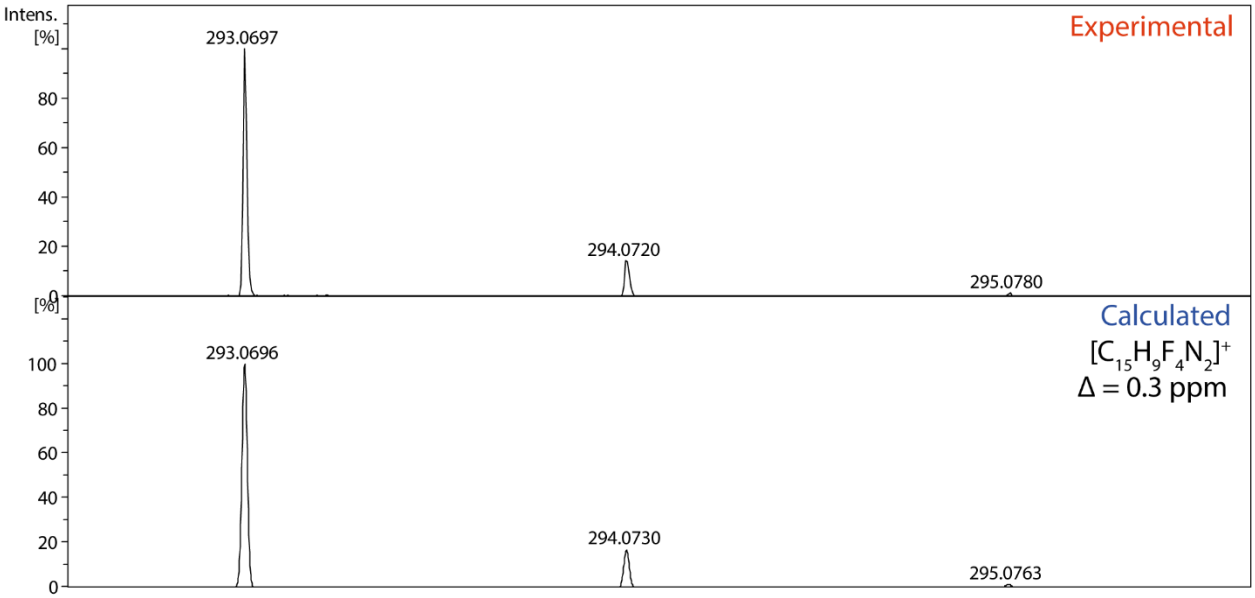

Figure S79. Experimental and theoretical ESI-(+)HRMS spectrum of **2c** in CH_3CN solution: experimental peak $[M]^+$ = 293.0697 Da, calculated for $C_{15}H_9F_4N_2$ = 293.0696, Δ = 0.3 ppm.

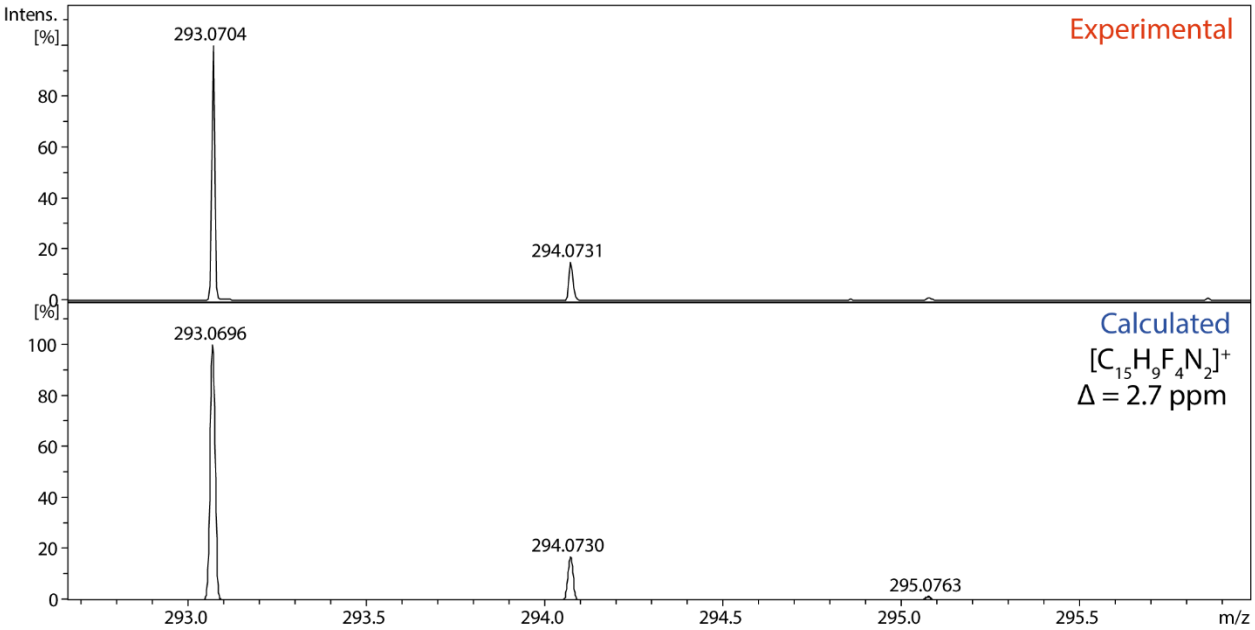

Figure S80. Experimental and theoretical ESI-(+)HRMS spectrum of **2d** in CH_3CN solution: experimental peak $[M]^+$ = 293.0704 Da, calculated for $C_{15}H_9F_4N_2$ = 293.0696, Δ = 2.7 ppm.

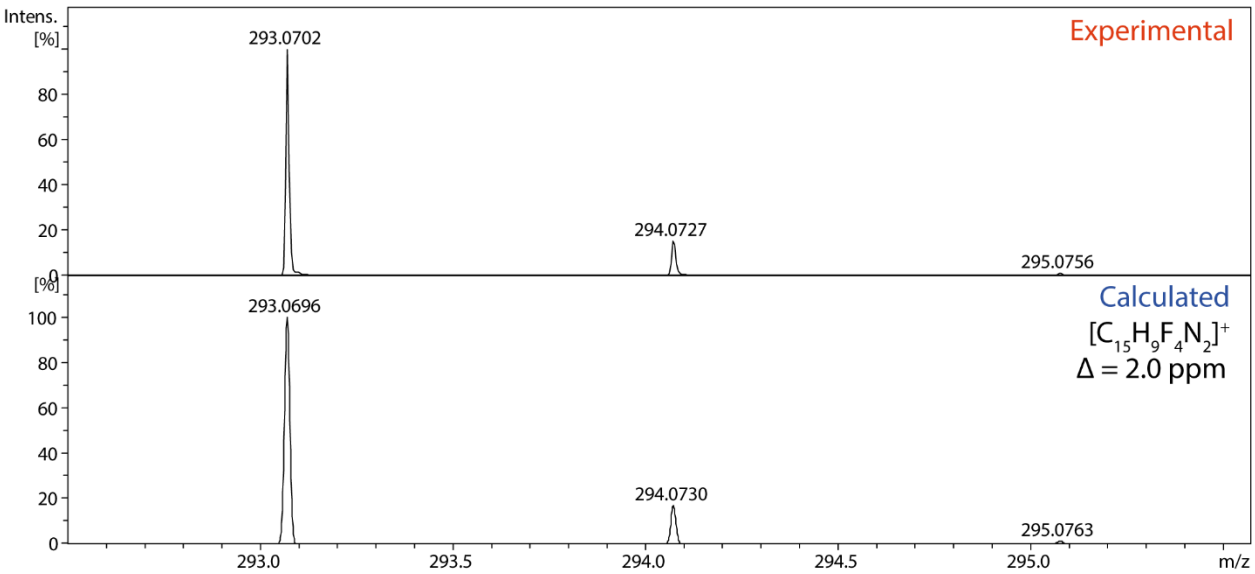

Figure S81. Experimental and theoretical ESI-(+)HRMS spectrum of **2e** in CH_3CN solution: experimental peak $[M]^+$ = 293.0702 Da, calculated for $C_{15}H_9F_4N_2$ = 293.0696, Δ = 2.0 ppm.

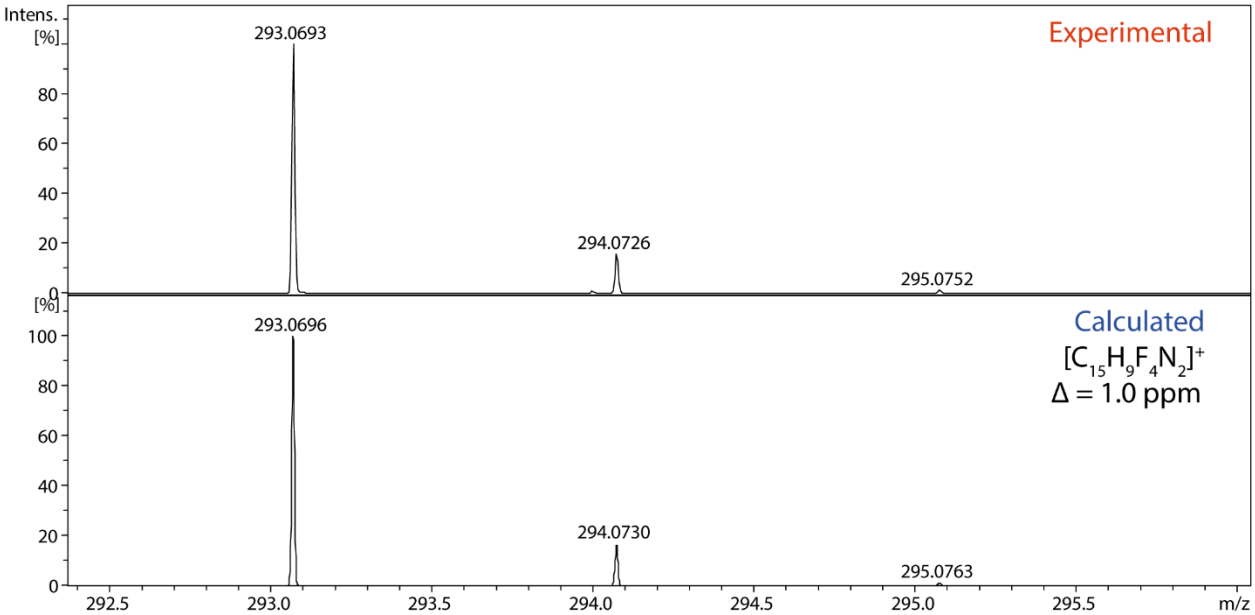

Figure S82. Experimental and theoretical ESI-(+)HRMS spectrum of **2f** in CH_3CN solution: experimental peak $[M]^+$ = 293.0693 Da, calculated for $C_{15}H_9F_4N_2$ = 293.0696, Δ = 1.0 ppm.

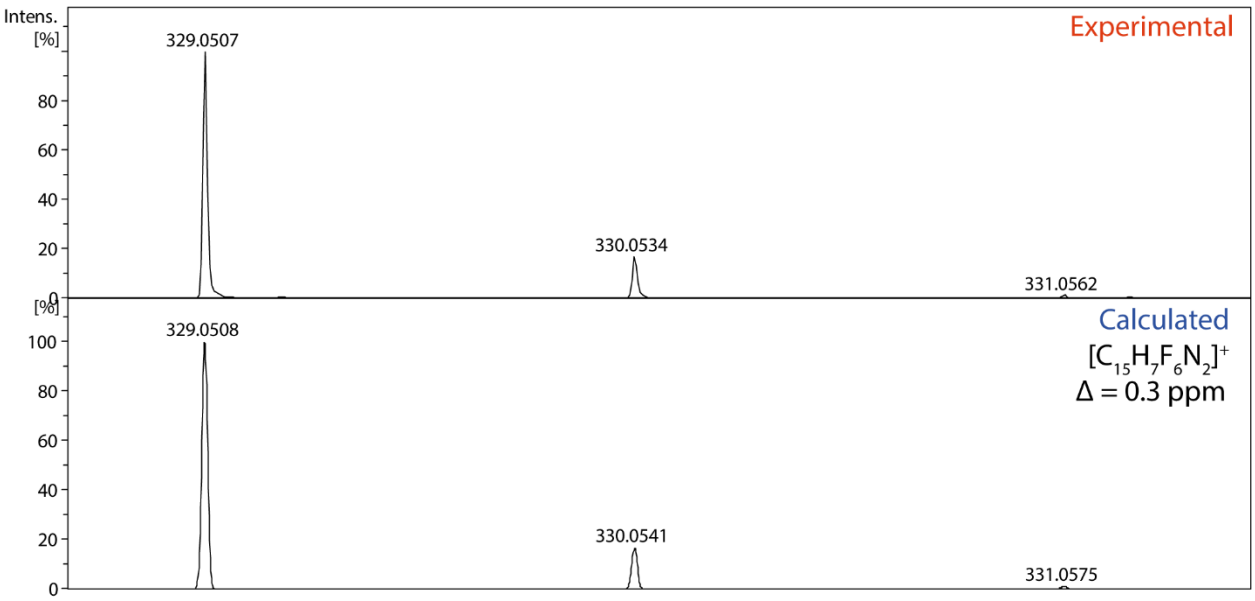

Figure S83. Experimental and theoretical ESI-(+)HRMS spectrum of **2g** in CH_3CN solution: experimental peak $[M]^+$ = 329.0507 Da, calculated for $C_{15}H_7F_6N_2$ = 329.0508, Δ = 0.3 ppm.

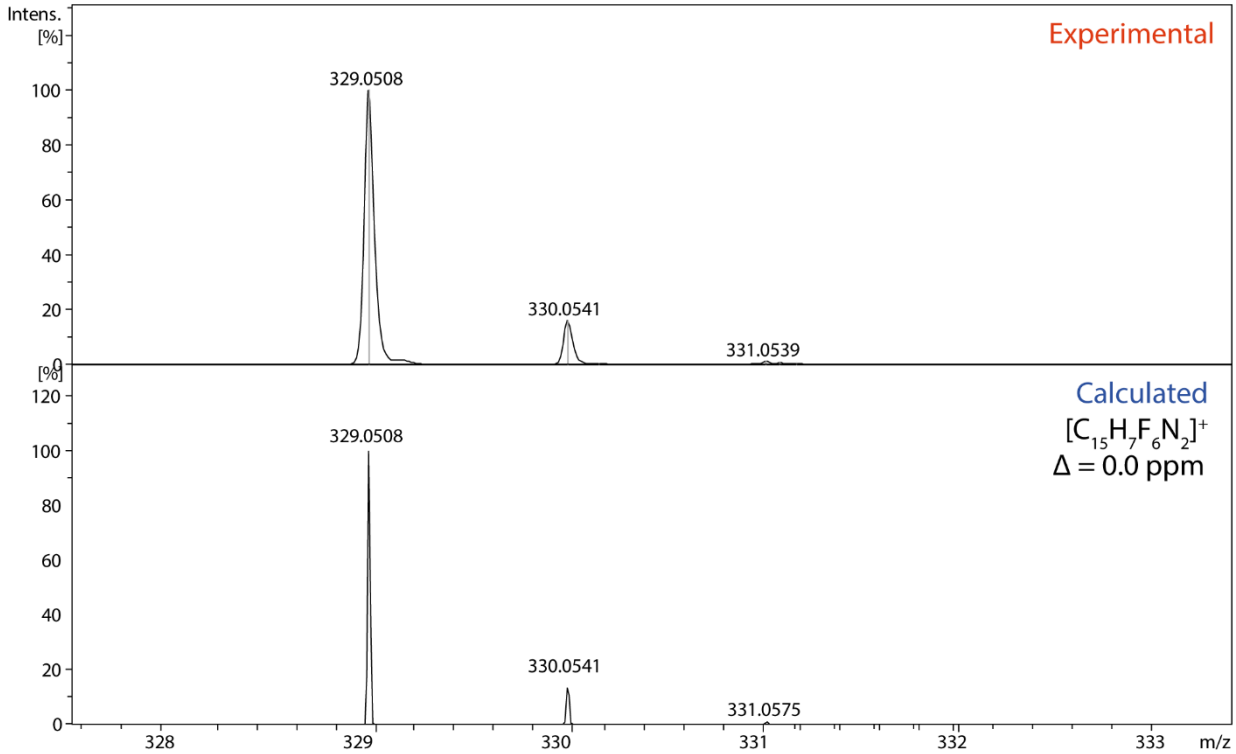

Figure S84. Experimental and theoretical ESI-(+)HRMS spectrum of **2j** in CH_3CN solution: experimental peak $[M]^+$ = 329.0508 Da, calculated for $C_{15}H_7F_6N_2$ = 329.0508, Δ = 0.0 ppm.

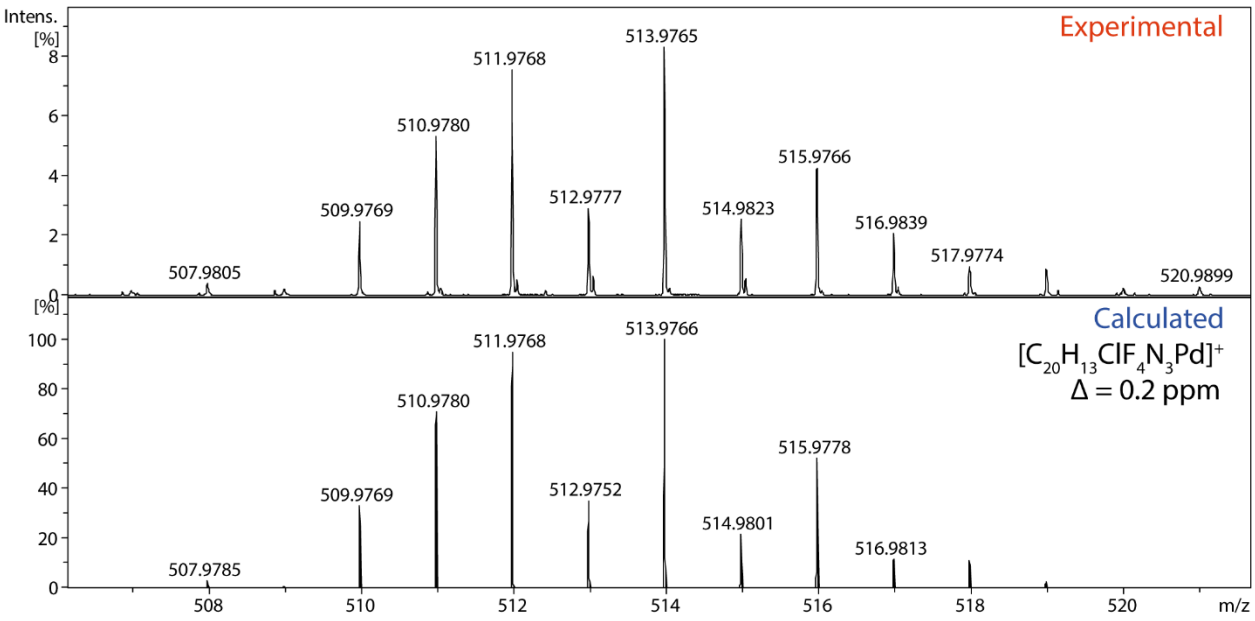

Figure S85. Experimental and theoretical ESI-(+)HRMS spectrum of **3c** in CH_3CN solution: experimental peak $[M]^+$ = 513.9765 Da, calculated for $C_{20}H_{13}ClF_4N_3Pd$ = 513.9766, Δ = 0.2 ppm.

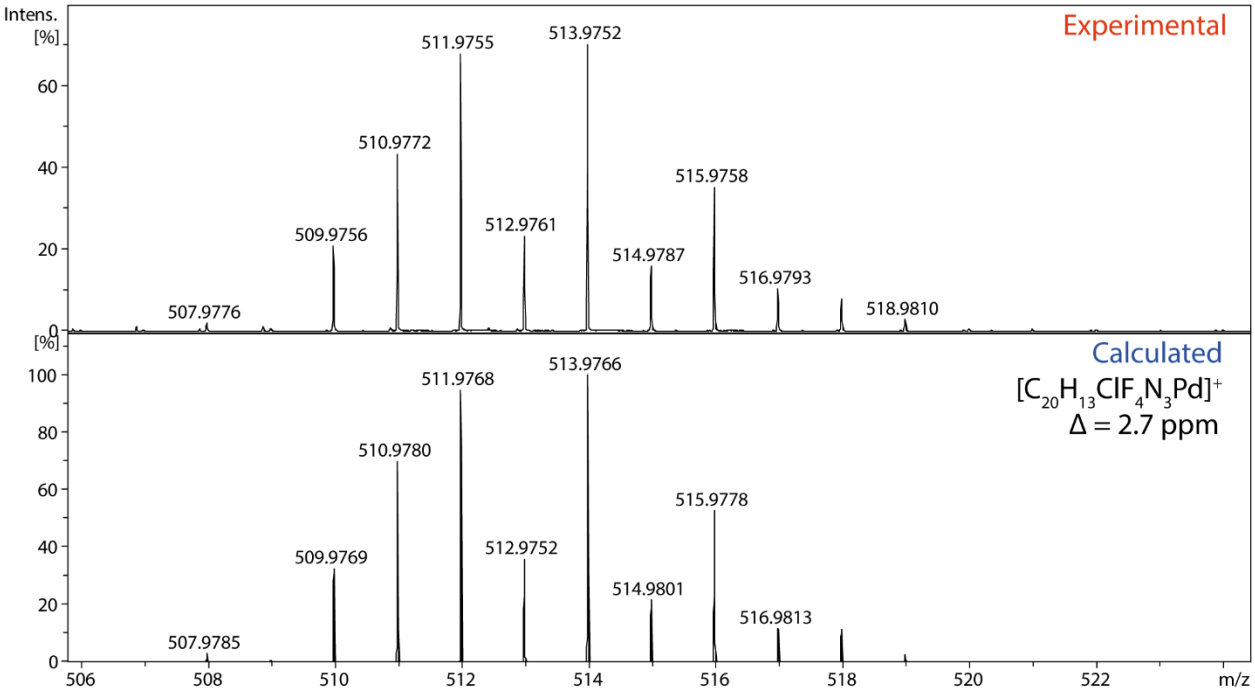

Figure S86. Experimental and theoretical ESI-(+)HRMS spectrum of **3d** in CH_3CN solution: experimental peak $[M]^+$ = 513.9752 Da, calculated for $C_{20}H_{13}ClF_4N_3Pd$ = 513.9766, Δ = 2.7 ppm.

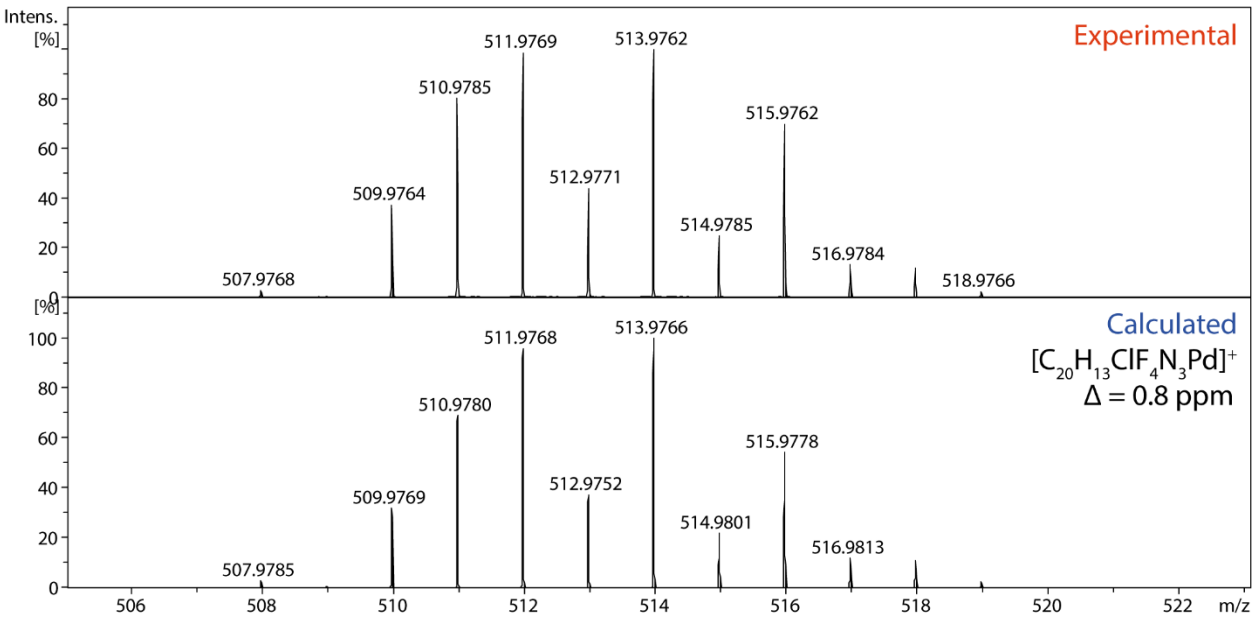

Figure S87. Experimental and theoretical ESI-(+)HRMS spectrum of **3e** in CH_3CN solution: experimental peak $[M]^+$ = 513.9762 Da, calculated for $C_{20}H_{13}ClF_4N_3Pd$ = 513.9766, Δ = 0.8 ppm.

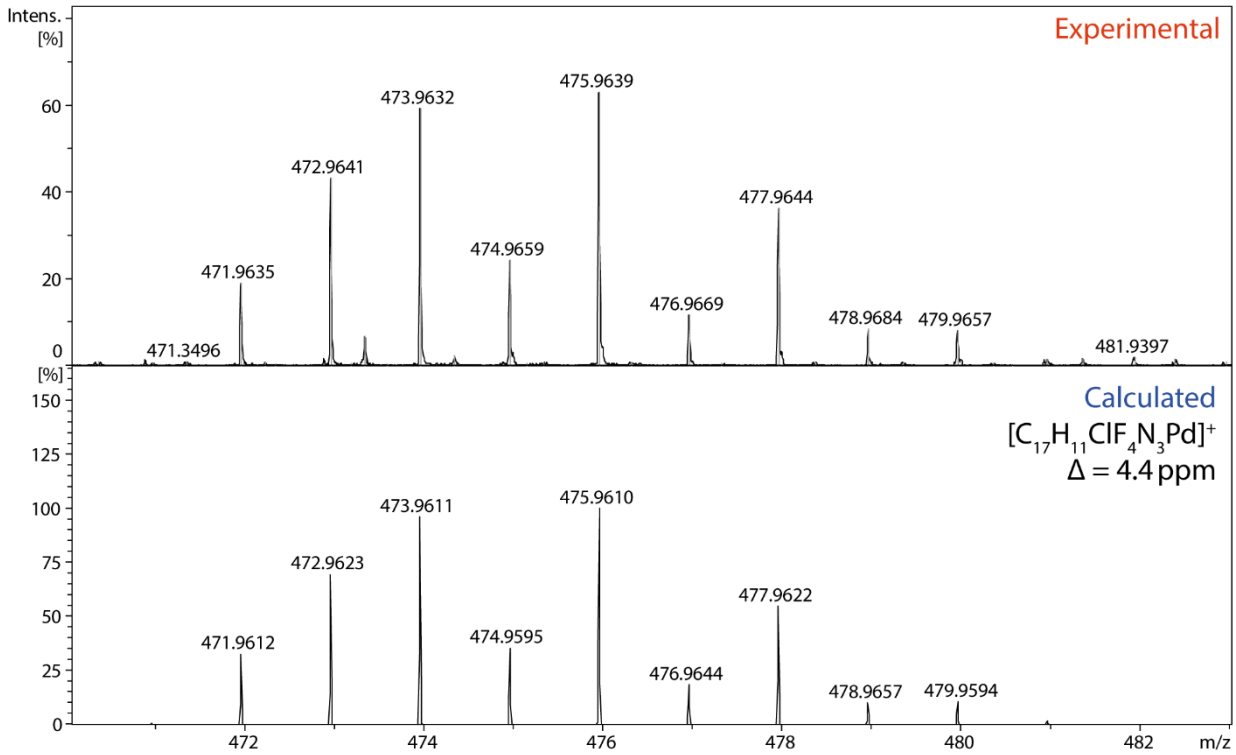

Figure S88. Experimental and theoretical ESI-(+)HRMS spectrum of **3f** in CH_3CN solution: experimental peak $[M]^+$ = 473.9632 Da, calculated for $C_{17}H_{11}ClF_4N_3Pd$ = 473.9611, Δ = 4.4 ppm.

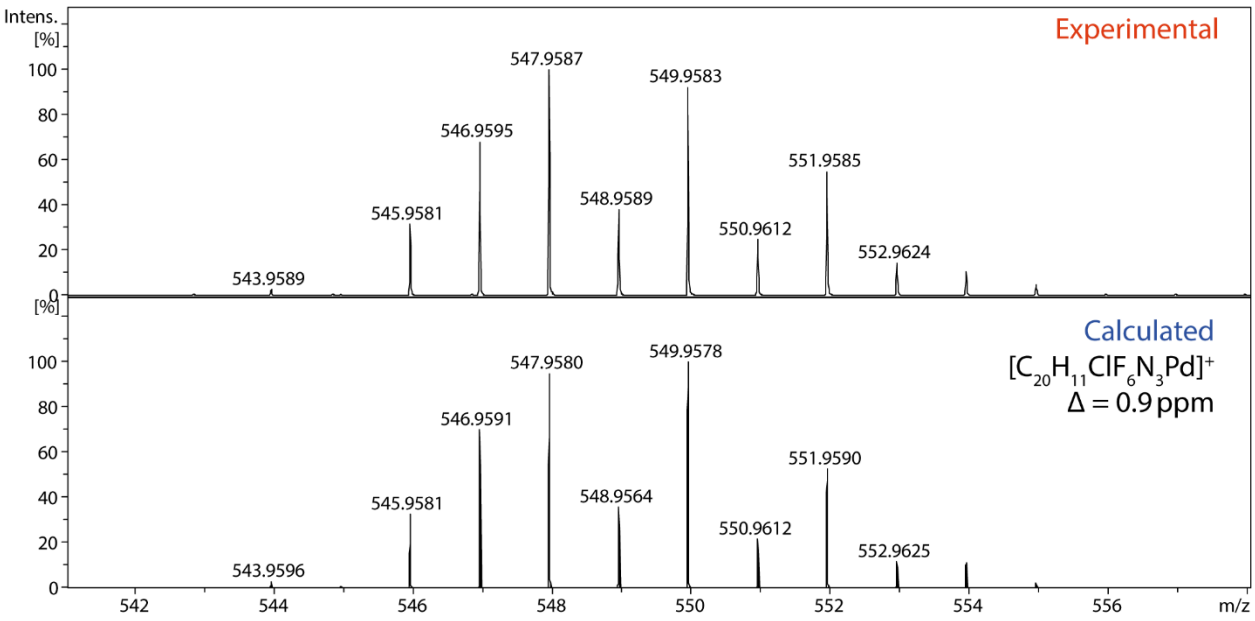

Figure S89. Experimental and theoretical ESI-(+)HRMS spectrum of **3g** in CH_3CN solution: experimental peak $[M]^+$ = 549.9583 Da, calculated for $C_{20}H_{11}ClF_6N_3Pd$ = 549.9578, Δ = 0.9 ppm.

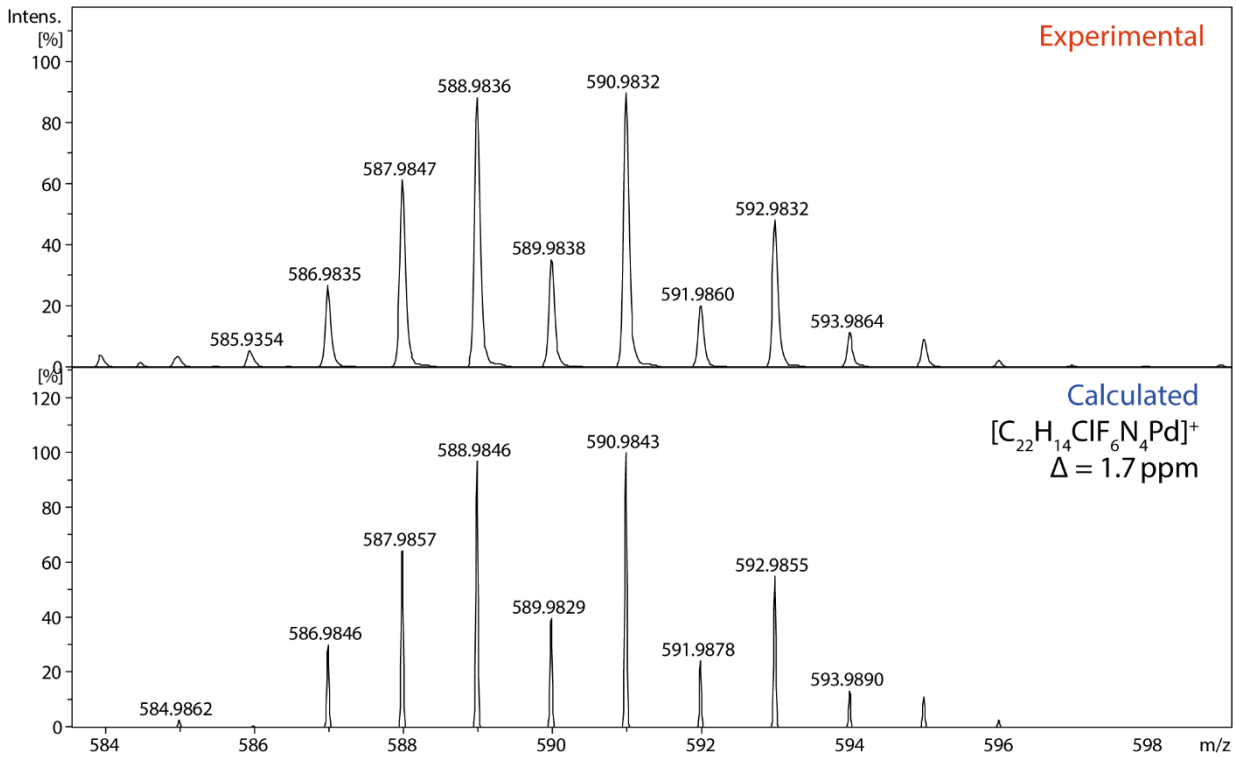

Figure S90. Experimental and theoretical ESI-(+)HRMS spectrum of **3ja** in CH_3CN solution: experimental peak $[M]^+$ = 588.9836 Da, calculated for $C_{22}H_{14}ClF_6N_4Pd$ = 588.9846, Δ = 1.7 ppm.

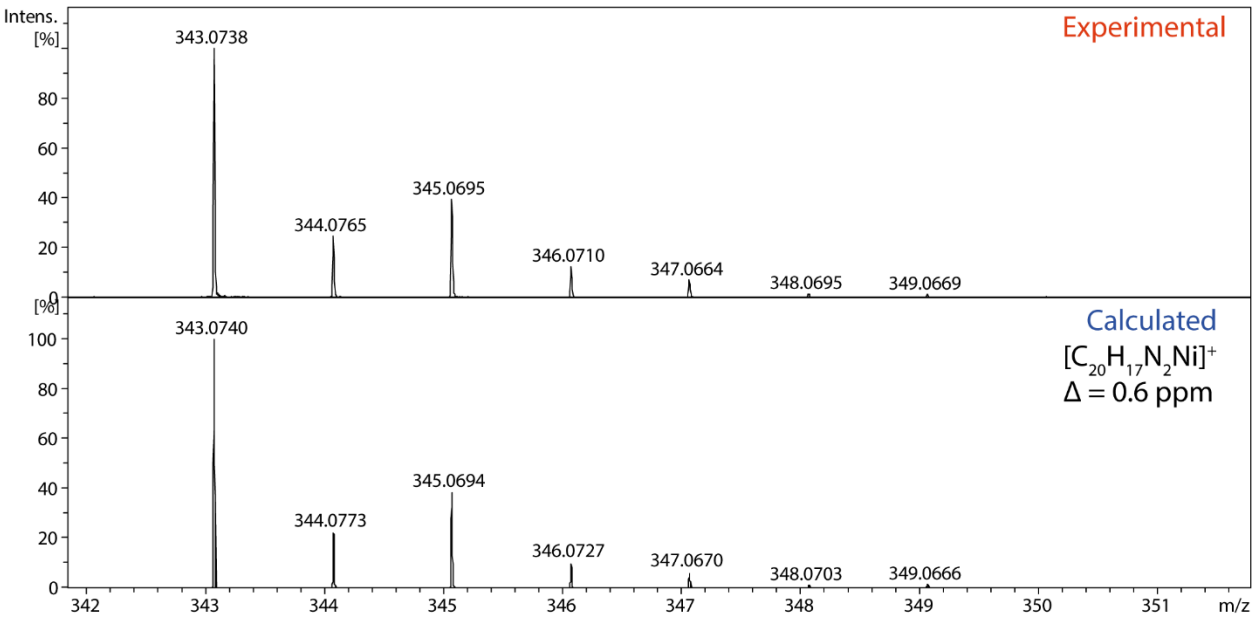

Figure S91. Experimental and theoretical ESI-(+)HRMS spectrum of **4a** in CH_3CN solution: experimental peak $[M]^+$ = 343.0738 Da, calculated for $C_{20}H_{17}N_2Ni$ = 343.0740, Δ = 0.6 ppm.

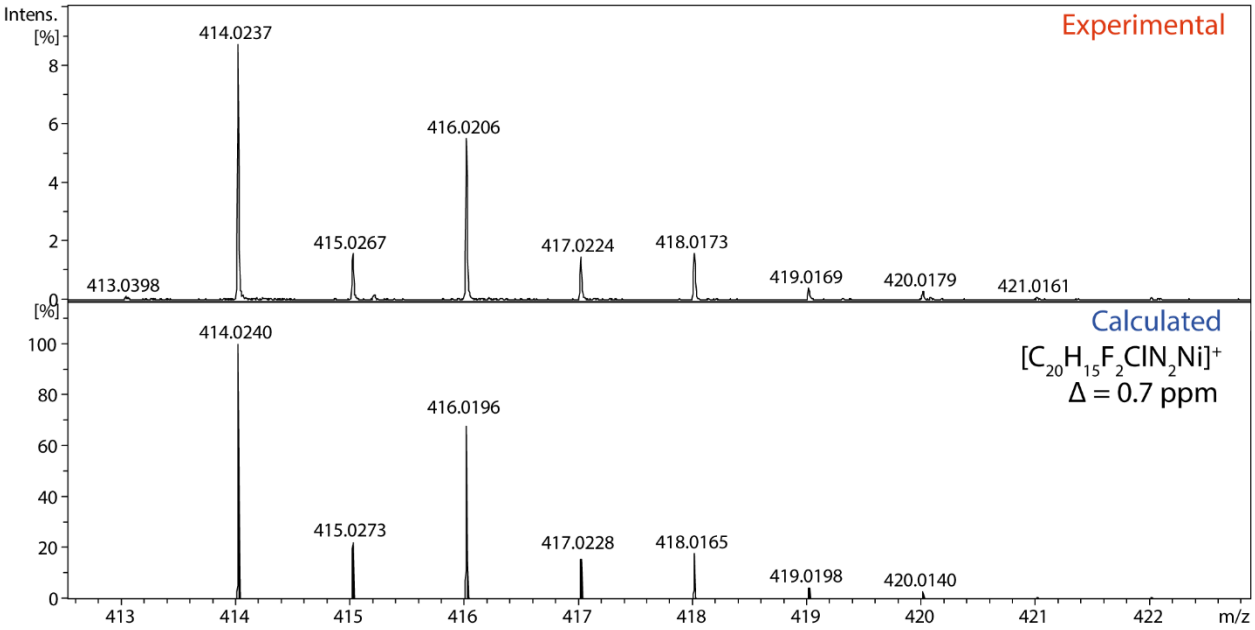

Figure S92. Experimental and theoretical ESI-(+)HRMS spectrum of **4b** in CH_3CN solution: experimental peak $[M]^+$ = 414.0237 Da, calculated for $C_{20}H_{15}ClF_2N_2Ni$ = 414.0240, Δ = 0.7 ppm.

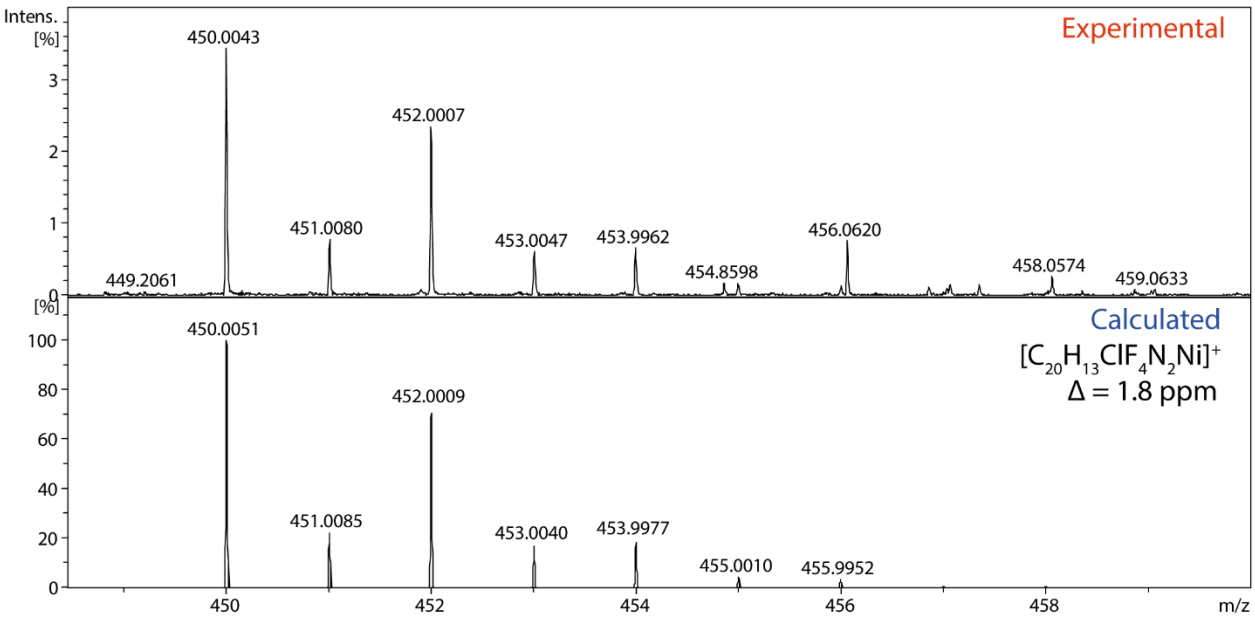

Figure S93. Experimental and theoretical ESI-(+)HRMS spectrum of **4c** in CH_3CN solution: experimental peak $[M]^+$ = 450.0043 Da, calculated for $C_{20}H_{13}ClF_4N_2Ni$ = 450.0051, Δ = 1.8 ppm.

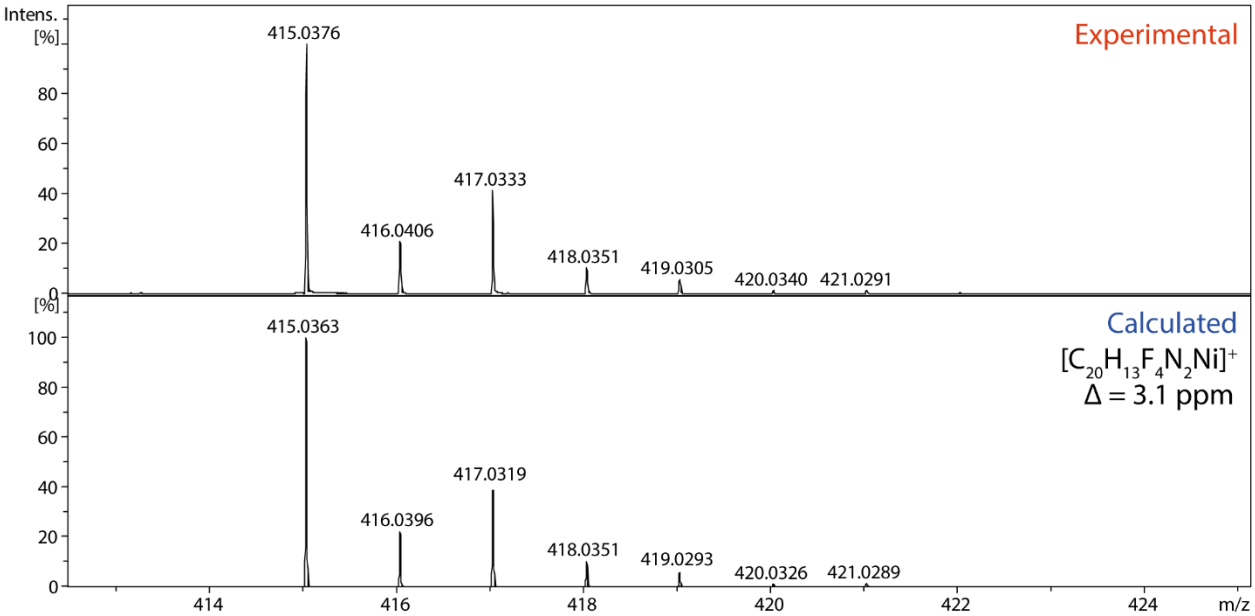

Figure S94. Experimental and theoretical ESI-(+)HRMS spectrum of **4d** in CH_3CN solution: experimental peak $[M]^+$ = 415.0376 Da, calculated for $C_{20}H_{13}F_4N_2Ni$ = 415.0363, Δ = 3.1 ppm.

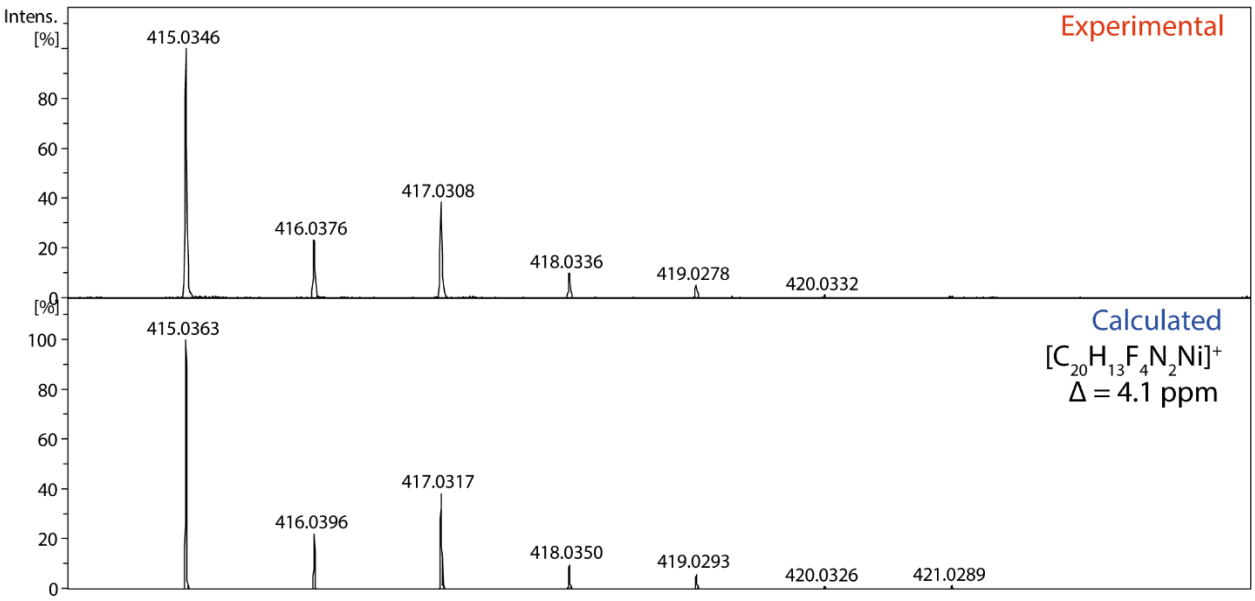

Figure S95. Experimental and theoretical ESI-(+)HRMS spectrum of **4e** in CH_3CN solution: experimental peak $[M]^+$ = 415.0346 Da, calculated for $C_{20}H_{13}F_4N_2Ni$ = 415.0363, Δ = 4.1 ppm.

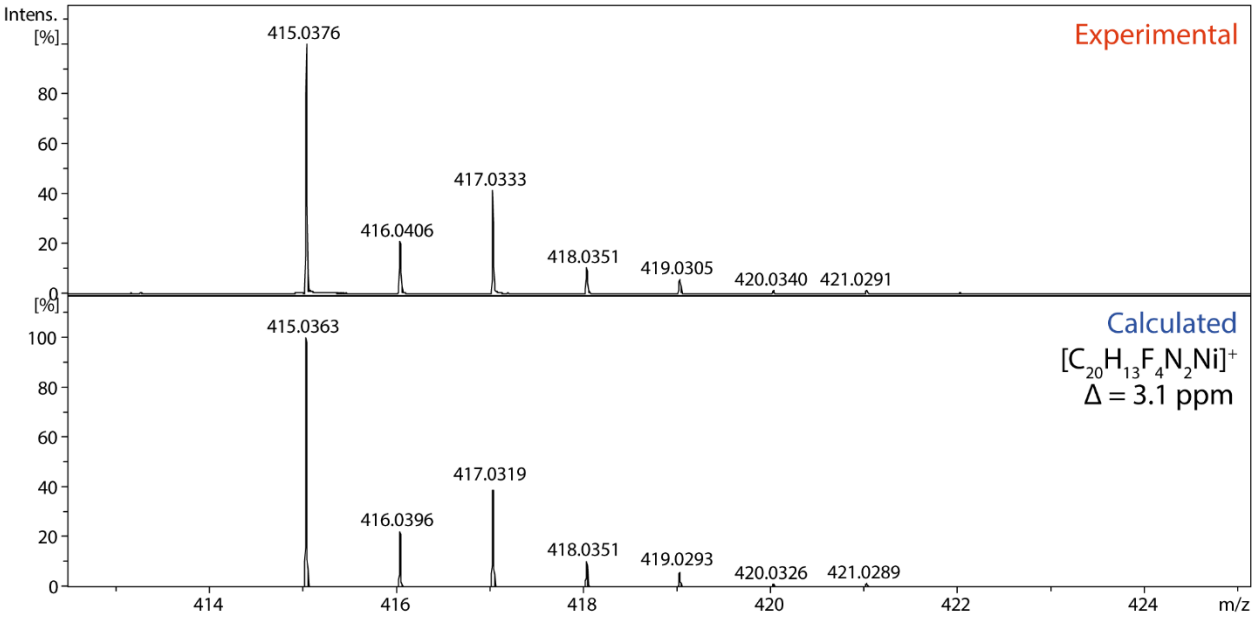

Figure S96. Experimental and theoretical ESI-(+)HRMS spectrum of **4f** in CH_3CN solution: experimental peak $[M]^+$ = 415.0376 Da, calculated for $C_{20}H_{13}F_4N_2Ni$ = 415.0363, Δ = 3.1 ppm.

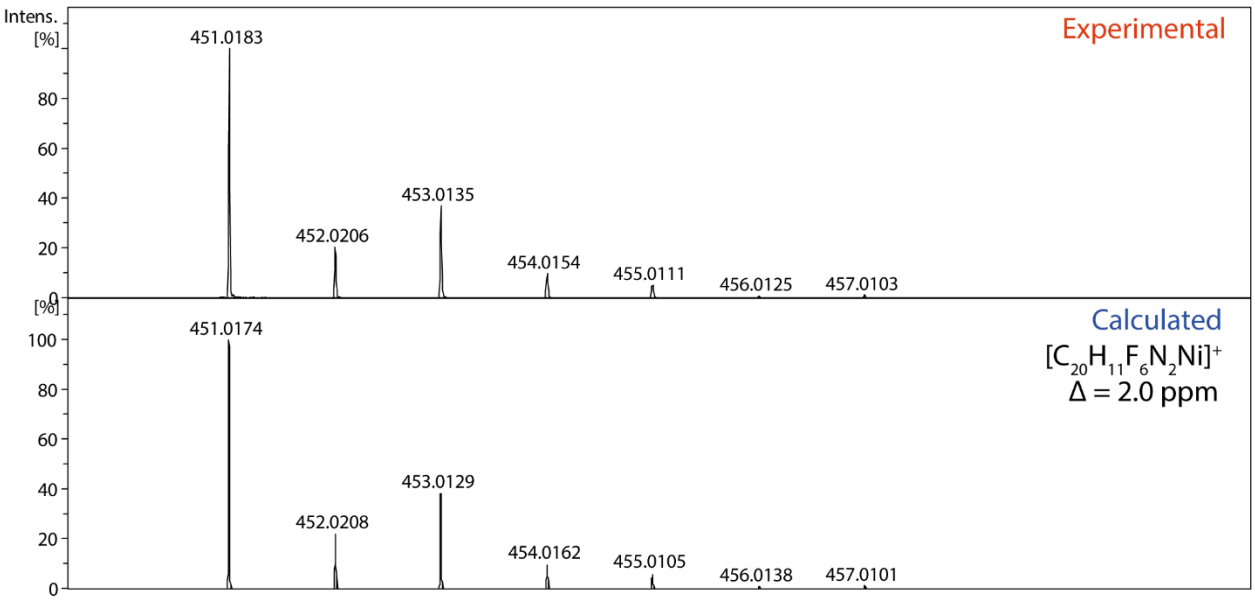

Figure S97. Experimental and theoretical ESI-(+)HRMS spectrum of **4g** in CH_3CN solution: experimental peak $[M]^+$ = 451.0183 Da, calculated for $C_{20}H_{11}F_6N_2Ni$ = 451.0174, Δ = 2.0 ppm.

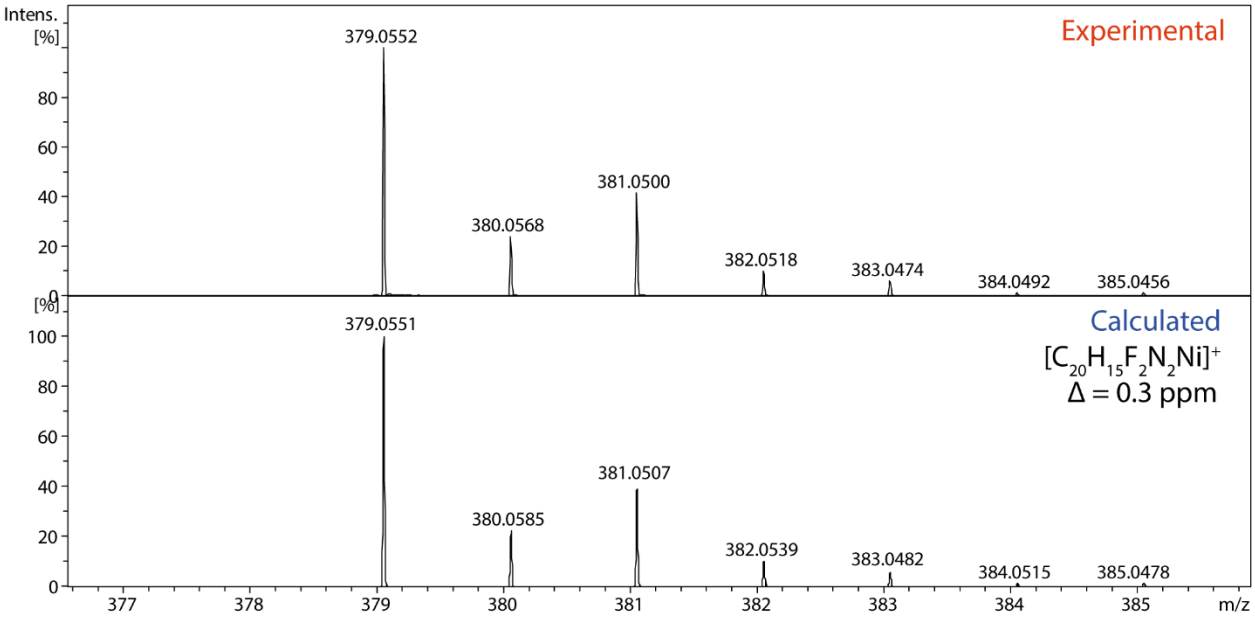

Figure S98. Experimental and theoretical ESI-(+)HRMS spectrum of **4h** in CH_3CN solution: experimental peak $[M]^+$ = 379.0552 Da, calculated for $C_{20}H_{15}F_2N_2Ni$ = 379.0551, Δ = 0.3 ppm.

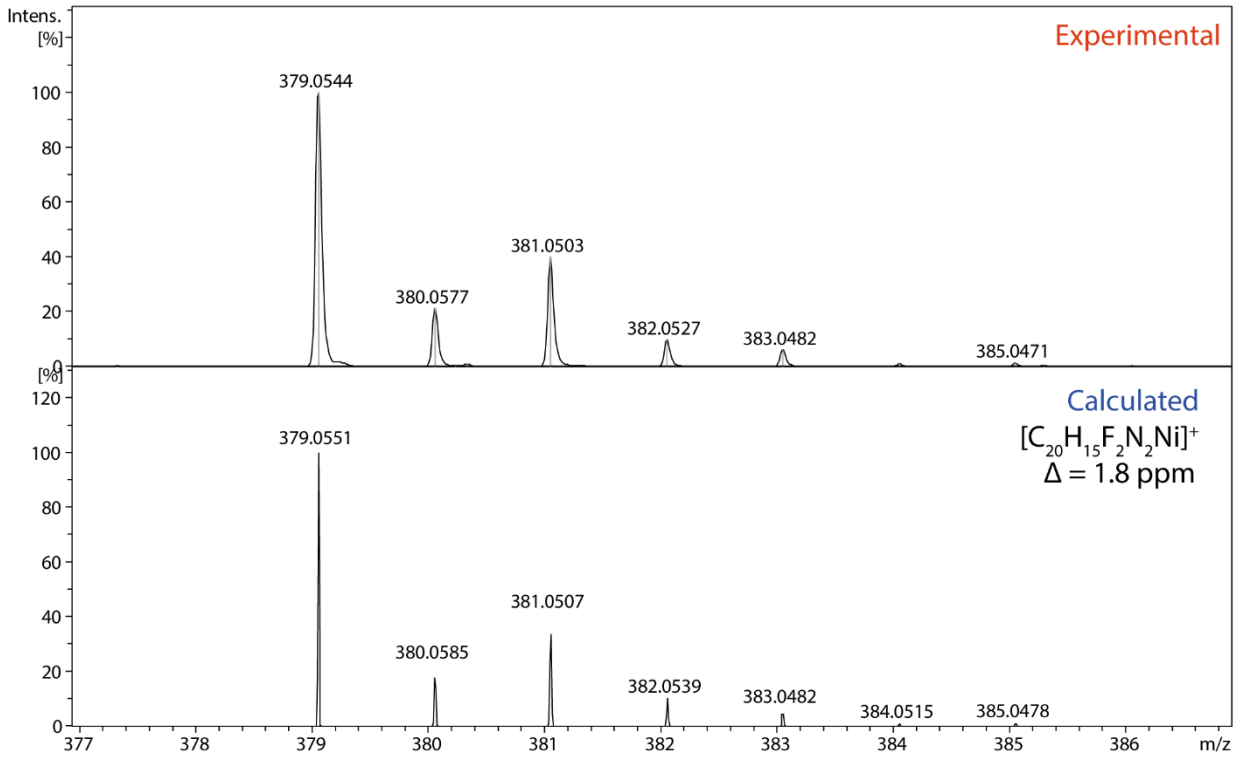

Figure S99. Experimental and theoretical ESI-(+)HRMS spectrum of **4i** in CH_3CN solution: experimental peak $[M]^+$ = 379.0544 Da, calculated for $C_{20}H_{15}F_2N_2Ni$ = 379.0551, Δ = 1.8 ppm.

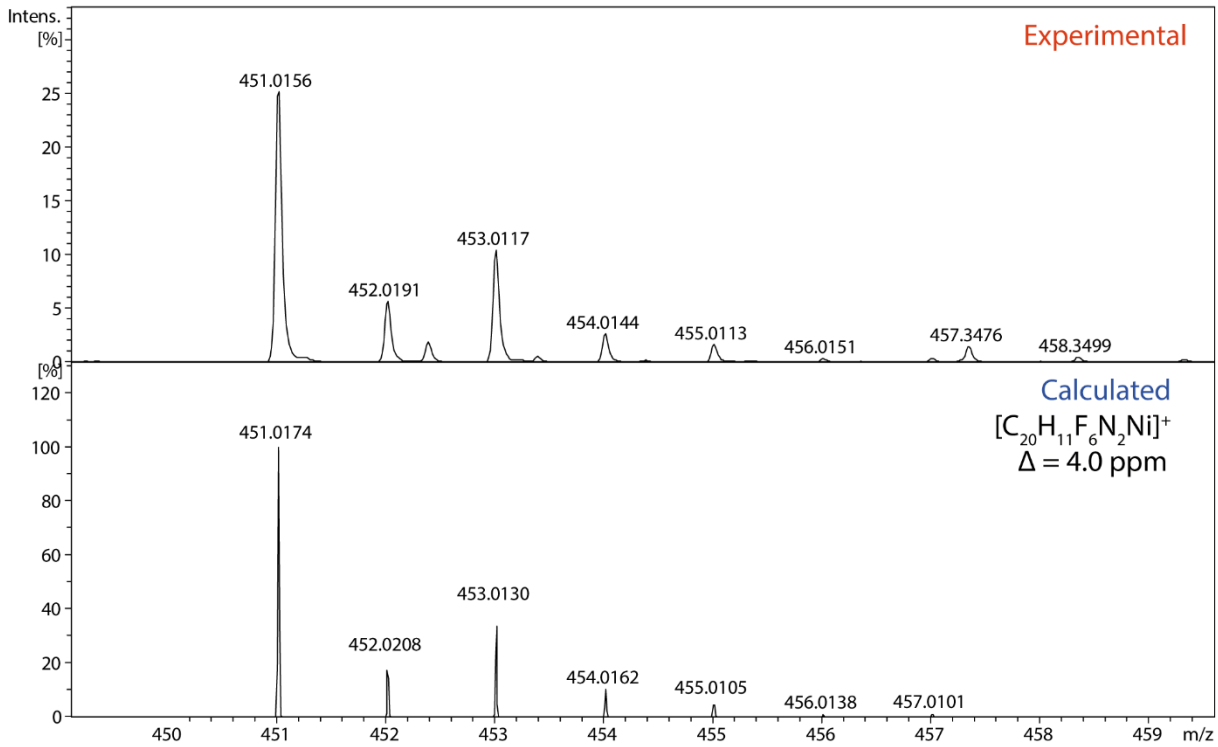

Figure S100. Experimental and theoretical ESI-(+)HRMS spectrum of **4j** in CH_3CN solution: experimental peak $[M]^+$ = 451.0156 Da, calculated for $C_{20}H_{11}F_6N_2Ni$ = 451.0174, Δ = 4.0 ppm.

4. Cyclic voltammetry

Table S2. CVs data for complexes **4** (recalculated to Fc^+/Fc, $2.5\cdot10^{-3}$ M) in CH_3CN**.** Working electrode: glassy carbon (*d* = 1.7 mm), scan rate 100 mVs^{-1}, 0.1 M Bu_4PF_6/ CH_3CN, 298 K.

Compound	E^p_{ox}, mV
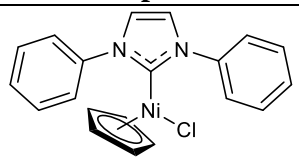 **4a**	-14
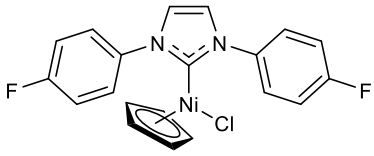 **4b**	+15
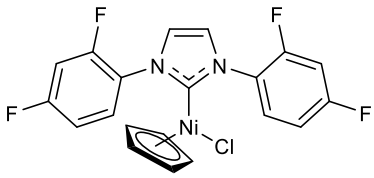 **4c**	+87
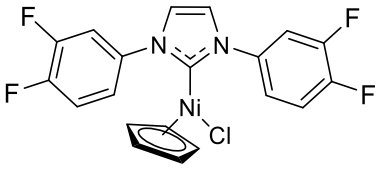 **4d**	+145
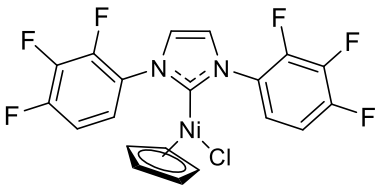 **4g**	+155
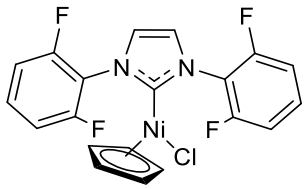 **4e**	+205

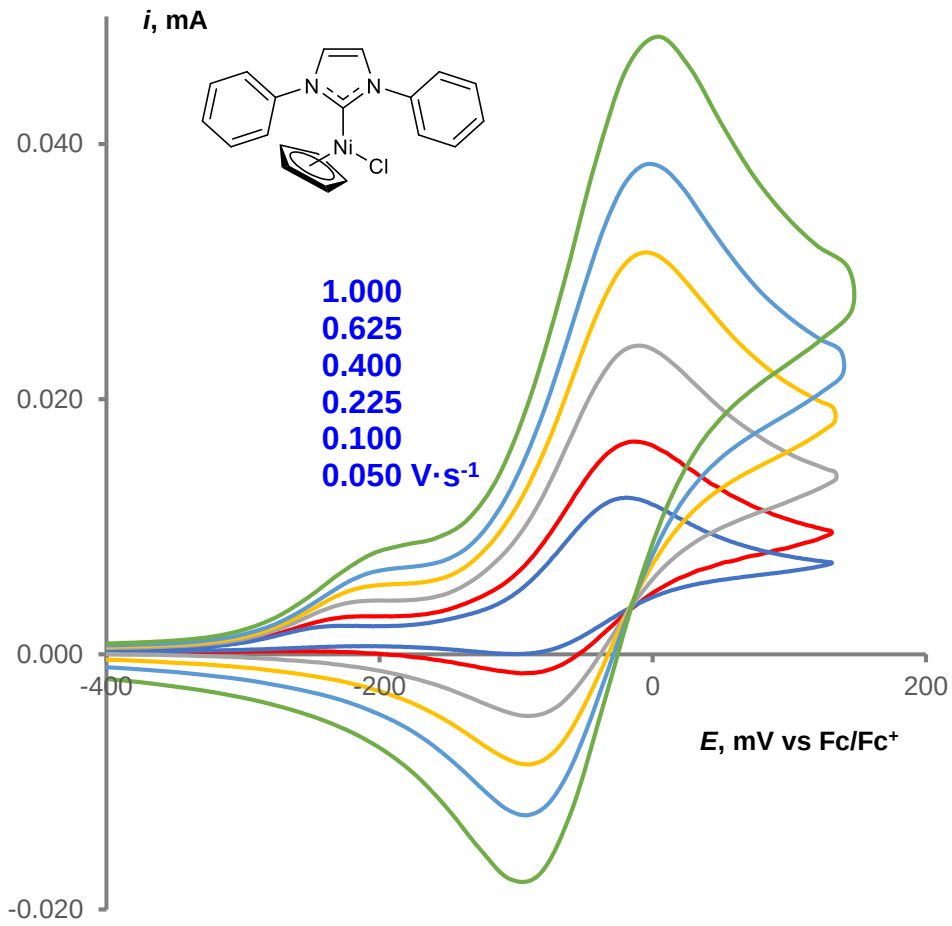

Figure S101. CVs data for **4a** ($2.5 \cdot 10^{-3}$ M) in CH_3CN**.** Working electrode: glassy carbon (*d* = 1.7 mm), 0.1 M Bu_4PF_6/ CH_3CN, 298 K.

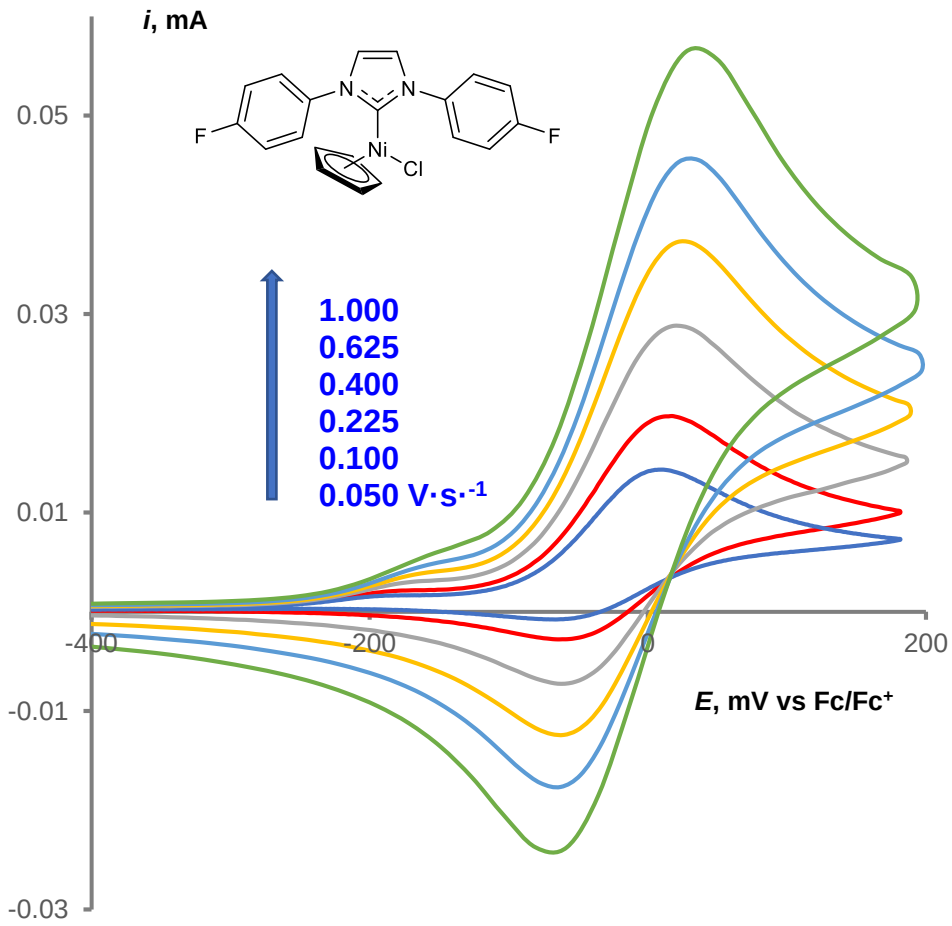

Figure S102. CVs data for **4b** ($2.5 \cdot 10^{-3}$ M) in CH_3CN**.** Working electrode: glassy carbon (*d* = 1.7 mm), 0.1 M Bu_4PF_6/ CH_3CN, 298 K.

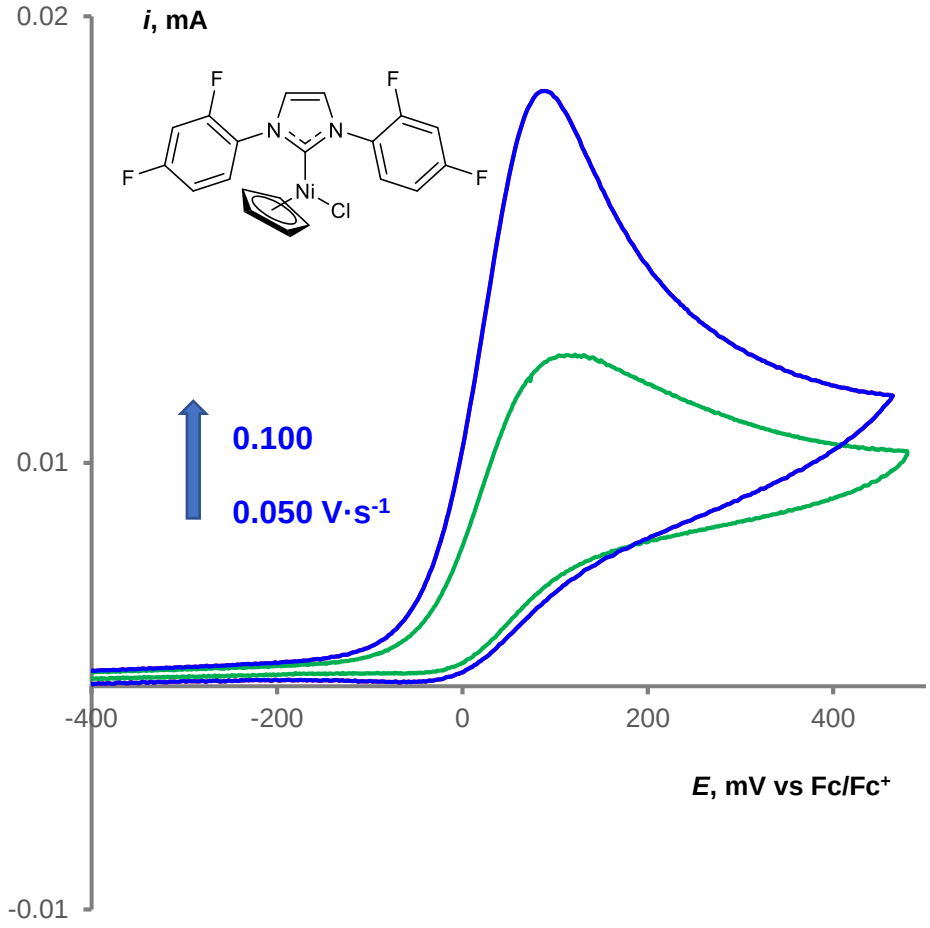

Figure S103. CVs data for **4c** ($2.5\cdot10^{-3}$ M) in CH_3CN**.** Working electrode: glassy carbon (*d* = 1.7 mm), 0.1 M Bu_4PF_6/ CH_3CN, 298 K.

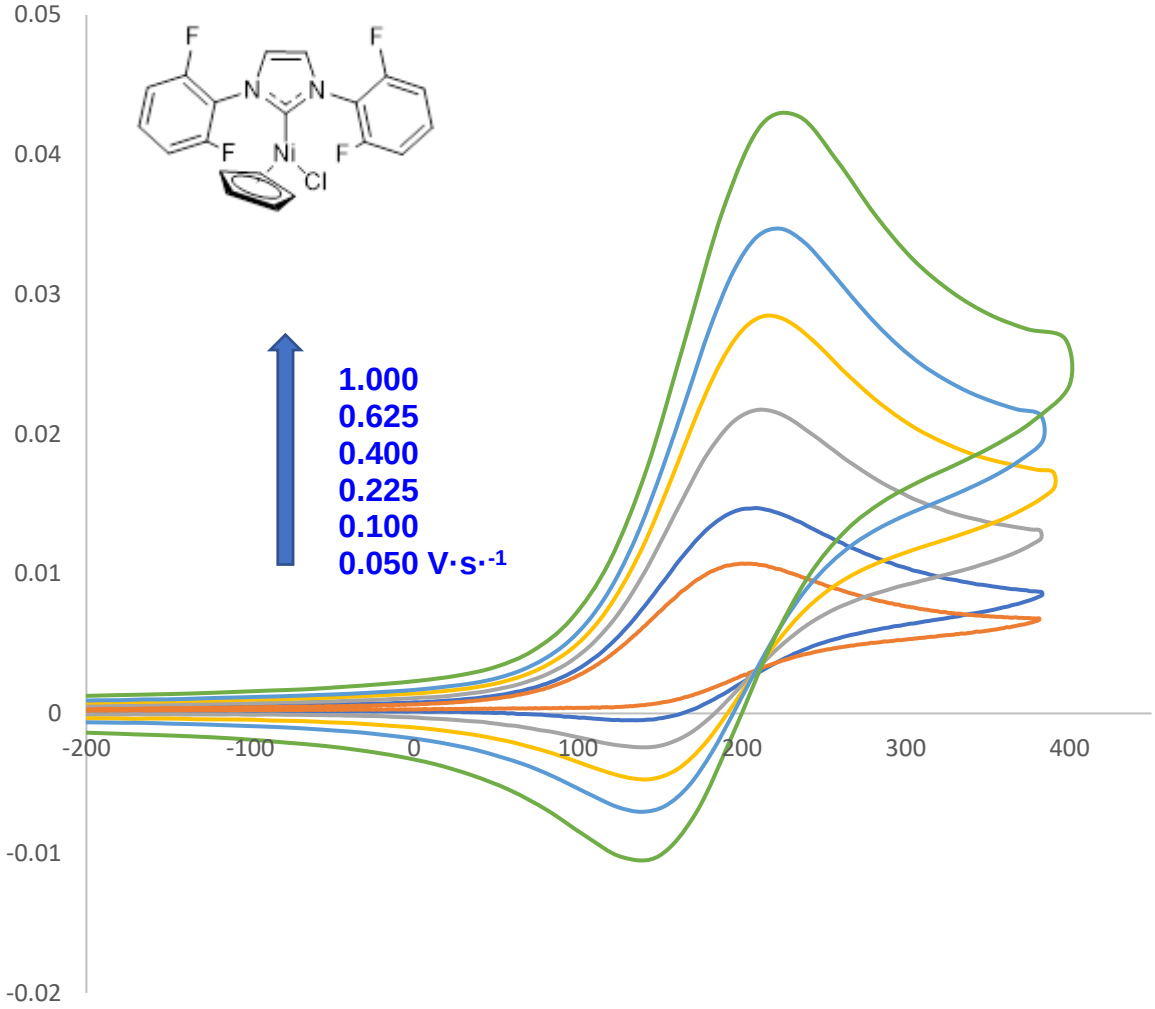

Figure S104. CVs data for **4e** ($2.5\cdot10^{-3}$ M) in CH_3CN**.** Working electrode: glassy carbon (*d* = 1.7 mm), 0.1 M Bu_4PF_6/ CH_3CN, 298 K.

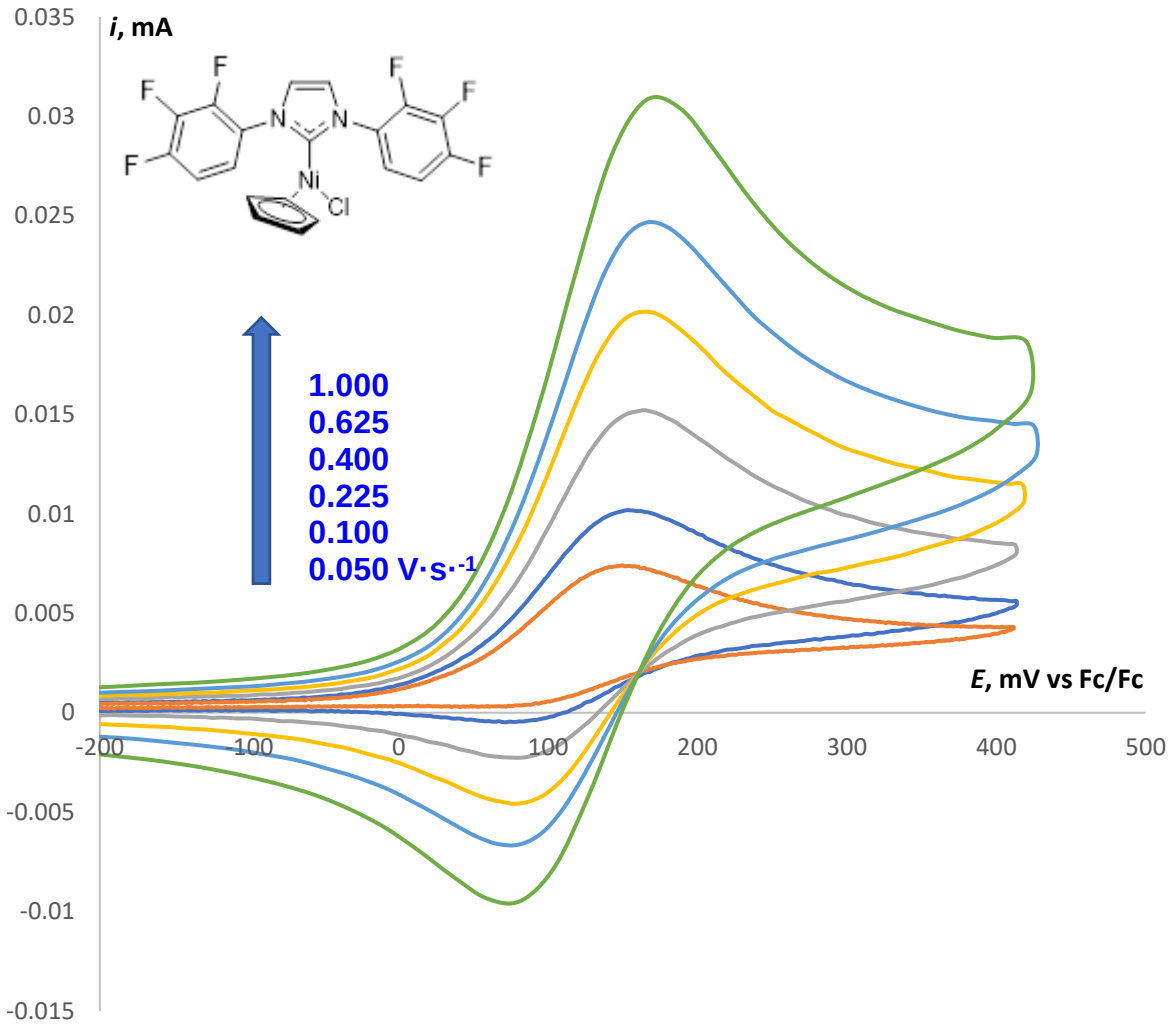

Figure S105. CVs data for **4g** ($2.5 \cdot 10^{-3}$ M) in CH_3CN**.** Working electrode: glassy carbon (*d* = 1.7 mm), 0.1 M Bu_4PF_6/ CH_3CN, 298 K.

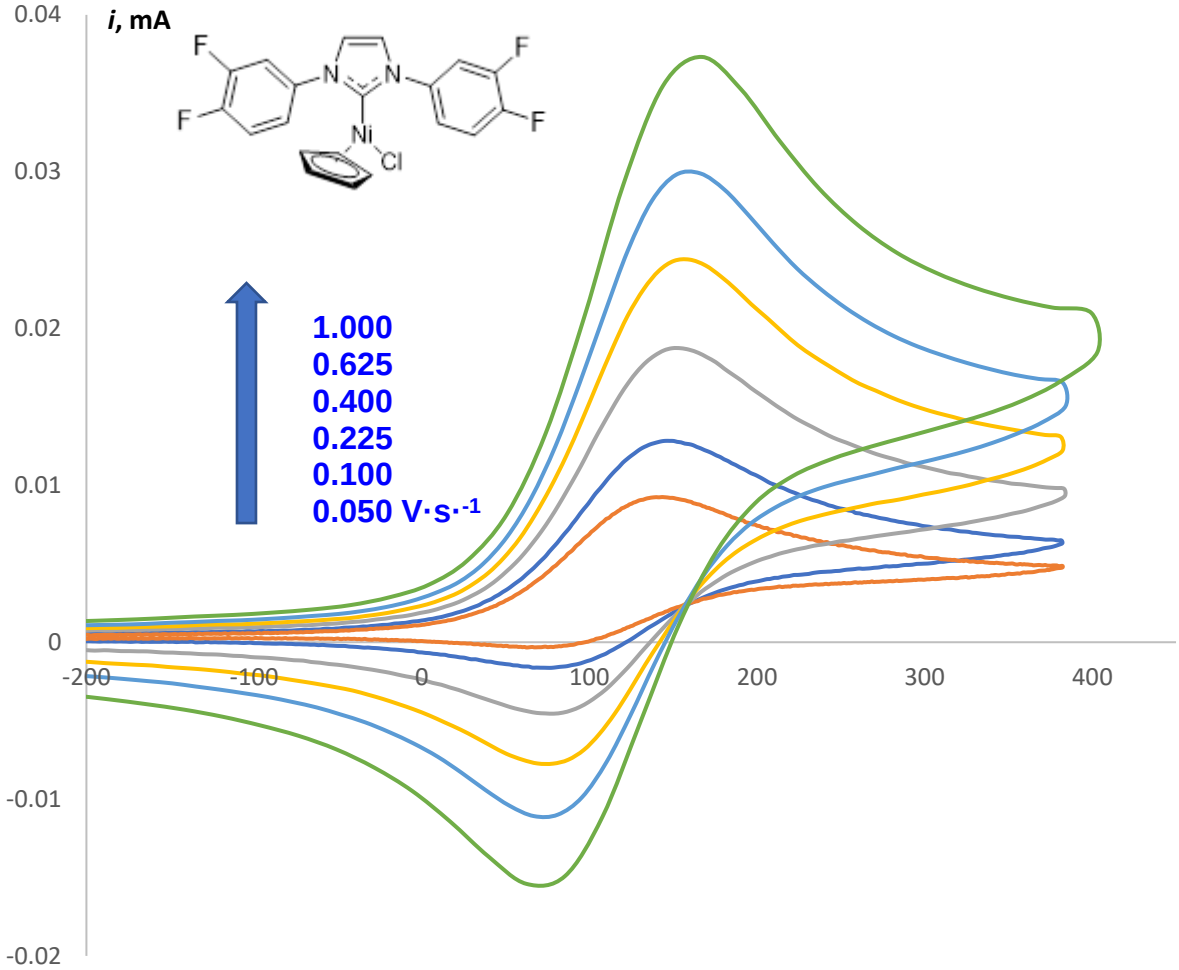

Figure S106. CVs data for **4d** ($2.5 \cdot 10^{-3}$ M) in CH_3CN**.** Working electrode: glassy carbon (*d* = 1.7 mm), 0.1 M Bu_4PF_6/ CH_3CN, 298 K.

5. X-ray crystallographic data and refinement details

X-ray diffraction data for **4h, 4b**, **4c**, **4d**, **4e**, **4g** and **3jb** were collected at 100K on a Rigaku XtaLAB Synergy-S diffractometer equipped with a HyPix6000HE area-detector (kappa geometry, shutterless ω-scan technique) using monochromatized Cu K_{α}-radiation. The intensity data were integrated and analytically corrected for absorption and decay by the CrysAlisPro program.[2] The structures were solved by direct methods using SHELXT[3] and refined by the full-matrix least-squares minimization method on F^2 using SHELXL-2018[4] in the OLEX2 program.[5] The positions of all atoms were found from the electron density-difference map except for the disordered H-atoms in **4c**. The disordered phenyl H-atoms in **4c** were positioned geometrically (C-H distance = 0.950 Å). Atoms were refined with individual anisotropic (non-hydrogen atoms) or relatively isotropic (hydrogen atoms) displacement parameters (U_{iso}(H)=1.2U_{eq}(C)). The H/F disorder in **4c** and Cl disorder in **4h** were refined in a regular manner, including the same isotropic displacement parameters for similar F or Cl atoms and restraining C-F or Ni-Cl bond distances to be equal within 0.02 Å.

The *SHELXTL* program suite[6] and the *Mercury* program[7] were used for molecular graphics herein and in the manuscript, respectively. The crystal data, data collection and structure refinement details are summarized in Table S1. The structures have been deposited at the Cambridge Crystallographic Data Center with the reference CCDC numbers 2362710, 2348102, 2338060-2338063 and 2362711; they also contain supplementary crystallographic data. These data can be obtained free of charge from the CCDC *via* https://www.ccdc.cam.ac.uk/structures/

Table S3. Crystal data and structure refinement for **4c**, **4d**, **4e** and **4g**.

Identification code	**4h**	**4b**	**4c**	**4d**
Empirical formula	$C_{20}H_{16}ClF_2N_2NiO_{0.5}$	$C_{20}H_{15}ClF_2N_2Ni$	$C_{20}H_{13}ClF_4N_2Ni$	$C_{20}H_{13}ClF_4N_2Ni$
Formula weight	424.51	415.50	451.48	451.48
Temperature (K)	100.00(10)	100.00(10)	100.00(10)	100.00(10)
Wavelength (Å)	1.54184	1.54184	1.54184	1.54184
Crystal system	Monoclinic	Monoclinic	Monoclinic	Monoclinic
Space group	$P2_1/c$	$P2_1/c$	$P2_1/c$	$P2_1/c$
Unit cell dimensions				
a (Å)	8.53819(6)	10.82250(6)	7.99026(4)	10.87858(6)
b (Å)	18.09252(12)	7.90636(4)	19.21028(11)	10.65567(5)
c (Å)	12.13920(8)	20.14341(12)	11.91822(6)	15.41970(8)
β (°)	105.5562(7)	95.3896(5)	100.8923(5)	92.6788(5)
Volume ($Å^3$)	1806.54(2)	1715.982(17)	1796.430(17)	1785.476(16)
Z	4	4	4	4
Calculd. density ($g \cdot cm^{-3}$)	1.561	1.608	1.669	1.680
μ (mm^{-1})	3.167	3.298	3.372	3.393
F(000)	868	848	912	912
Crystal size (mm)	0.56×0.36×0.09	0.35×0.25×0.20	0.56×0.44×0.21	0.56×0.27×0.23
θ range (°)	4.502-80.311	4.103-80.065	4.424-80.377	4.068-80.226
Index ranges	$-10 \le h \le 10$,	$-13 \le h \le 13$,	$-10 \le h \le 10$,	$-13 \le h \le 13$,
	$-23 \le k \le 22$,	$-7 \le k \le 10$,	$-24 \le k \le 23$,	$-13 \le k \le 13$,
	$-15 \le l \le 14$	$-25 \le l \le 24$	$-15 \le l \le 14$	$-19 \le l \le 19$
Reflections				
Collected	26603	27642	24230	24172
Independent [R_{int}]	3948 [0.0309]	3728 [0.0225]	3931 [0.0221]	3896 [0.0216]
Observed	3841	3699	3907	3876
Completeness to θ_{full} / θ_{max}	0.999 / 0.998	1.000 / 0.997	1.000 / 0.999	1.000 / 0.998
Max. / min. transmission	1.000 / 0.287	1.000 / 0.223	1.000 / 0.105	1.000 / 0.328
Data/restraints/parameters	3948 / 12 / 305	3728 / 0 / 295	3931 / 0 / 293	3896 / 19 / 295
Goodness-of-fit on F^2	1.053	1.072	1.104	1.100
R1 / wR2 for I>2σ(I)	0.0319 / 0.0845	0.0263 / 0.0648	0.0274 / 0.0666	0.0277 / 0.0676
R1 / wR2 for all data	0.0326 / 0.0851	0.0265 / 0.0650	0.0277 / 0.0668	0.0279 / 0.0677
Extinction coefficient	0.00067(12)	-	0.00311(12)	0.00057(8)
$\Delta\rho(\mathbf{r})_{max}$ / $\Delta\rho(\mathbf{r})_{max}$ ($\bar{e} \cdot Å^{-3}$)	0.412 / -0.410 e.$Å^{-3}$	0.331 / -0.279	0.328 / -0.274	0.342 / -0.304
CCDC numbers	2362710	2348102	2338060	2338061

Table S3. Crystal data and structure refinement for **4c**, **4d**, **4e** and **4g**.

Identification code	**4e**	**4g**	**3jb**
Empirical formula	$C_{20}H_{13}ClF_4N_2Ni$	$C_{20}H_{11}ClF_6N_2Ni$	$C_{20}H_{11}F_4N_3O_2Pd$
Formula weight	451.48	487.47	507.72
Temperature (K)	100.00(10)	99.99(10)	100.00(11)
Wavelength (Å)	1.54184	1.54184	1.54184
Crystal system	Monoclinic	Monoclinic	Triclinic
Space group	$P2_1/n$	$P2_1/n$	$P\bar{1}$
Unit cell dimensions			
a (Å)	7.95480(7)	10.34845(5)	3.68882(7)
b (Å)	17.60556(13)	17.63964(7)	11.4296(2)
c (Å)	13.33453(10)	10.81434(6)	20.0470(3)
α (°)	90	90	88.7087(14)
β (°)	106.8036(9)	108.9317(5)	84.9983(14)
g (°)	90	90	82.4843(17)
Volume ($Å^3$)	1787.74(3)	1867.293(15)	834.71(3) $Å^3$
Z	4	4	2
Calculated density ($g \cdot cm^{-3}$)	1.677	1.734	2.020
μ (mm^{-1})	3.389	3.457	9.614
F(000)	912	976	500
Crystal size (mm)	0.12×0.10×0.08	0.27×0.22×0.19	0.08×0.03×0.02
θ range (°)	4.278-79.980	4.998-80.164	2.212-79.654
Index ranges	$-9 \le h \le 10$,	$-13 \le h \le 12$,	$-4 \le h \le 4$,
	$-22 \le k \le 22$,	$-22 \le k \le 22$,	$-14 \le k \le 14$,
	$-17 \le l \le 16$	$-13 \le l \le 13$	$-25 \le l \le 25$
Reflections			
Collected	28249	33931	12853
Independent [R_{int}]	3890 [0.0183]	4083 [0.0205]	3473 [0.0313]
Observed	3779	4059	3248
Completeness to θ_{full} / θ_{max}	1.000 / 0.997	1.000 / 0.999	0.981 / 0.953
Max. / min. transmission	1.000 / 0.695	1.000 / 0.253	0.888 / 0.551
Data/restraints/parameters	3890 / 0 / 292	4083 / 0 / 305	3473 / 0 / 304
Goodness-of-fit on F^2	1.060	1.098	1.094
R1 / wR2 for I>2σ(I)	0.0241 / 0.0654	0.0246 / 0.0622	0.0312 / 0.0743
R1 / wR2 for all data	0.0246 / 0.0657	0.0248 / 0.0623	0.0341 / 0.0754
Extinction coefficient	-	0.00144(9)	-
$\Delta\rho(\mathbf{r})_{max}$ / $\Delta\rho(\mathbf{r})_{max}$ ($\bar{e} \cdot Å^{-3}$)	0.336 / -0.380	0.309 / -0.291	1.140 / -0.884
CCDC numbers	2338062	2338063	2362711

In all the structures, the Cp ring is symmetrically coordinated to Ni^{2+}, since the ring slippage is not observed: the distances Cp(centroid)···Ni and Cp(plane)···Ni are nearly identical. The Ni^{2+} cation (C.N. = 5) is located in a pseudotrigonal environment: the Ni, Cl and C1 atoms and the Cp(centroid) are located in the same plane. Selected geometrical parameters for the Cp-Ni(Cl)-C crystallographic node are provided in Table S11.

The structure of **4h**.

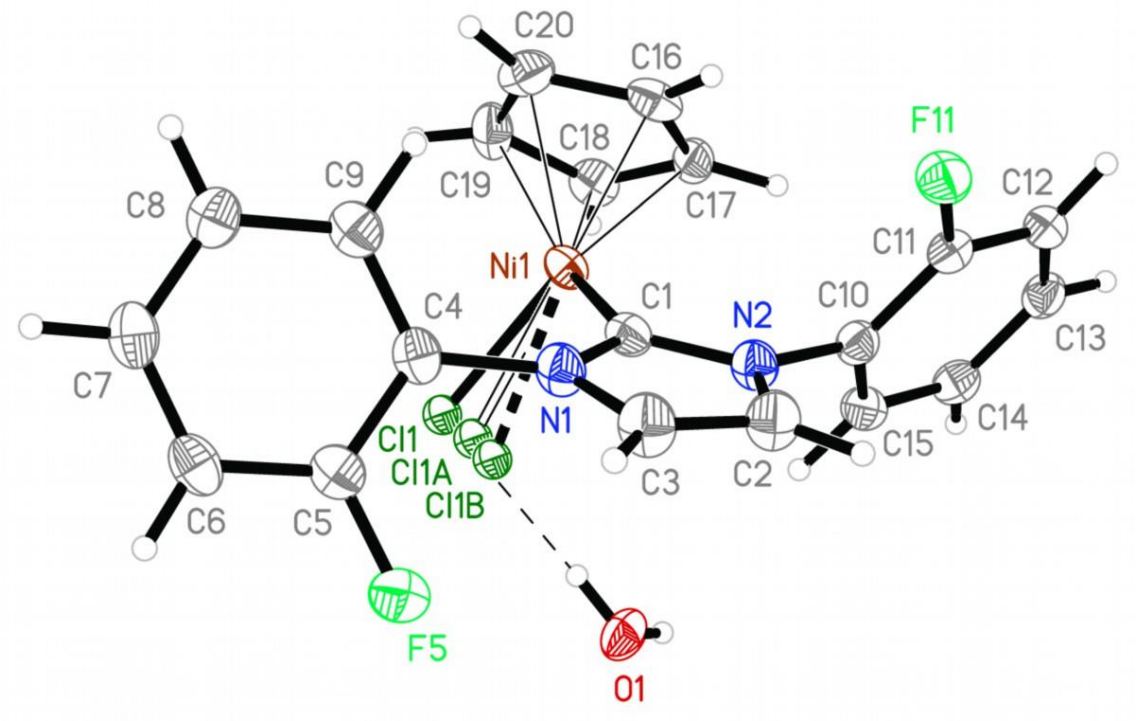

Figure S107. The structure of **4h** in anisotropic approximation (p=50%). The Cl atom is disordered over three positions with the disorder ratio of 0.501(3): 0.307(3):0.192(3). The water molecule has a site occupancy of 0.501(3). The hydrogen atoms of the water molecule form two hydrogen bonds with the Cl1 atoms of two molecules (one of the bonds is shown with a thin dashed line).

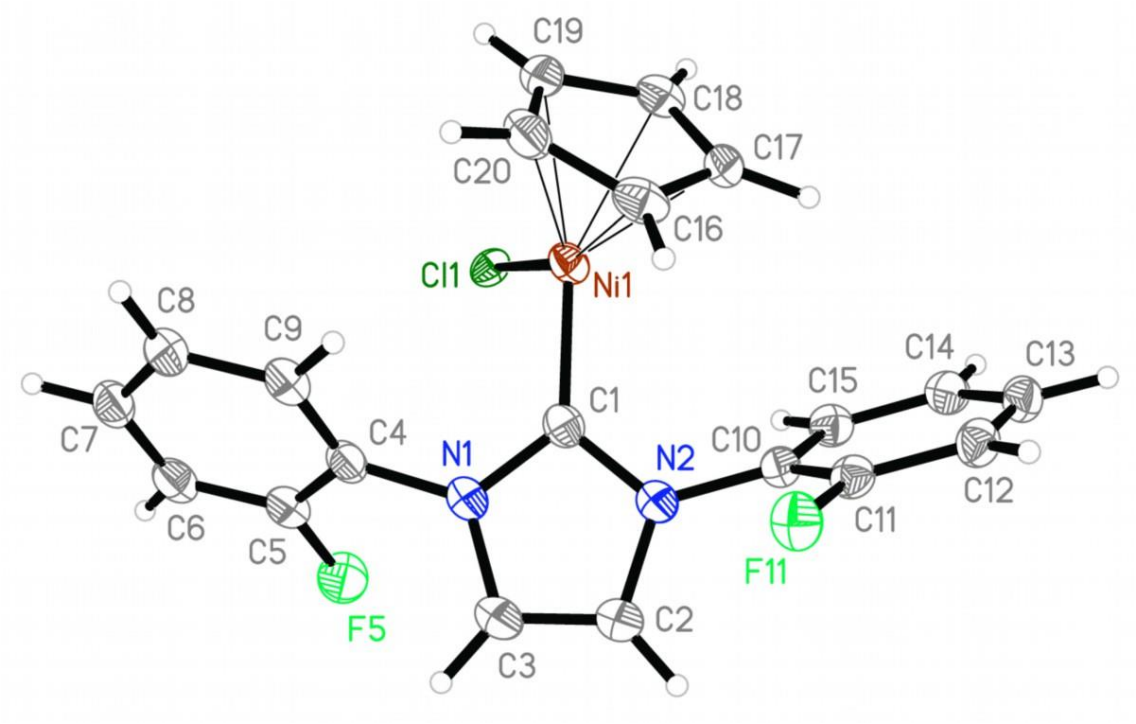

Figure S108. The structure of the complex **4h** (p=50%). The disorder is omitted.

Table S4. Selected bond distances in **4h** (Å).

Ni1-Cl1	2.2131(11)	C1-N2	1.360(2)	C10-C15	1.388(2)
Ni1-Cl1A	2.2217(19)	N2-C2	1.388(2)	C11-F11	1.3576(18)
Ni1-Cl1B	2.312(3)	N2-C10	1.4307(19)	C11-C12	1.379(2)
Ni1-C1	1.8772(16)	C2-C3	1.342(2)	C12-C13	1.389(2)
Ni1-C16	2.0422(16)	C4-C5	1.388(2)	C13-C14	1.391(2)
Ni1-C17	2.1754(15)	C4-C9	1.385(2)	C14-C15	1.389(2)
Ni1-C18	2.1756(16)	C5-F5	1.346(2)	C15-H15	1.00(2)
Ni1-C19	2.1553(17)	C5-C6	1.379(2)	C16-C17	1.430(2)
Ni1-C20	2.1468(17)	C6-C7	1.387(3)	C16-C20	1.427(3)
N1-C1	1.362(2)	C7-C8	1.391(3)	C17-C18	1.385(2)
N1-C3	1.388(2)	C8-C9	1.391(2)	C18-C19	1.446(3)
N1-C4	1.433(2)	C10-C11	1.383(2)	C19-C20	1.391(3)

Table S5. Hydrogen bonds for **4h** (Å and °).

D-H...A	d(D-H)	d(H...A)	d(D...A)	<(DHA)
O1-H1A...Cl1	0.83(2)	2.32(2)	3.150(3)	175(5)
O1-H1B...Cl1#1	0.82(2)	2.89(3)	3.665(3)	157(5)

Symmetry transformation to generate equivalent atoms: #1 -x+1, -y+1, -z+1

The structure of **4b**.

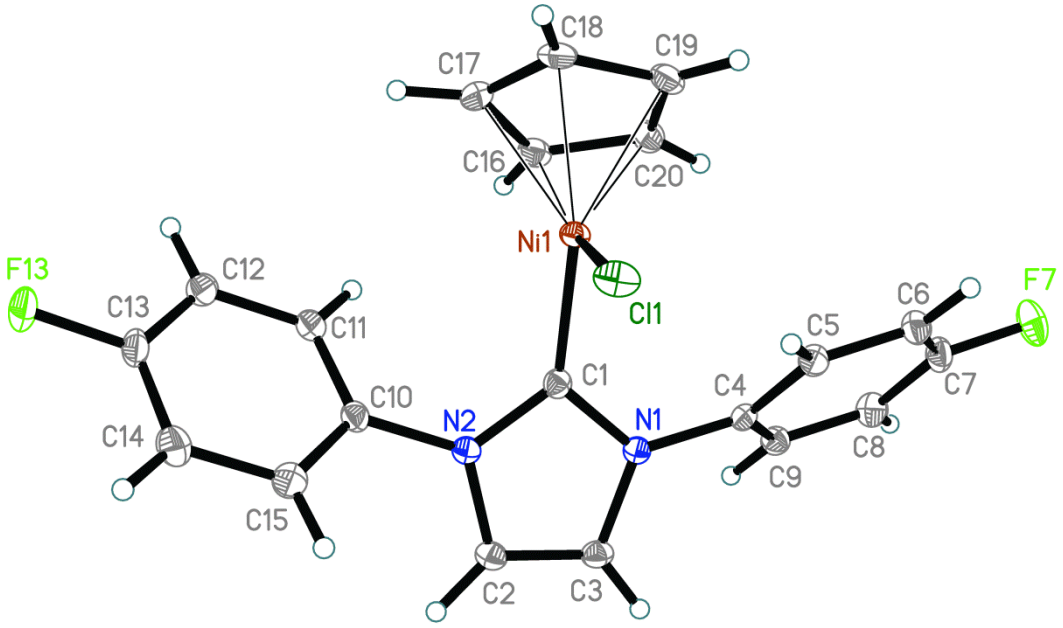

Figure S109. The structure of **4b** in anisotropic approximation (p=50%).

Table S6. Selected bond distances in **4c** (Å).

Ni1-Cl1	2.1905(4)	N2-C2	1.3959(18)	C10-C15	1.390(2)
Ni1-C1	1.8879(14)	N2-C10	1.4353(17)	C11-C12	1.392(2)
Ni1-C16	2.0666(14)	C2-C3	1.347(2)	C12-C13	1.378(2)
Ni1-C17	2.1539(14)	C4-C5	1.391(2)	C13-F13	1.3566(16)
Ni1-C18	2.1201(14)	C4-C9	1.3867(19)	C13-C14	1.379(2)
Ni1-C19	2.1848(14)	C5-C6	1.393(2)	C14-C15	1.393(2)
Ni1-C20	2.1708(14)	C6-C7	1.381(2)	C16-C17	1.425(2)
N1-C1	1.3608(17)	C7-F7	1.3651(16)	C16-C20	1.448(2)
N1-C3	1.3949(18)	C7-C8	1.377(2)	C17-C18	1.404(2)
N1-C4	1.4338(17)	C8-C9	1.392(2)	C18-C19	1.449(2)
C1-N2	1.3624(18)	C10-C11	1.388(2)	C19-C20	1.388(2)

The structure of **4c**.

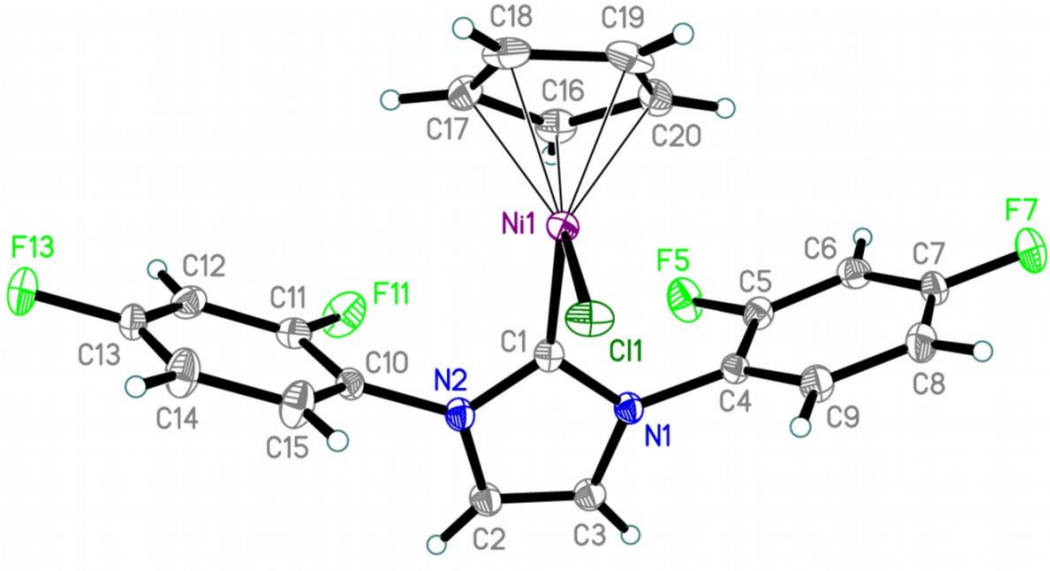

Figure S110. The structure of **4c** in anisotropic approximation (p=50%).

Table S7. Selected bond distances in **4c** (Å).

Ni1-Cl1	2.1953(4)	N2-C10	1.4310(18)	C11-F11	1.3483(17)
Ni1-C1	1.8630(14)	C2-C3	1.342(2)	C11-C12	1.379(2)
Ni1-C16	2.0323(15)	C4-C5	1.385(2)	C12-C13	1.376(2)
Ni1-C17	2.1548(15)	C4-C9	1.389(2)	C13-F13	1.3562(17)
Ni1-C18	2.1710(15)	C5-F5	1.3473(17)	C13-C14	1.376(2)
Ni1-C19	2.1574(15)	C5-C6	1.381(2)	C14-C15	1.393(2)
Ni1-C20	2.1507(15)	C6-C7	1.383(2)	C16-C17	1.437(2)
N1-C1	1.3570(18)	C7-F7	1.3511(17)	C16-C20	1.432(2)
N1-C3	1.3977(18)	C7-C8	1.377(2)	C17-C18	1.388(2)
N1-C4	1.4325(17)	C8-C9	1.391(2)	C18-C19	1.444(2)
C1-N2	1.3555(18)	C10-C11	1.384(2)	C19-C20	1.388(2)
N2-C2	1.3967(18)	C10-C15	1.384(2)		

The structure of **4d**.

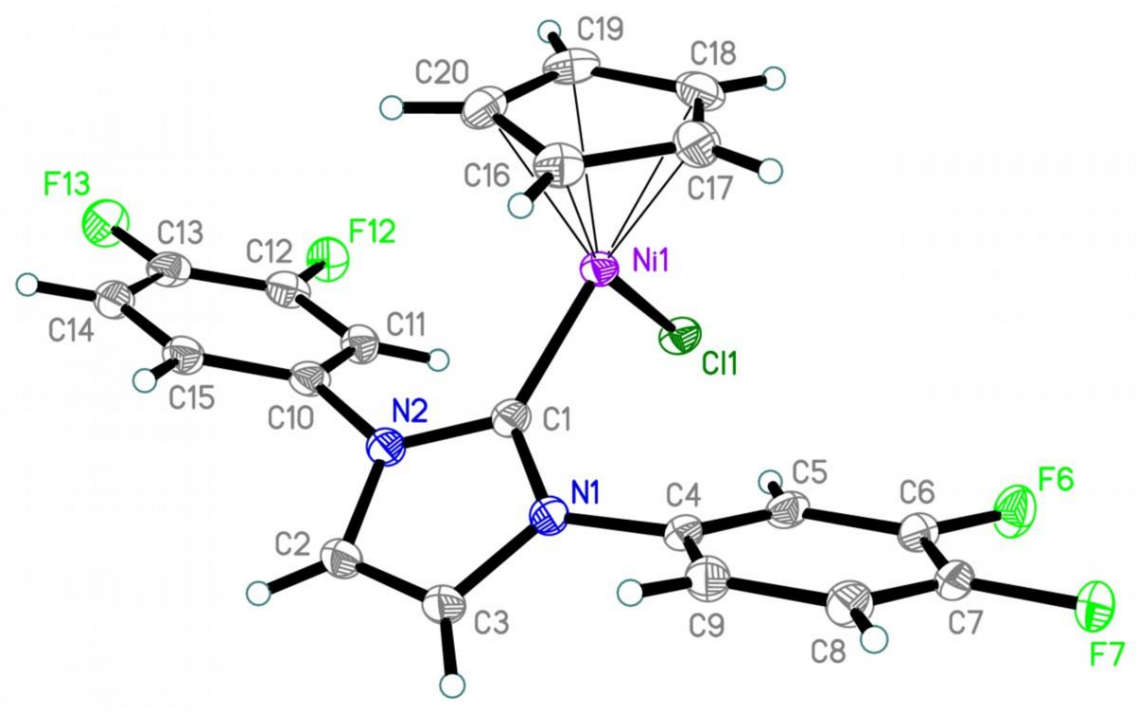

Figure S111. The structure of **4d** in anisotropic approximation (p=50%). The H/F disorder is omitted.

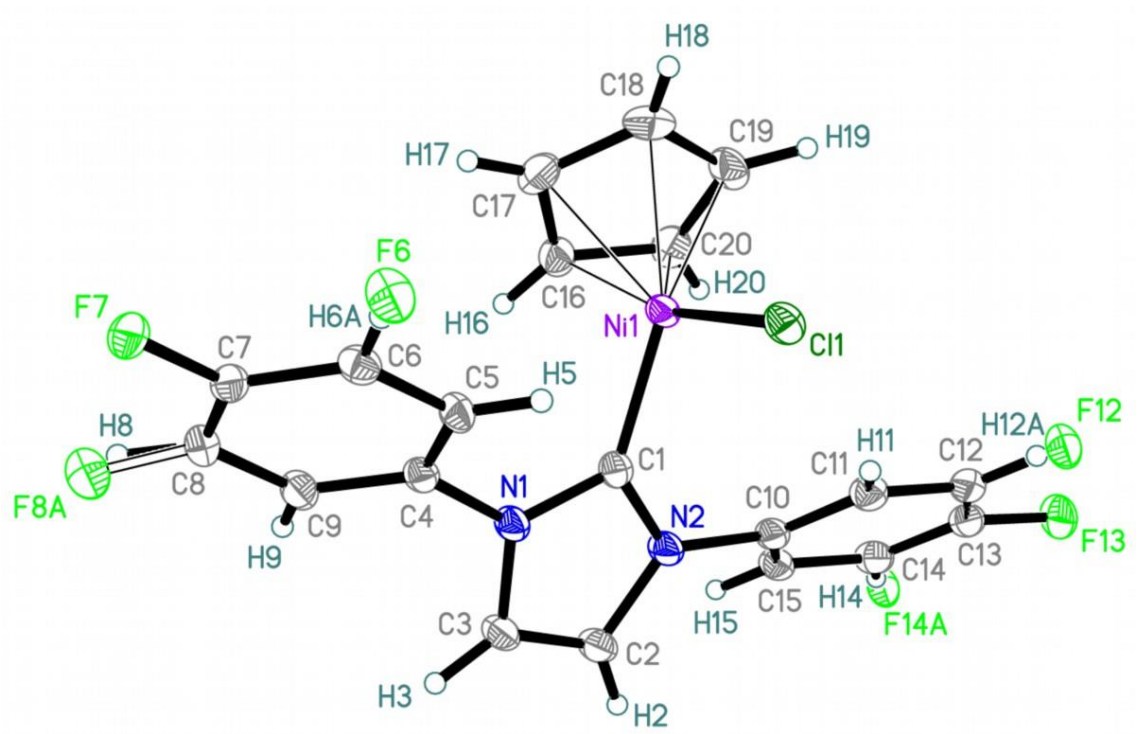

Figure S112. The structure of **4d** in anisotropic approximation (p=50%). The disorder ratios for F6, H8 / H6A, F8A and F12, H14 / H12A, F14A disorders are 0.980(2) : 0.020(2) and 0.6303(19) : 0.3697(19), correspondingly.

Table S8. Selected bond distances in **4d** (Å).

Ni1-Cl1	2.2154(4)	C2-C3	1.343(2)	C11-C12	1.385(2)
Ni1-C1	1.8826(15)	C4-C5	1.391(2)	C12-F12	1.289(2)
Ni1-C16	2.0419(16)	C4-C9	1.390(2)	C12-C13	1.379(2)
Ni1-C17	2.1499(16)	C5-C6	1.380(2)	C13-F13	1.3467(17)
Ni1-C18	2.1354(16)	C6-F6	1.3435(18)	C13-C14	1.374(2)
Ni1-C19	2.1811(15)	C6-C7	1.385(2)	C14-F14A	1.253(3)
Ni1-C20	2.1481(16)	C7-F7	1.3489(17)	C14-C15	1.391(2)
N1-C1	1.3651(18)	C7-C8	1.375(2)	C16-C17	1.417(2)
N1-C3	1.3966(19)	C8-F8A	1.286(16)	C16-C20	1.451(2)
N1-C4	1.4340(18)	C8-C9	1.394(2)	C17-C18	1.398(2)
C1-N2	1.3622(19)	C10-C11	1.391(2)	C18-C19	1.449(3)
N2-C2	1.3964(19)	C10-C15	1.388(2)	C19-C20	1.383(2)
N2-C10	1.4350(18)				

The structure of **4e**.

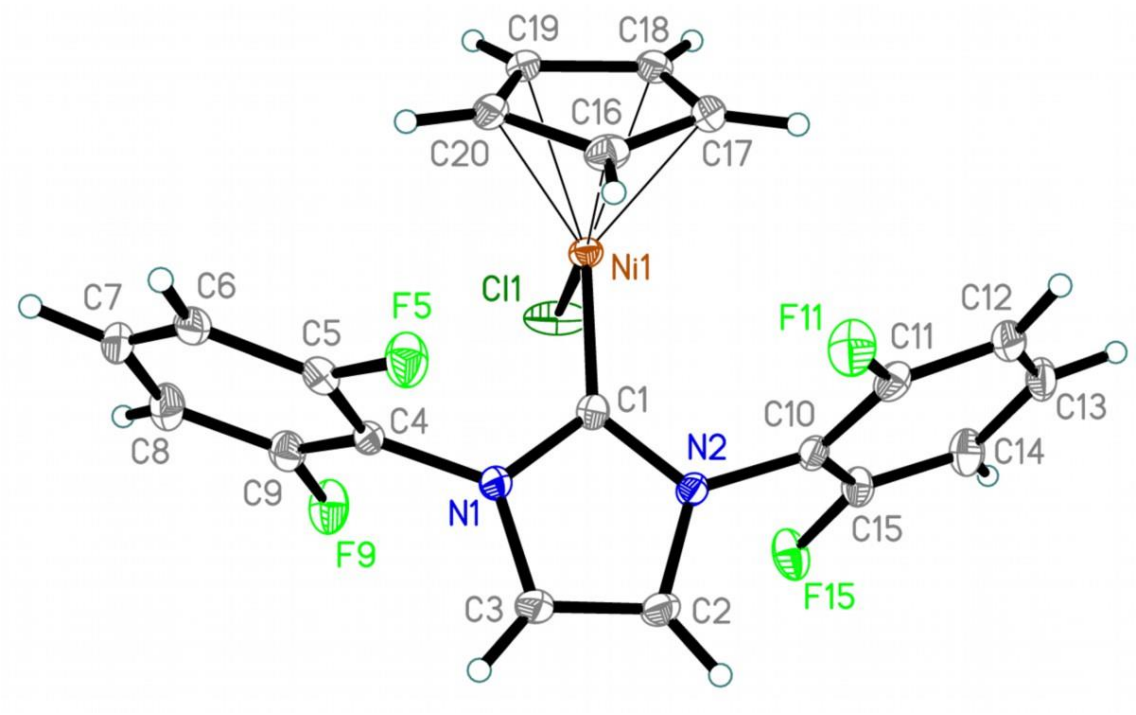

Figure S113. The structure of **4e** in anisotropic approximation (p=50%).

Table S9. Selected bond distances in **4e** (Å).

Ni1-Cl1	2.1860(4)	N2-C10	1.4246(15)	C11-F11	1.3419(14)
Ni1-C1	1.8644(13)	C2-C3	1.3410(19)	C11-C12	1.3818(18)
Ni1-C16	2.0342(13)	C4-C5	1.3898(17)	C12-C13	1.3878(19)
Ni1-C17	2.1781(13)	C4-C9	1.3861(18)	C13-C14	1.3933(19)
Ni1-C18	2.2059(12)	C5-F5	1.3497(15)	C14-C15	1.3796(18)
Ni1-C19	2.1719(12)	C5-C6	1.3799(18)	C15-F15	1.3439(14)
Ni1-C20	2.1383(12)	C6-C7	1.388(2)	C16-C17	1.4373(19)
N1-C1	1.3591(15)	C7-C8	1.389(2)	C16-C20	1.4347(18)
N1-C3	1.3952(16)	C8-C9	1.3830(18)	C17-C18	1.3878(19)
N1-C4	1.4251(15)	C9-F9	1.3473(15)	C18-C19	1.4485(17)
C1-N2	1.3575(15)	C10-C11	1.3855(17)	C19-C20	1.3986(17)
N2-C2	1.3912(16)	C10-C15	1.3860(17)		

The structure of **4g**.

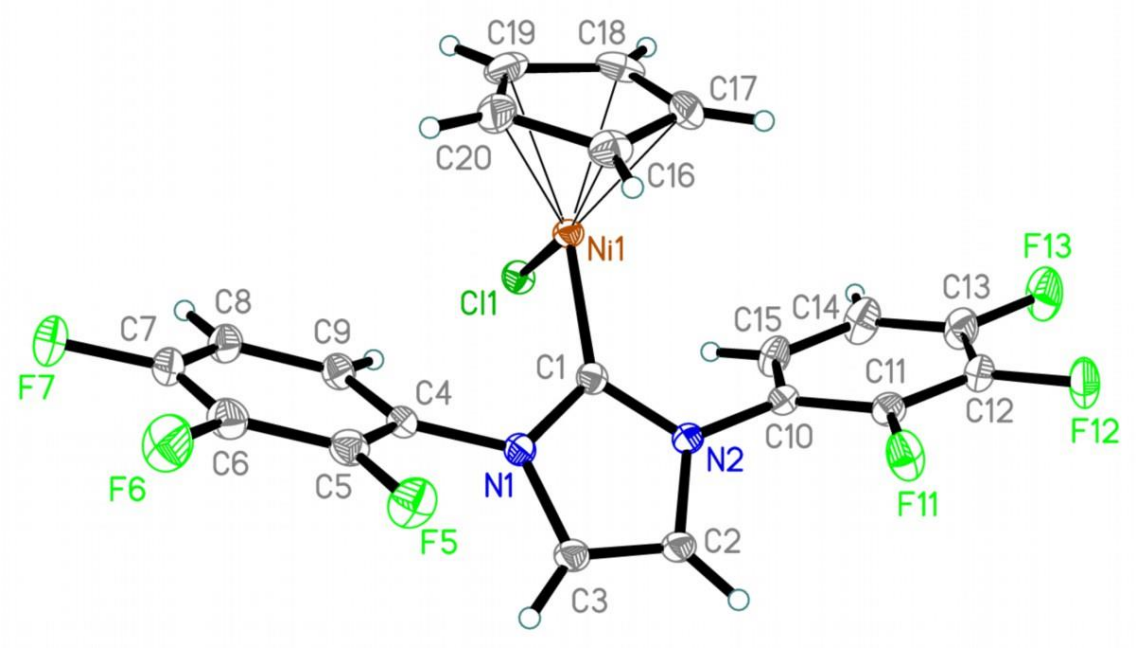

Figure S114. The structure of **4g** in anisotropic approximation (p=50%).

Table S10. Selected bond distances in **4g** (Å).

Ni1-Cl1	2.2059(4)	C2-C3	1.3409(19)	C11-F11	1.3443(15)
Ni1-C1	1.8741(13)	C4-C5	1.3855(18)	C11-C12	1.3815(19)
Ni1-C16	2.0368(14)	C4-C9	1.3920(18)	C12-F12	1.3414(16)
Ni1-C17	2.1618(14)	C5-F5	1.3448(15)	C12-C13	1.378(2)
Ni1-C18	2.1527(14)	C5-C6	1.3873(19)	C13-F13	1.3467(16)
Ni1-C19	2.1407(14)	C6-F6	1.3413(16)	C13-C14	1.377(2)
Ni1-C20	2.1370(14)	C6-C7	1.380(2)	C14-C15	1.389(2)
N1-C1	1.3643(16)	C7-F7	1.3510(15)	C16-C17	1.439(2)
N1-C3	1.3979(16)	C7-C8	1.377(2)	C16-C20	1.433(2)
N1-C4	1.4286(16)	C8-C9	1.3914(19)	C17-C18	1.386(2)
C1-N2	1.3604(16)	C10-C11	1.3868(18)	C18-C19	1.448(2)
N2-C2	1.3976(16)	C10-C15	1.3886(18)	C19-C20	1.388(2)
N2-C10	1.4273(16)				

Table S11. Geometrical parameters for the Cp-Ni(Cl)-C crystallographic node (Å, °).

Distances/angles	**4h**	**4b**	**4c**	**4d**	**4e**	**4g**
Ni1-Cl1	2.1953(4)	2.1905(4)	2.1953(4)	2.2154(4)	2.1860(4)	2.2059(4)
Ni1-C1	1.8630(14)	1.8879(14)	1.8630(14)	1.8826(15)	1.8644(13)	1.8741(13)
$Cp_{centroid}$···Ni1	1.7688(8)	1.7647(7)	1.761(2)	1.757(2)	1.774(1)	1.751(1)
Cp_{plane}···Ni1	1.7662(8)	1.7633(7)	1.758(2)	1.755(2)	1.769(1)	1.749(1)
C1-Ni-Cl1	99.77(6)	94.42(4)	94.32(4)	100.66(5)	93.17(4)	98.13(4)
$Cp_{centroid}$···Ni1-Cl1	127.3	128.7	133.8	131.4	134.1	130.6
$Cp_{centroid}$···Ni1-C1	132.9	136.6	131.8	127.9	132.7	131.2
The sum	360.0	359.7	359.9	360.0	360.0	359.9

Table S12. The Ph···N_2C_3 dihedral angles (°).

Complex	Ph = C4..C9	Ph = C10..C15
4h	61.62(7)	67.11(6)
4b	49.91(4)	53.14(6)
4c	80.13(5)	78.55(5)
4d	40.79(6)	42.92(6)
4e	88.01(4)	77.68(5)
4g	45.38(6)	49.47(5)

The structure of **3jb**.

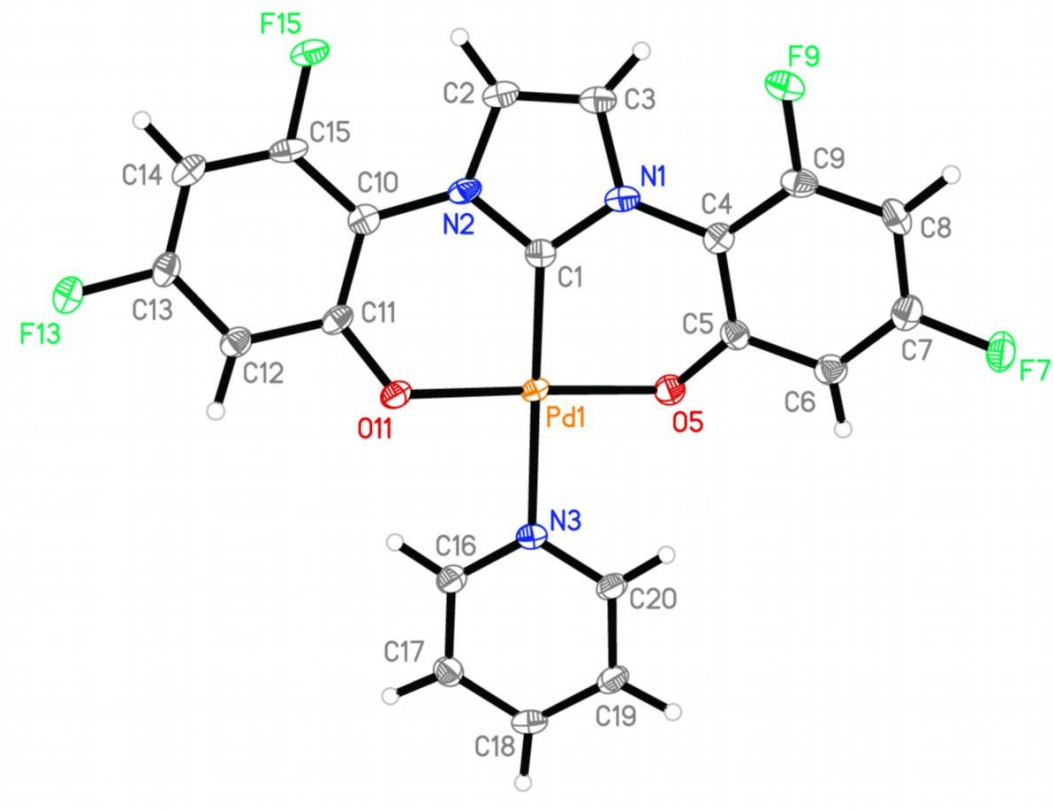

Figure S115. The structure of **3jb** in anisotropic approximation (p=50%).

Table S13. Selected bond distances in **3jb** (Å).

Pd1-C1	1.918(4)	C4-C9	1.395(5)	C12-C13	1.367(5)
Pd1-O5	1.994(3)	C5-O5	1.308(4)	C13-F13	1.357(4)
Pd1-O11	1.977(3)	C5-C6	1.415(5)	C13-C14	1.381(5)
Pd1-N3	2.116(3)	C6-C7	1.366(6)	C14-C15	1.376(6)
N1-C1	1.358(5)	C7-F7	1.369(4)	C15-F15	1.369(4)
N1-C3	1.392(5)	C7-C8	1.374(6)	N3-C16	1.338(5)
N1-C4	1.436(5)	C8-C9	1.376(5)	N3-C20	1.345(5)
C1-N2	1.359(4)	C9-F9	1.359(4)	C16-C17	1.385(5)
N2-C2	1.407(5)	C10-C11	1.424(5)	C17-C18	1.384(5)
N2-C10	1.437(5)	C10-C15	1.398(5)	C18-C19	1.386(6)
C2-C3	1.333(6)	C11-O11	1.309(4)	C19-C20	1.385(5)
C4-C5	1.419(5)	C11-C12	1.415(5)		

Table S14. The Ph···N_2C_3 dihedral angles (°).

Complex	Ph = C4..C9	Ph = C10..C15
3jb	24.09(14)	6.56(19)

6. Literature references

1. Malyshev D.A., Scott N.M., Marion N., Stevens E.D., Ananikov V.P., Beletskaya I.P., Nolan S.P., Homogeneous Nickel Catalysts for the Selective Transfer of a Single Arylthio Group in the Catalytic Hydrothiolation of Alkynes, *Organometallics*, **2006,** 25, 4462-4470.
2. CrysAlisPro. Versions 1.171.42 and 1.171.43. *Rigaku Oxford Diffraction*, **2023**.
3. Sheldrick, G. M. SHELXT - Integrated space-group and crystal-structure determination. *Acta Cryst.* **2015**, A71(1), 3-8. https://doi.org/10.1107/S2053273314026370
4. Sheldrick, G. M. Crystal structure refinement with SHELXL. *Acta Cryst.* **2015**, C71(1), 3-8. https://doi.org/10.1107/S2053229614024218
5. Dolomanov O.V.; Bourhis L.J.; Gildea R.J.; Howard J.A.K.; Puschmann H. OLEX2: a complete structure solution, refinement and analysis program. *J. Appl. Cryst.* **2009**, 42(2), 339-341. https://doi.org/10.1107/S0021889808042726
6. Sheldrick, G.M. A short history of SHELX. *Acta Cryst., Sect. A* **2008**, A64(1), 112-122. https://doi.org/10.1107/S0108767307043930
7. Macrae, C. F.; Sovago, I.; Cottrell, S. J.; Galek, P. T. A.; McCabe, P.; Pidcock, E.; Platings, M.; Shields, G. P.; Stevens, J. S.; Towler, M.; Wood, P. A. Mercury 4.0: from visualization to analysis, design and prediction. *J. Appl. Cryst.* **2020**, 53(1), 226-235. https://doi.org/10.1107/S1600576719014092